EVALUATION OF AN HF HELICOPTER ANTENNA MEASUREMENTS AND NUMERICAL TECHNIQUES

© Youssef Bahsoun

A Thesis

in

The Faculty

of

Engineering

Presented in Partial Fulfillment of the Requirements
for the degree of Master of Engineering at
Concordia University
Montréal, Québec, Canada

March 1982

ABSTRACT

EVALUATION OF AN HF HELICOPTER ANTENNA MEASUREMENTS AND NUMERICAL TECHNIQUES

YOUSSEF BAHSOUN

This thesis presents a complete evaluation of the radiation characteristics of an HF loop antenna mounted on the Sea-King helicopter. Scale model measurements of the antenna's radiation patterns are carried out. Power-related assessment parameters are computed directly from the radiation patterns. These assessment parameters form the basis of a meaningful evaluation of antenna performance, and they are being used throughout this thesis to compare the performace of various HF wire antennas to the loop antenna.

In this work wire grid models of different levels of complexity are developed for the Sea-King helicopter. These models are analyzed using the moment method techniques. It is found that a computer model can produce good results at resonant frequencies when a proper tuning of the model is applied.

Thus a carefully optimized computer model provides a useful means for comparing the operational performance of various antenna designs

ACKNOWLEDGEMENT

My sincerest thanks goes to my supervisor, Dr. S.J. Kubina for his assistance and constant support, but most of all for his wonderful attitude. I would like to thank Dr. C.W. Trueman for reviewing the first draft of this thesis. His guidance and useful discussions were very much appreciated.

I am grateful to Miss Iona Farrell for making the PDP-11/45 readily available. Many thanks to my friend Michael Marak for his help in maintaining the PDP-11/20. I wish to thank Concordia's Computer Centre for the use of the university's CDC computer.

The radiation pattern measurements described in this thesis were a joint NRCC/Concordia measurements project arranged with Dr. J.Y. Wong and carried out with the co-operation of Mr. W. Lavrench and with the collaboration of Mr. J. Hazell. The author extends his sincere thanks for this successful team effort.

The work described in this project was funded partially by NSERC Grant No. A9340 and DREO/DSS Contract No. 2SU80-00136. Messrs. Ken Peebles and Prakash Bhartia, Ph.D. served as

Technical Authorities for the D.R.E.O. contract. Their support and encouragement are gratefully acknowledged.

I wish to thank Miss Pamela Fox and Miss Janice Robinson for their help in typing and reproducing this thesis.

TABLE OF CONTENTS

GLOSSARY OF TERMS

E_θ : Far field vertical polarization, measured or computed.
E_ϕ : Far-field horizontal polarization, measured or computed.
P_r : Power radiated by the helicopter antenna.
P_{av} : Average power radiated by an isotropic antenna.
H/V : 20 log(E_ϕ max / E_θ max).
η_p : Radiation pattern efficiency.
$\%E_\theta$: Relative power contained in E_θ.
$\%E_\theta^*$: Useful power contained in E_θ.

TRN11 : Simple wire grid model of the Sea-King helicopter.
TRN18 : Modified version of the TRN11 model.
TRN30 : Intermediate wire grid model of the Sea-King helicopter.
TRN40 : Complex wire grid model of the Sea-King helicopter.

NEC : Numerical Electromagnetic Code.
ISOLEV : Program to calculate the isotropic level.
WAP : Wire Analysis Program.
MODEL : Model display program.
MODDIS : Model display program.
CDDP : Current Distribution Display Program.
IDIS : Current display program.
PATCMP : Radiation pattern display program.
SURPAT : Surface plot program.

CHAPTER 1

INTRODUCTION

1.1 Purpose of the Work

When designing an aircraft antenna many factors are taken into consideration. The aircraft is comparable to one wavelength at the lower end of the HF band, and so the metallic skin of the aircraft presents paths to the RF current which can be resonant in the HF frequency range. The antenna and the airframe act together as a radiator, and the behaviour of the antenna must be analyzed by including the effect of the RF current on the body of the aircraft. In addition, when the aircraft is a helicopter, the rotor blade motion introduces amplitude modulation onto the RF signal by presenting a path for the induced RF currents which changes in geometrical configuration at the frequency of rotation of the blades. This also causes a variation in the antenna impedance. The effect of rotor blade modulation can be assessed by techniques presented in this thesis.

An aerospace vehicle may have many antennas mounted on it. Each serves a different application. Frequencies can range from the LF to the VHF band. Helicopter HF antennas are required to radiate maximum far field in the vertical polarization. In this

thesis it is shown that the HF wire antenna presently used on the Canadian Sea-King "CHSS-2" helicopter does not satisfy this requirement. Loop antennas are considered here as a possible replacement for the wire antenna. Such a loop strongly couples to the airframe and is physically easier to install. Chapter 2 describes a specific design of loop antenna called "Tranline"*. This is a shunt-type antenna using a shorted transmission line to excite RF currents on the helicopter itself. Due to its inductive impedance, a loop or Tranline antenna has a 90% coupler efficiency at the lower end of the HF band, whereas the coupler efficiency of a wire antenna is about 20%. This enables a loop antenna to transmit 4 times more power than the wire antenna for a given input power. The loop therefore has significant advantage over the wire antenna.

The work in this thesis consists of closely related antenna measurements and numerical modelling analysis. In Chapter 2 and 3, scale model measurements are reported on the full set of radiation patterns for the Tranline antenna on the CHSS-2 Sea-King helicopter over the full HF frequency band. The antenna performance as derived from these radiation patterns is evaluated in Chapter 3. This evaluation includes a description of the "assessment parameters", as well as a comparison of the Tranline antenna with the wire antenna and other HF antennas. Chapter 4 presents the theoretical basis of the computer program which is used to model aircraft. The program determines the RF

---

* Proprietory item: Cincinnati Electronics Corp.

currents flowing on an antenna consisting of interconnected electrically "thin" wires, based on the fundamental integral equation giving the RF current and the surface electric field. Its solution by numerical techniques using the "moment method" is presented. The "wire-grid" modelling technique represents the helicopter with a grid of thin wires. The special software developed for the evaluation of the antenna's radiation patterns and of the RF current distribution is described. This integrated package of hardware and software makes possible the effective computer-aided analysis of the design and evaluation of aircraft antennas. Chapter 5 presents the wire-grid analysis of the HF antenna for the Sea-King helicopter. Three wire-grid models of the Sea-King are studied, namely the simple, the intermediate and the complex model. Parametric studies of the wire radius and of the position of the Tranline antenna are presented. The resonant behaviour of the helicopter is examined using the complex model. A study of the effect of the antenna location is then considered using the complex wire-grid model of the Sea-King helicopter. Several locations of the Tranline antenna are evaluated and suggestions of an optimized location are made.

In summary this thesis presents a complete radiation pattern analysis of the "Tranline" loop antenna using both scale model measurements and computer modelling techniques, and concluding that the performance of a loop antenna is significantly better than that of the wire antenna presently used.

1.2 Previous Work

The Sea-King helicopter has been in service for many years now. Radiation patterns of different HF antennas were previously measured on this helicopter. The following is a brief history of the radiation patterns, measurements, numerical techniques and evaluation methods as related to the Sea-King helicopter.

1.2.1 Measurements

It has become a common practice to use scale model techniques when measuring HF antenna radiation patterns on an aircraft [1]. This eliminates the very costly pattern measurements on a full scale aircraft. A description of scale model measurement techniques is included in Chapter 2. Radiation patterns of various HF antennas on scale models of the Sea-King helicopter have been previously reported. In 1964, radiation patterns of five wire antennas installed on a scale model of the Sea-King helicopter were measured at Canadair [2]. Pattern modulation due to the rotor blade position was measured in 1965 on one of these five wire antennas, at the National Research Council (NRC), Ottawa [3]. In 1967 pattern measurements of a tuned monopole antenna, mounted on the Sea-King helicopter were reported at an AGARD conference [4]. It was found then that the usual aircraft HF antenna systems do not satisfy the requirements for a helicopter communication system, and it was observed that a monopole antenna might be superior. In 1978 the

Department of National Defence (DND), Ottawa, had occasion to evaluate a trial installation of a Tranline antenna on the Sea-King helicopter. Limited full scale model radiation patterns were measured at that time [5]. In 1979, radiation patterns of an HF loop antenna were done in England using a scale model of the Sea-King helicopter [6]. A complete set of a scale model radiation patterns of the Sea-King/Tranline combination were measured by the author in 1980 at NRC [7]. These measured patterns of the Tranline antenna are the experimental basis for the work in this thesis. They are presented in detail in Chapters 2 and 3.

1.2.2 Numerical Techniques

Extensive measurements of radiation patterns as a function of, say, antenna location over the whole band, is very difficult, costly and time consuming. Measurements of RF current is so difficult that it is rarely done. Computer models do not do away with the need for some measurements of radiation patterns, because as will be seen in this thesis, a set of measured patterns is essential for the validation of the computer model. But a validated computer model provides information that is only available with much difficulty by direct measurements. Thus the computer model reveals the RF current on each part of the aircraft and this current provides insight into resonance modes on the airframe, and also it is possible to associate specific features of the radiation with strong currents on specific parts of the aircraft. In addition,

a validated computer model can be used for studies such as the effect of the position of the antenna, or its length or its spacing from the fuselage, on the radiation patterns over the whole frequency band.

The available computer modelling methods either approximate a surface by flat "facets" or "patches", either rectangular or triangular in shape and solve for the two components of surface current on each facet, or represent the surface by an "equivalent" grid of "thin wires" and find the current flowing on each wire. In each case electromagnetic theory is used to formulate an integral equation which states the boundary condition at the surface, and then the "moment method" is used to convert the integral equation into a matrix equation solvable for the complex currents on the patches or wires. The procedure is summarized in Chapter 4 of this thesis.

The wire-grid modelling technique was introduced by Richmond in 1966 [8]. Since then complex structures such as aircraft and helicopters have been the subject of ongoing investigation using this technique. Miller and Maxum (1970) [9] model communication antennas on the OH-6A helicopter using a wire-grid model with about 200 RF current unknowns, to predict radiation patterns at the low end of the 30 to 70 MHZ band. Kubina (1972) [10] has developed a wire-grid model for the Bell 47G-4A helicopter using 250 unknowns. J.I.R. Owen (1977) [11] has modelled the Sea-King helicopter using a complex wire-grid model using 340 unknowns. This model is used to predict the

radiation patterns of loop antennas located at various positions on the helicopter. This model is described and used in Chapter 5 of this thesis.

Early studies implied that accurate results could only be obtained by increasing the complexity of the wire-grid model [12]. However systematic parametric studies can produce good results using a simple stick model [13]. Miller et al (1974) [14] models the Boeing 747 aircraft at 1.8 and 6.0MHZ with a tail cap antenna using a simple stick model. Trueman (1979) [15] uses the stick model approach to model HF antennas on the CL-28 Argus aircraft, using his wire antenna analysis program "WG3". In Section 5.2 of this thesis a stick model of the Sea-King helicopter is used to predict the radiation characteristics of the Tranline antenna from 2.6 to 6MHZ.

1.2.3 Evaluation

In choosing among several antennas for a given application on an aerospace vehicle, each possible antenna system may meet the requirements well in some sense but be very far from the ideal in other aspects of performance. For example, a given antenna might have satisfactory coverage in its radiation patterns and very low overall efficiency because of poor impedance characteristics. In practice coverage of an HF aircraft antenna deviates so far from ideal that no obvious advantage can be seen by inspecting the radiation patterns of one antenna over another, and so quantitative "assessment

parameters" are needed to compare such antennas.

Quantitative evaluation of the performance of an aircraft HF communication antenna assesses the fraction of the total power radiated that is considered useful to the receiver. The angular sector in which this useful power is contained is defined as ±30 degrees from the horizon. This useful power has become a standard in the military specification of reference [16] for aircraft liaison antennas. Chapter 3 discusses assessment parameters which are derived from the full set of conical patterns for the antenna mounted on the aircraft. One such assessment parameter called "radiation pattern efficiency" was introduced by Granger (1951) [17]. It is defined as the ratio of power radiated in the useful sector to the total power radiated by the antenna. Another assessment parameter considers that only power radiated in the vertical component is useful to the receiver and so compares the total power radiated in E_θ to the total power radiated by the antenna. Such an assessment parameter is usually used to evaluate helicopter antennas for which a maximum vertical component is desired. Kubina (1972) [10] defines a new assessment parameter, which compares the fraction of the power radiated in the vertical component in the useful angle sector 30 degrees from the horizon to the total power radiated by the antenna. Another parameter called "H to V ratio" is used to compare the relative strength of the horizontal and vertical polarization in the azimuth pattern [6]. It is defined as the ratio of the maximum field strength in the horizontal component E_ϕ to the maximum field strength in the

vertical component E_θ .

Previous numerical prediction of radiation patterns did not use such "assessment parameters" to evaluate the overall performance on the aircraft. In this thesis these assessment parameters are the basis of evaluating results obtained by the wire-grid modelling of the aircraft. In addition, interactive computer graphics is used to compare measured and computed radiation patterns. Surface plots of a complete set of conical cuts are used to identify the location of nulls and the sector where maximum radiation occurs.

The above evaluation methods are considered effective when exploring the usefulness of an antenna system for a certain application. They have been used for many years now. Their use in the numerical modelling evaluation is expected to provide a new, useful and reliable tool.

1.3 Importance of the Work

The ideal performance or "performance criterion" for an HF helicopter antenna is identified in this work. The actual performance for practical antenna design is evaluated and compared with the "performance criteria" using a number of "assessment parameters" which are defined in Chapter 3. In this thesis, these parameters are derived from the complete set of measured or computed conical patterns using a numerical integration over the angle sector containing these patterns [18], as given in Chapter 3. This work reports the first

complete set of measured radiation patterns for the Tranline antenna on the Sea-King helicopter [7]. These patterns allow a detailed investigation of the radiation characteristics of this type of HF antenna using the "assessment parameters". Also, the performance of this antenna is compared with others of similar type using this technique.

The "assessment parameters" have been used in Chapter 5 in the development and validation of computer models for the Sea-King helicopter and the Tranline antenna. The assessment parameters are derived from the computer model's patterns, and are compared to those obtained from the measured patterns. This new method of evaluating numerical models is effective, and it does not overwhelm the antenna engineer with the task of comparing a huge number of conical patterns, when in fact one set of such patterns has no obvious advantage over another set. For a simple model, these assessment parameters are used to quantify the changes in the patterns that come about as a function of parameters such as wire radius, number of current unknowns or the antenna locations.

A detailed model, including a true "wire-grid" representation of the surface of the helicopter is called a "complex model". Such a model is used to study the resonant behaviour of the helicopter/antenna combination in Chapter 5. The model can be tuned by varying the length of certain wires on it. The complex model is flexible in terms of antenna relocation studies. It produces results in which the assessment

parameters are derived for different antenna locations. This provides the designer with information prior to the antenna installation on the actual aircraft.

The importance of this work is identified in the evaluation of the Tranline antenna, and the development and evaluation of computer models using the assessment parameters. Once a computer model has been validated via comparison of the assessment parameters with the measured ones, a set of guidelines can be obtained to carry on studies on resonance behaviour, antenna location, rotor modulation and other factors affecting the performance of the antenna.

CHAPTER 2

MEASUREMENTS OF THE RADIATION PATTERNS OF A TRANLINE ANTENNA

2.1 Introduction

In 1978, the Department of National Defence had occasion to evaluate a trial installation of a "Tranline" antenna on the CHSS-2 Sea-King helicopter, as a possible replacement for the present HF wire antenna. Such a performance evaluation would not be complete without the measurement of the radiation patterns of the Tranline antenna on the helicopter, over the full HF band. This chapter presents these patterns, which were obtained at the National Research Council's antenna range in Ottawa [7], in June 1980.

The antenna measurements were carried out using a 1/24 scale factor, copper-flame-sprayed wooden model of the Sea-King helicopter, equipped with a replica of the Tranline antenna.

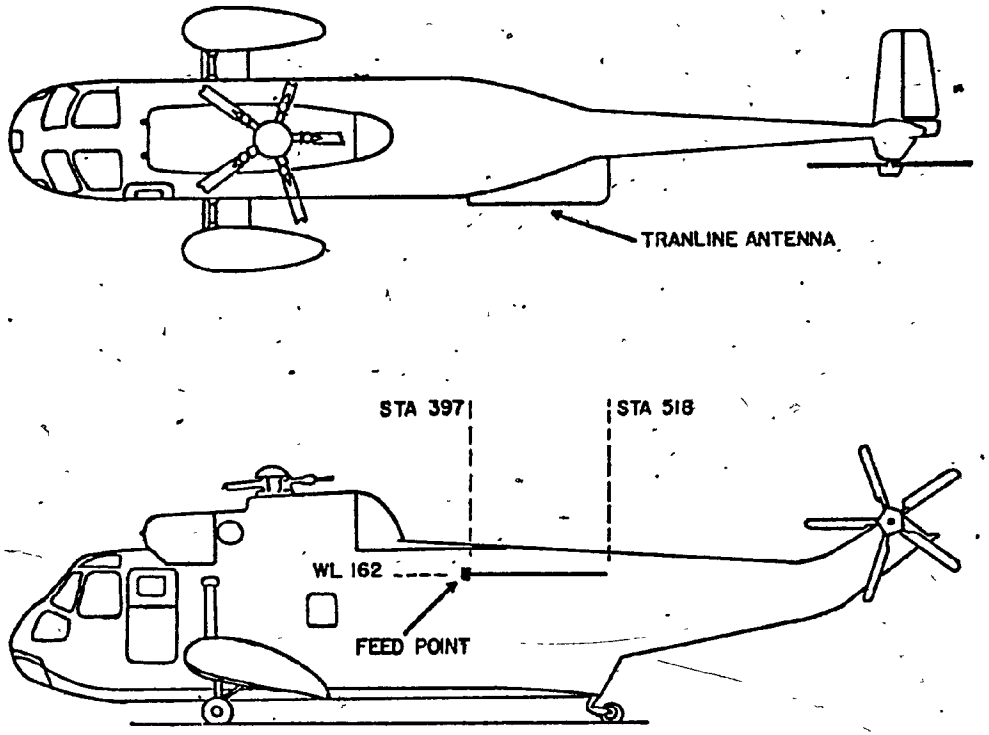

Fig. 2.1 Tranline antenna configuration on the CHSS-2 Sea-King helicopter

As shown in Fig. 2.1, the antenna is located on the port side of the fuselage, with the feed point at "station" 396.5 inches (STA 396.5)*, and "waterline" 162.0 (WL 162.0)**, where the coordinates are defined in Fig. 2.1. The antenna runs aft to STA 517.0 and WL 162.0 . This feed point is identical to that used for the existing wire antenna installation and has been maintained for convenience since the antenna coupler is physically located inside the fuselage at this position. In the following, first the measurement system will be described, and then the problems associated with outdoor ranges are discussed, and finally the radiation pattern requirements are described.

2.2 Components of the Measuring System

The NRC range was developed for the purpose of measuring the radiation patterns of antennas, and is particularly well adapted for measuring the patterns of antennas on scale models of aircraft. It is described in reference [19], and is block-diagrammed in Fig.2.2. The helicopter model is mounted on the tower spindle in order to measure its radiation patterns. The signal originates from a battery-powered oscillator in the model, is radiated by the Tranline antenna, is received by the corner reflector's dipole, and is fed to a receiver, and then to the recorder system. The following describes each of the components of the measuring system.

---

* STA 0.0 is located at the nose of the helicopter.

** WL 0.0 is located at the wheel level of the helicopter.

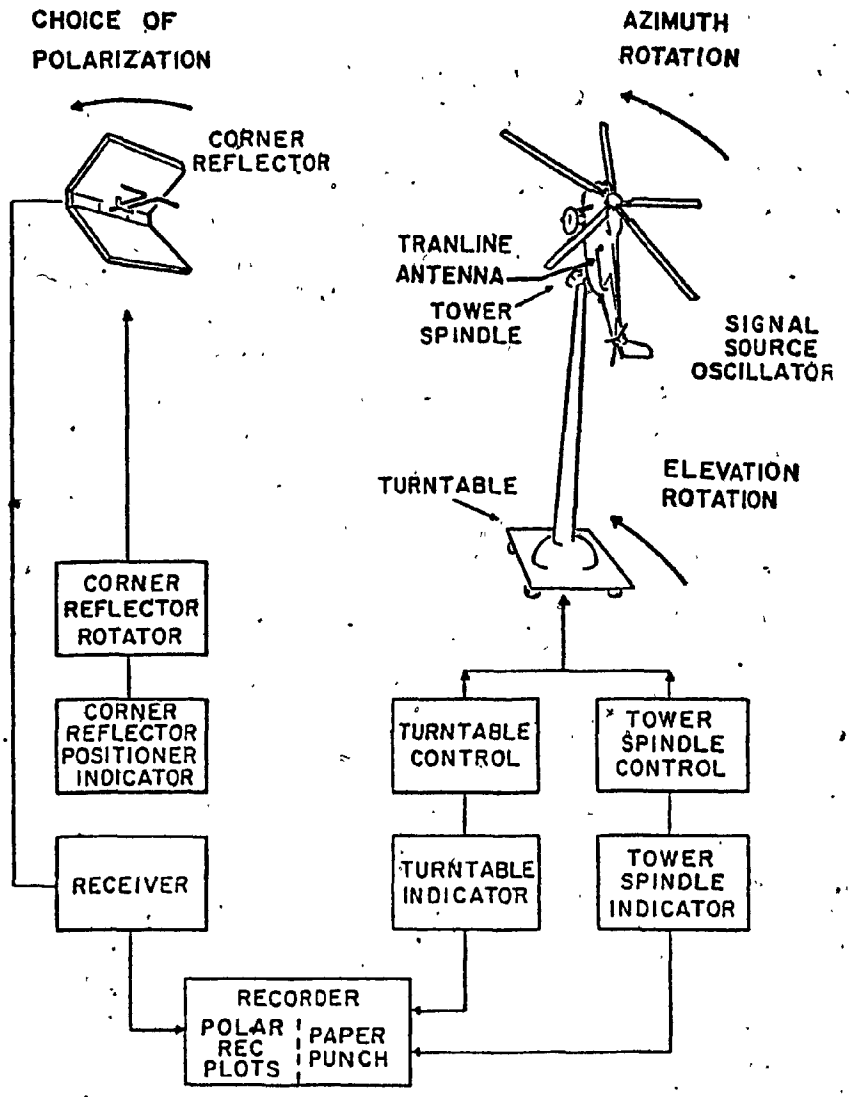

Fig. 2.2 Antenna range block diagram

2.2.1 Transmitting System

In the past, radiation pattern measurments were done using high resistive cable techniques. The resistive cable was used to provide a non-metallic electrical path between the model and the base of the turntable, because a trailing coaxial cable would alter the radiation patterns of the antenna under test. The resistive cable technique is used in the receive mode. A detector is mounted in the model and the cables feed the rectified signal from the model to the recorder. This measurement technique is subject to numerous problems as described in reference [20], such as spurious RF signals induced on the high resistive cable. To overcome these difficulties, a miniature solid state battery-powered oscillator is mounted inside the scale model of the helicopter, and drives the Tranline antenna as a transmitter. To cover several octaves of the full range of the HF band, a series of four oscillators are used. The average size of each unit is approximately 5x2.5x2.5 cm. The unit is fitted inside the helicopter model. These oscillators are frequency-stable to within 0.5 MHz for between one and two hours, after which a minor tuning adjustment is required to compensate for the drop in battery voltage.

2.2.2 Positioning and Control System

There are three segments of the measuring system which are provided with remote control. Fig. 2.2 shows that the corner reflector's position determines the polarization of the field to be measured. The turntable permits the helicopter model to be

rotated around its elevation axis, whereas the tower spindle supplies the azimuth rotation of the model. Each of these functions is controlled using a synchro arrangement, as shown in the block diagram of Fig.2.3. The positioner control unit controls the angle of rotation of the corner reflector, and controls the elevation angle of the turntable, and the azimuth angle of the tower spindle rotator. The position angles of each is fed back to an indicator unit, and then fed via a suitable switching network to either a polar or rectangular recorder, and also to the paper tape punch, which provides a record in digital form, as described below.

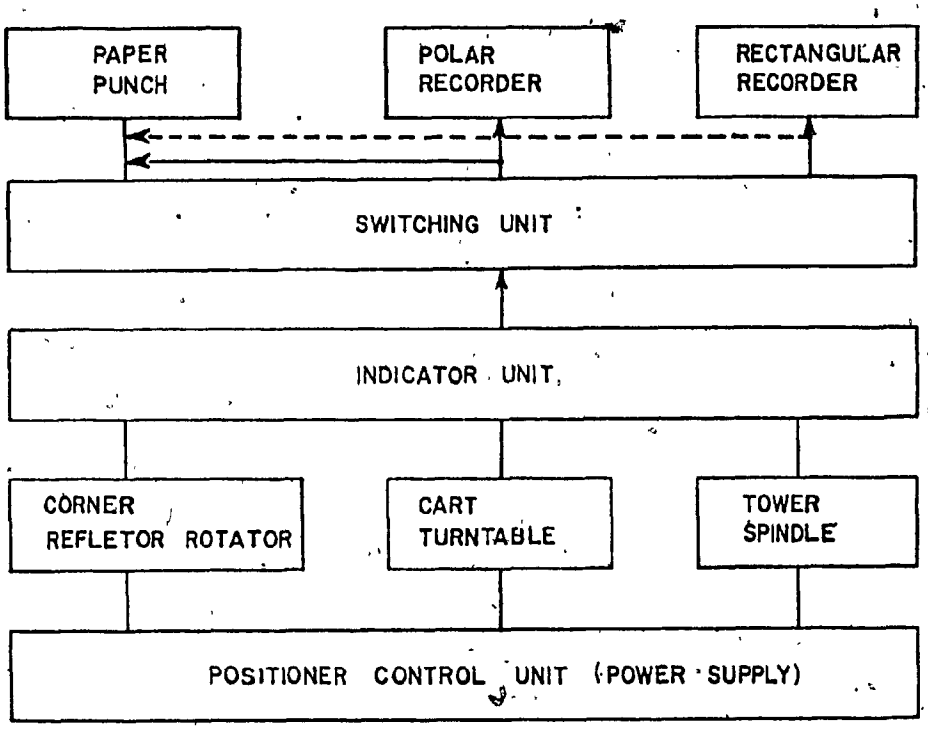

Fig. 2.3 Synchro arrangement used to control the measuring system.

2.2.3 Receiving System

The receiving antenna consists of a dipole mounted in a corner reflector as shown in Fig 2.2. The arrangement provides an antenna which is somewhat directional, over a wide bandwidth. The dipole is a removable one, so that a suitable dipole can be used for each range of frequency. The corner reflector's beam points toward the tower spindle, so that the helicopter model is uniformly illuminated, and a maximum direct signal can be detected from the antenna. The corner reflector antenna feeds a Scientific Atlanta (S.A.) "Precision Amplitude Receiver" Model Number 1742, which detects the radio frequency (RF) signal and supplies an audio frequency voltage proportional to the received RF signal strength. The audio signal is then fed to the recording system, which is described next.

2.2.4 Antenna Pattern Recorder

The radiation pattern is recorded in relative amplitude as a function of angular position, on an S.A. polar recorder series APR 20/30. The recorder's angular position is synchronised to either the azimuth or elevation rotation of the model, via the switching network. The pattern can be recorded on a logarithmic (dB) or a linear scale as desired. For the Tranline antenna measurements, a logarithmic plot is used. The

field strength value in decibels is punched simultaneously onto a paper tape using an S.A. "Radiation Distribution Printer" series 1800 [7]. The paper tapes are recorded in a binary format as described in reference [24]. A program was written by the author [18], to convert the tape records into ASCII code, and to store them as an RK05 disc file on Concordia University's PDP-11/20 "MIDAS" minicomputer system. In this way a digital "data base" of measured patterns is assembled. This "data base" is used effectively later in this thesis for direct comparison with analytical/numerical modelling, using computer graphics. Also, an isotropic reference level and other HF antenna performance criteria, such as radiation pattern efficiency, are readily computed, as described in Chapter 3.

2.2.5 Range Siting Consideration

On an outdoor or "open" antenna range, there are usually surfaces such as ground or nearby structures which give rise to reflected waves arriving at the receiving antenna. The primary reflection is from the range's ground plane surface, and in the present measurements this was minimized by using diffraction fences and low frequency absorber. The fences consisted of wooden frames, approximately six feet by four feet in height, covered with a metallic mesh screen with mesh size less than 0.1 wavelength. Different ideas are presented in the literature [21-23] concerning the proper placement of the fences. It is recommended that a trial-and-error study be used

for the required number of fences and their position. The range's surface is surveyed so as to determine the points of specular reflection, at various frequencies. The survey is done by sliding a one meter square metallic sheet over the flat range's surface, to provide a strong signal reflection from a small area, and observing the variation in the detected signal at the receiver. A location of the metal sheet which causes a large change in the received signal strength is a specular reflection point and hence the required location for a fence. The absorber sheets were composed of rubberized lossy fiber, and were two feet square by one foot thick. This material is listed by the manufacturer as attenuating the reflected wave by 20 dB, at frequencies between 0.3 and 40 GHz. Fig 2.4 shows a typical absorber configuration.

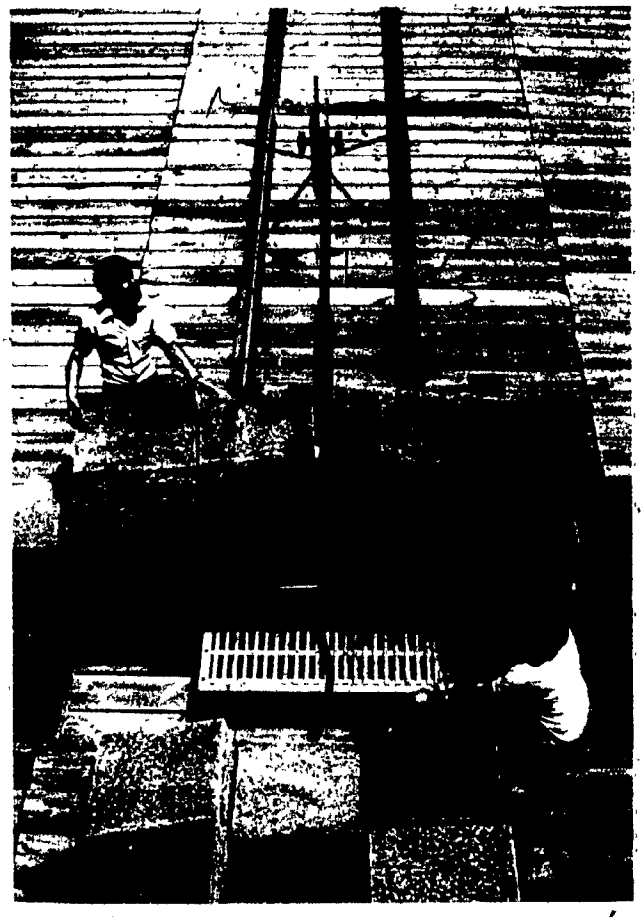

Fig. 2.4 Model tower typical absorber placement.

Additional reflection suppression was achieved by varying the path length between the helicopter and the receiving dipole, keeping in mind the far field distance requirements. Fig.2.5 shows the receiving corner reflector and the helicopter model at two different separations from each other. Fig.2.5(a) illustrates the case in which the direct wave is received by the main lobe whereas the reflected wave is received by either a null or a side lobe of the receiving corner reflector, thereby reducing the effects of the wave reflected off the range's surface. Fig. 2.5(b) shows the direct and reflected waves being received by the main lobe of the receiving corner reflector. This can introduce an error of more than 10 dB in the radiation pattern, depending on the frequency of operation..

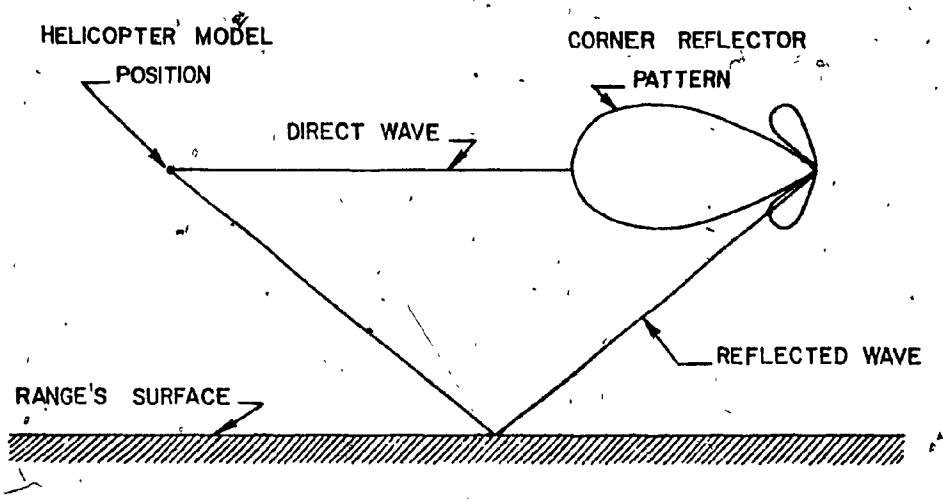

Fig. 2.5(a) Direct wave received by the main lobe of the receiving antenna, whereas the reflected wave is received by the minor lobe.

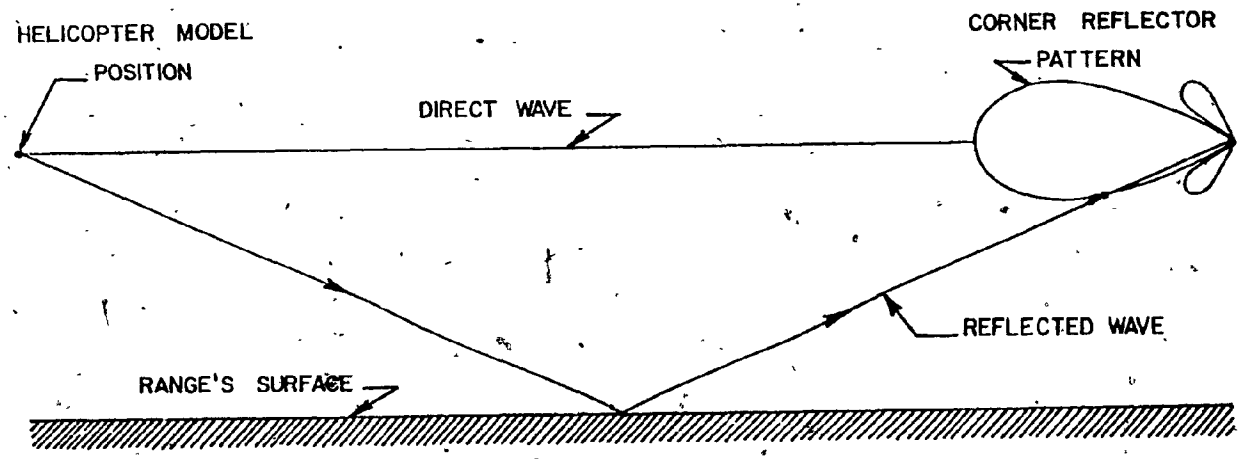

Fig. 2.5(b) Direct and reflected waves are received by the main lobe of the receiving antenna.

This completes the description of the antenna range. The following section describes the set of patterns which were measured on this range for the Tranline antenna on the CHSS-2 helicopter.

2.3 Standard Radiation Pattern Set

The NRC antenna range described above was used to measure radiation patterns in accordance with the military standard MIL-A-9080 (USAF) [16], which has previously been used for the measurements of the patterns of the wire antenna on the CHSS-2 helicopter [2]. The standard specifies the three principal plane patterns to be measured, and also a set of conical cuts to be obtained for the following theta values: 0, 25, 37, 45, 53, 60, 66, 72, 78, 84, 96, 102, 108, 114, 120, 127, 135, 143, 155 and 180 degrees, where theta is defined in Fig. 2.6. These patterns were measured for both E-theta and E-phi polarizations. The measurements were carried out with the rotor blades mainly in the forward position as shown in Fig. 2.7 . The effects of the position of the blades are considered below. The measurements were done over the full HF frequency range, at scale frequencies corresponding to 2.6, 4.1, 6.0, 8.1, 10.0, 12.0, 14.0, 16.0, 18.0, 20.0, 22.0, 24.0, 26.0, 28.0, and 30.0 MHz.

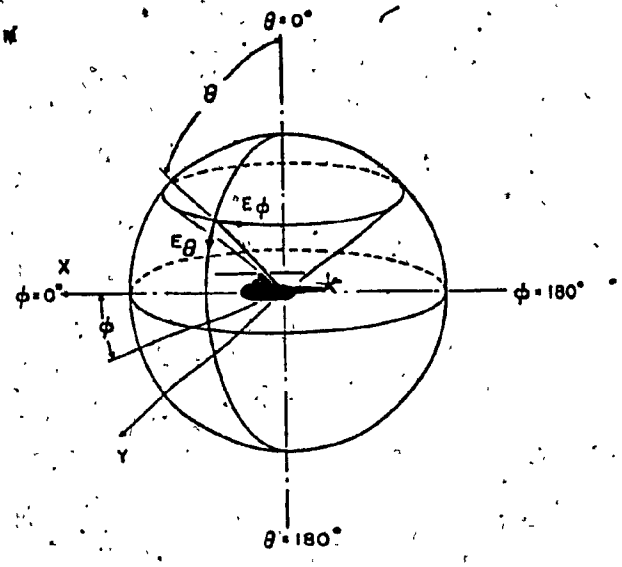

Fig. 2.6 Standard spherical coordinate system used in the measurements.

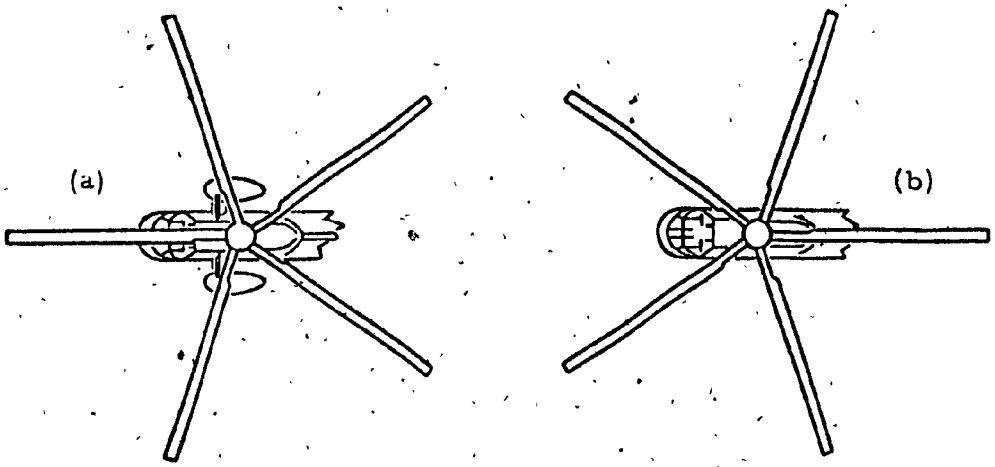

Fig. 2.7 (a) Forward blade position (F-Blade)
(b) backward blade position (B-Blade)

2.4 Summary

This chapter has described the basic components of the NRC antenna range, namely the transmitting system, the positioning and control system, the receiving system and the recording system. The use of a miniature solid state battery-powered oscillator has been most helpful in presenting the helicopter model as a self-contained transmitter, which eliminated the problems associated with other techniques. The use of punched paper tapes of the radiation patterns as a part of the recording system resulted in the construction of an extensive digital "data base", without the need to resort to the tedious process of manual digitization of individual patterns.

In the next chapter, the characteristics and the procedure for the assessment of the radiation patterns of the tranline antenna will be discussed in detail. Techniques are introduced to compute the isotropic level of a set of patterns. A powerful method is introduced for the comparative evaluation of the performance of the Tranline antenna relative to other types of antennas.

CHAPTER 3

EVALUATION OF THE TRANLINE ANTENNA

3.1 Introduction

The assessment of the performance of an HF antenna such as the "Tranline" mounted on a helicopter, is based on the need to excite propagation modes which are effective for communication beyond the line of sight, because the helicopter is normally flown at low altitudes but at distances of up to 350 km from the receiving station. For a highly conductive ground such as sea water, the most suitable mode of propagation uses a ground wave [4]. Because power radiated as a horizontal electric field component is attenuated very rapidly in a ground wave mode [25], the performance of the antenna is optimum when it radiates as much power as possible in the vertical (E-theta) component. The manoeuvers a helicopter usually performs result in attitude changes which make it necessary to maintain good communication over the sector $60 < \theta < 120$ degrees, where theta is defined in Fig 2.6 . Thus in the high ground conductivity case the HF antenna performance is optimum when it radiates as much power as

possible in the vertically polarized component in the sector between $60^\circ < \theta < 120^\circ$ degrees. In the case of inadequate ground conductivity, a skywave mode of propagation dominates. This requires radiation at high elevation angles within ± 30 degrees of the zenith for paths under 350 km in length for frequencies from 2 to 12 MHz [4]. No special emphasis is placed on the polarization to be radiated, because of the polarization rotation in the ionosphere [25]. It will be shown in this chapter that high elevation angle radiation is present with all the HF helicopter antennas that are considered, and so the problem of maximizing the performance of the HF antenna can be defined as that of maximizing the power radiated in the vertically polarized component over the sector $60^\circ < \theta < 120^\circ$ degrees.

In this chapter a number of "performance criteria" or parameters are defined, as aids to the assessment of HF helicopter antenna performance. The Tranline antenna is evaluated, and compared to other HF antennas using these parameters. The effects of the rotor blade position on the Tranline communication system are also considered in a quantitative manner.

3.2 Presentation of Measured Patterns

A full set of 620 patterns for the Tranline antenna was measured on the antenna range described in Chapter 2. These

patterns consisted of the twenty one conical cuts in both polarizations, and two elevation cuts at each frequency as described in Section 2.3. Appendix A gives the three principal plane patterns at fifteen frequencies.

The Tranline antenna of Fig.2.1 with its image in the highly conductive skin of the helicopter constitutes a loop oriented in a horizontal plane and so radiates mainly a horizontally polarized electric field. This is seen in the pricipal plane patterns in Appendix A, where E-phi generally has a higher field strength than E-theta. Fig.3.1. shows the radiation patterns for the theta equals 25 degrees conical cut, at frequencies between 2.6 to 12 MHz. The field strength of these patterns satisfies the requirements for exciting the skywave mode of propagation described in Section 3.1. The coupling of the Tranline antenna to the airframe results in patterns that are more complex than those due to the antenna element alone. It is seen from the principal plane patterns in Appendix A that the patterns of the Tranline antenna change considerably with increasing frequency. The full conical cuts [7] also show that the radiation pattern is dependent on the conical angle (theta) at a given frequency, which makes a direct assessment of the radiation patterns a difficult task. Thus a method is needed which summarizes into a simple parameter the performance of the HF antenna at each frequency, and such parameters are the subject of this chapter.

2.6 MHz

4.1 MHz

6 MHz

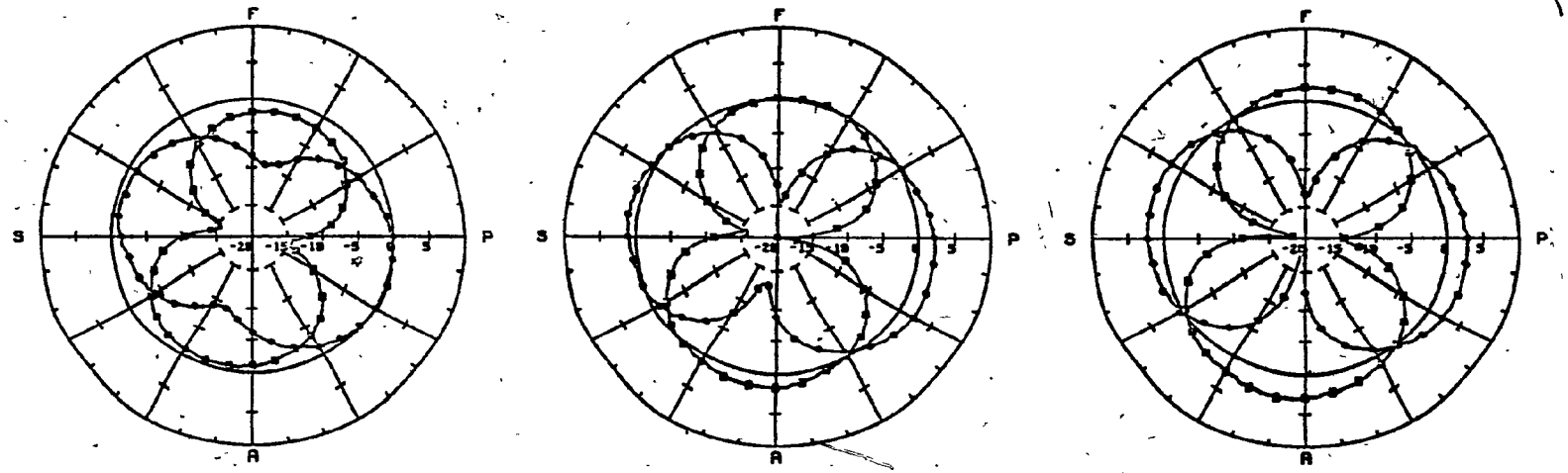

Fig. 3.1 Tranline antenna measured conical patterns (theta = 25 degrees) for both polarizations (E_θ ▫——▫) and (E_ϕ o——o), dB-scale.

8.1 MHz

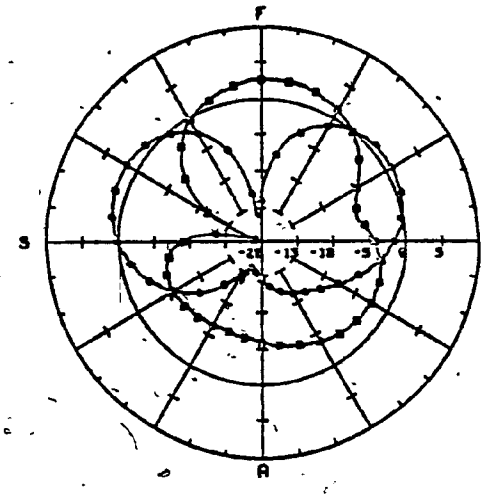

10 MHz

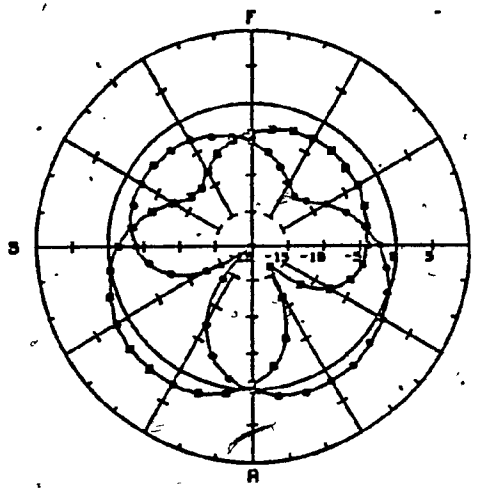

12 MHz

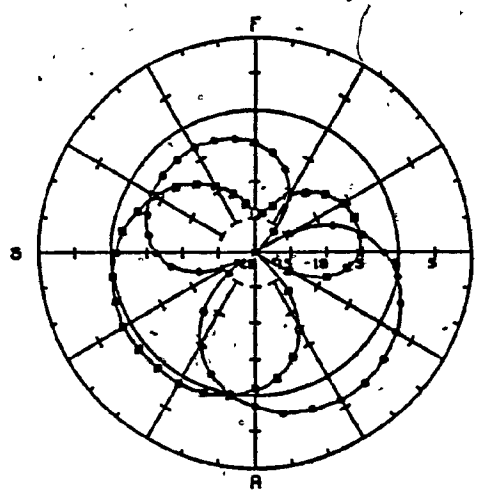

Fig. 3.1 (cont'd)

Tranline antenna measured conical patterns (theta = 25 degrees) for both polarizations (E_θ ▫——▫) and (E_ϕ o——o), dB-scale.

The full set of the twenty one conical patterns for both E-theta and E-phi at each frequency can be used to evaluate the total amount of power radiated by the antenna. Also the power radiated in each polarization over a specified sector of angles can be computed, and the isotropic level can be calculated. The details of these power calculation are given in the next section.

3.3 Radiated Power and Isotropic Level

Most of the performance criteria to be considered in this chapter require a knowledge of the total power radiated by the antenna. This power is obtained by taking the closed surface integral of the average Poynting vector over any surface enclosing the antenna [26].

$$P_r = \oiint \bar{S}_{av} \cdot \bar{ds} \qquad \ldots\ldots\ldots\ldots\ldots (1)$$

where P_r is the total power radiated in watts, $\bar{S}_{av}$ is the average Poynting vector given by

$$\bar{S}_{av} = 1/2 \; Re(\bar{E} \times \bar{H}^*)$$

where $\bar{E}$ and $\bar{H}$ are the peak values of the sinusoids, and ds is a spherical surface element given by

$$ds = r^2 \sin\theta \, d\theta \, d\phi$$

Using a closed sphere centered on the helicopter as a closed surface as defined in Fig 2.6, after some vector manipulation the total power radiated becomes

$$P_r = \frac{1}{2\eta} \int_0^{2\pi} \int_0^{\pi} \left(|E'_\theta|^2 + |E'_\phi|^2 \right) r^2 \sin\theta \, d\theta \, d\phi \quad \ldots\ldots\ldots(2)$$

where E'_θ and E'_ϕ depend inversely on r, and η is the characteristics impedance of the medium, taken here as 120π ohms. By defining $E_\theta = rE'_\theta$ and $E_\phi = rE'_\phi$, Equation (2) becomes

$$P_r = \frac{1}{2\eta} \int_0^{2\pi} \int_0^{\pi} \left(|E_\theta|^2 + |E_\phi|^2 \right) \sin\theta \, d\theta \, d\phi \quad \ldots\ldots\ldots(3)$$

where E_θ and E_ϕ are the field values of the measured patterns. The Power radiated in any sector Ω of theta angles is given by

$$P_r = \frac{1}{2\eta} \int_0^{2\pi} \int_{\Omega} \left(|E_\theta|^2 + |E_\phi|^2 \right) \sin\theta \, d\theta \, d\phi \quad \ldots\ldots\ldots(4)$$

where theta varies over the sector defined to be "Ω".

Once the total power radiated is known, a reference level called the "Isotropic Level" is defined as that field level which would be radiated by an "Isotropic antenna" [26], which radiates only one polarization, equally in all directions and radiates the same total power as the antenna being measured.

The isotropic level is used for a comparison with the actual radiated fields. Thus the actual E_θ pattern is compared with the isotropic level by imagining that the total power were radiated uniformly ("isotropically") into E_θ only. Similarly, the actual radiated E_ϕ is compared with the isotropic level as if the total power was radiated into E_ϕ.

The isotropic level is calculated as follows. For an isotropic antenna the average power radiated is given by Equation (3), where the isotropic level E replaces each E_θ (or E_ϕ) and E_ϕ (or E_θ) is zero. Thus

$$P_{av} = \frac{1}{2\eta} \oiint |E|^2 \, ds \qquad \text{.....(5)}$$

Since the isotropic level is independent of the direction

$$P_{av} = \frac{|E|^2}{2\eta} \oiint ds \qquad \text{.....(6)}$$

where the surface integral is equal to 4π hence

$$P_{av} = \frac{|E|^2}{2\eta} (4\pi) \qquad \text{.....(7)}$$

Assuming that the total power radiated P_r from Equation (3) is equal to the power in the isotropic patterns, E can be calculated as

$$|E| = \left[\frac{1}{4\pi} \int_0^{2\pi} \int_0^{\pi} \left(|E\theta|^2 + |E\phi|^2 \right) \sin\theta \, d\theta \, d\phi \right]^{1/2} \qquad \text{.....(8)}$$

For ready comparison, the isotropic level E has been plotted on the Tranline antenna radiation patterns of Fig 3.1 and Appendix A as a solid circles for comparison.

3.4 Evaluation Methods and Tranline Antenna Performance

This section presents definitions of a number of performance criteria or parameters, and applies these parameters to the Tranline antenna. Each performance criterion is examined to assess the degree to which it reflects the desired antenna performance described Section 3.1. The best parameters are those directly related to the power radiated in the vertical component over the desired sector of angles.

3.4.1 Isotropic Level Method

Although isotropic antennas are not achievable in practice, it is useful to compare the isotropic level obtained in Section 3.3 with the actual antenna patterns. The Tranline antenna patterns can be examined to see how they differ from an omidirectional pattern at the same power level. Wong [27] had introduced a deviation factor based on the pattern degradation when compared to the isotropic level. Another method defined here, is called the "isotropic level method". It uses interactive computer graphics to display a surface plot of

(AZIMUTH PATTERN / ISOTROPIC LEVEL) VS FREQUENCY

Thus the plot in Fig. 3.2 displays the Yaw angle (phi) on one horizontal axis and the frequency on the other, and the relative field strength in either E_θ or E_ϕ on the vertical axis. This method can be viewed as a qualitative evaluation of the "idealness" of the radiation patterns, where the ideal is considered to be a uniform pattern with a field strength higher or equal to the isotropic level. In this method the azimuth pattern is examined at various frequencies, and its amplitude strength is compared to the corresponding isotropic level. This type of evaluation gives the designer a quick appreciation of the pattern directivity as a function of frequency and its system performance ramifications.

In the case of the Tranline antenna, the isotropic level method has been applied to the set of azimuth plane patterns at 15 frequencies included in Appendix A, to produce Fig. 3.2. The vertical polarization of Fig. 3.2(a) shows the azimuth plane pattern at the 15 frequencies. There is a low level of radiation at 2.6, 4.1, and 6.0 MHz. The maximum radiation level occurs at 8.1 and 28 MHz. The pattern becomes more uniform and it has shallower nulls at frequencies higher than 6.0 MHz. Fig. 3.2(b) shows the horizontal polarization. The patterns are butterfly figures at frequencies below 20 MHz, with the main lobes at a higher level than the isotropic level. At frequencies above 20 MHz the horizontal polarization becomes more directional but maintains a high field strength.

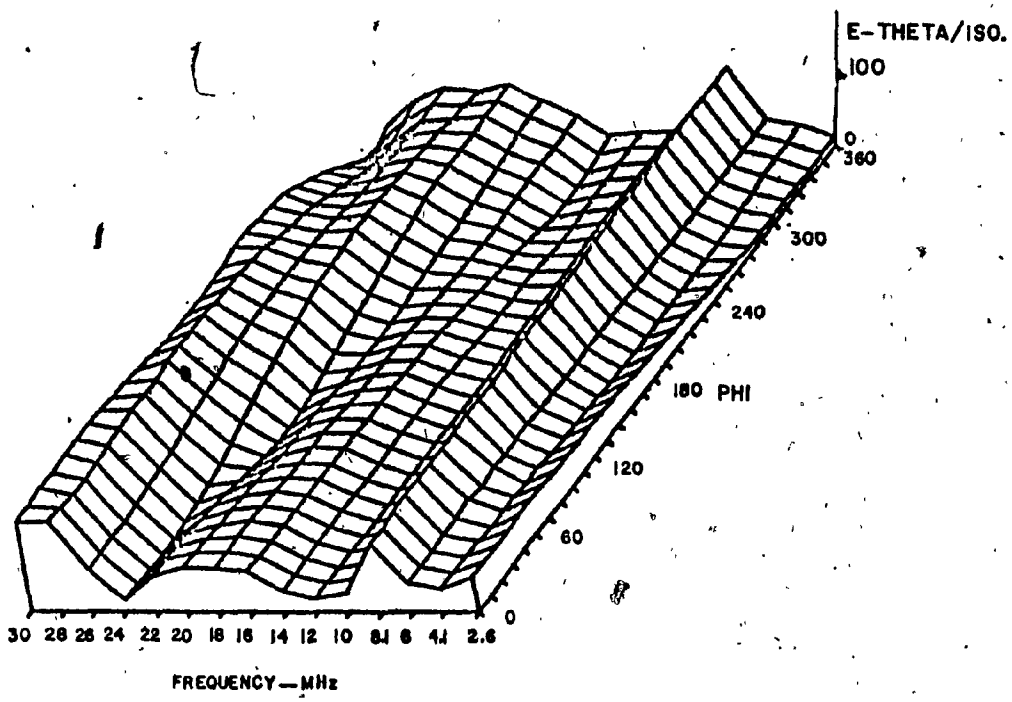

Fig. 3.2(a) Tranline antenna surface plot of the measured E_θ azimuth/isotropic level as a function of frequency

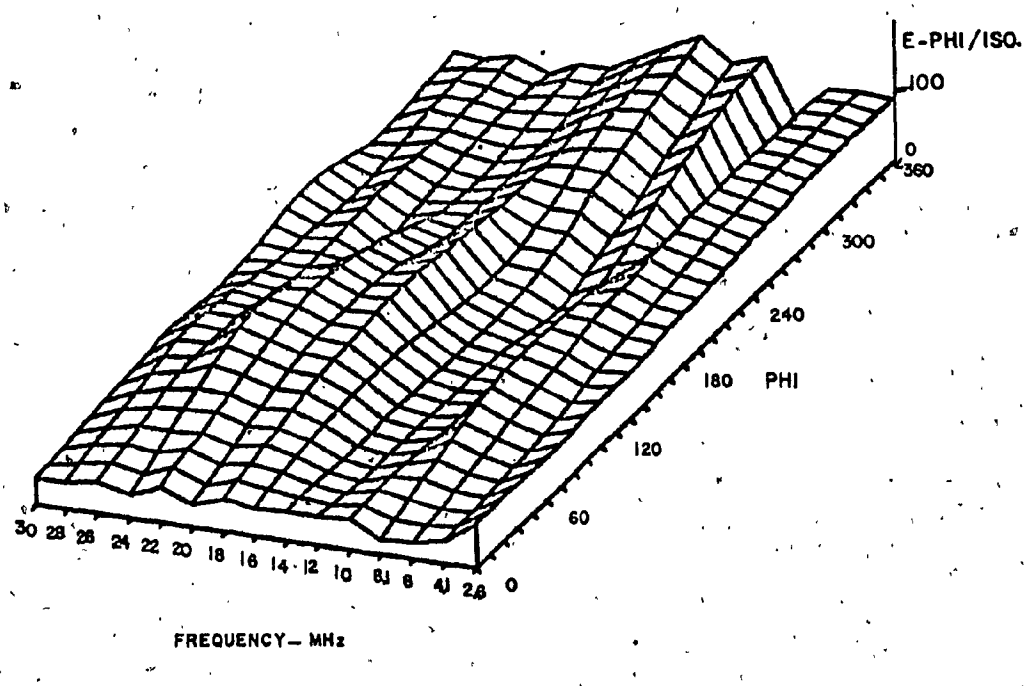

Fig. 3.2(b) Tranline antenna surface plot of the measured E_ϕ azimuth/isotropic level as a function of frequency

The above analysis of the azimuth plane patterns does not conclusively assess the quality of the Tranline antenna radiation patterns. In general these surface plots show that the Tranline antenna radiates a relatively weak vertical component at the lower end of the HF band. A more complete assessment of the Tranline antenna's performance must include information about the radiation patterns over the full $60 < \theta < 120$ degree sector.

3.4.2 H to V Method

In recent studies of HF helicopter antennas at the Royal Aircraft Establishment (RAE), Farnborough, England [28], the ratio of the maximum of the horizontal field component (E_ϕ) to the maximum of the vertical field component (E_θ) or horizontal to vertical ratio (H/V) in the azimuth plane is being used to evaluate the performance of the antenna, where it is preferred that the H/V ratio be very low so it reflects the high vertical radiation.

In order to apply comparative evaluation between the Tranline antenna and other loop antennas measured at Farnborough, later on in this chapter the H/V ratio of the Tranline antenna at different frequencies is plotted in Fig. 3.3 as

$$H/V = 20*\log(E_\phi \text{ max}/E_\theta \text{ max})$$

as a function of frequency. The figure shows that the Tranline antenna radiates a weak vertical component at the lower end of the HF band. Also at 12 MHz the figure shows that the antenna radiates mainly a horizontal component, with an H/V ratio of +20 dB. This is misleading because the full set of Tranline antenna patterns at 12 MHz shown in Fig 3.4 presents an overall stronger vertical component than is suggested by the H/V ratio alone at this frequency. The difficulties arise because H/V ratio is based solely on the azimuth plane pattern. Other performance criteria are presented below which overcome the limitations of the H/V ratio.

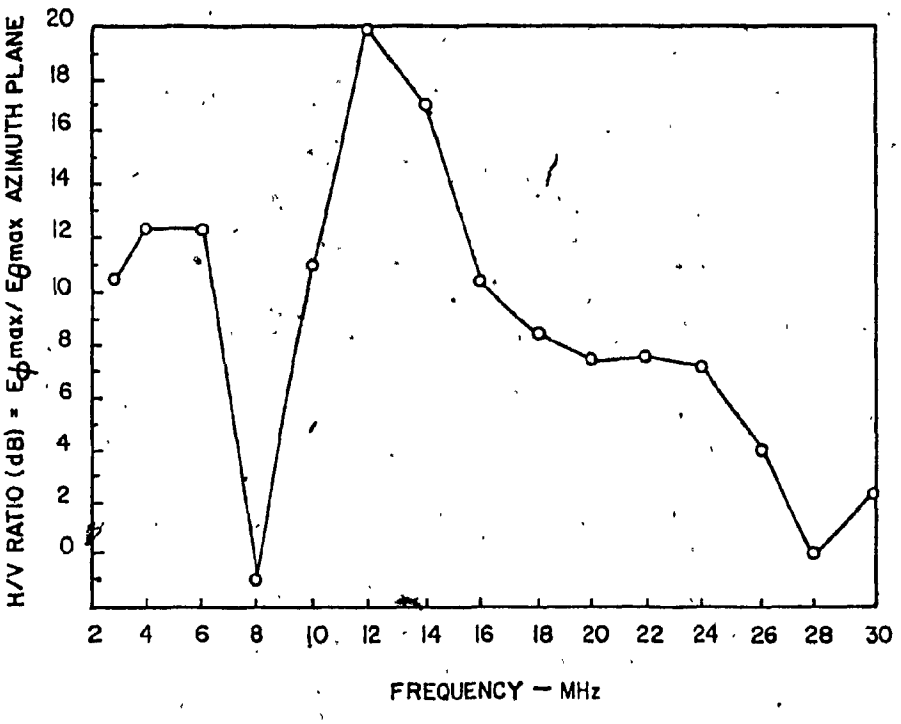

Fig. 3.3 Tranline antenna H/V ratio as a function of frequency

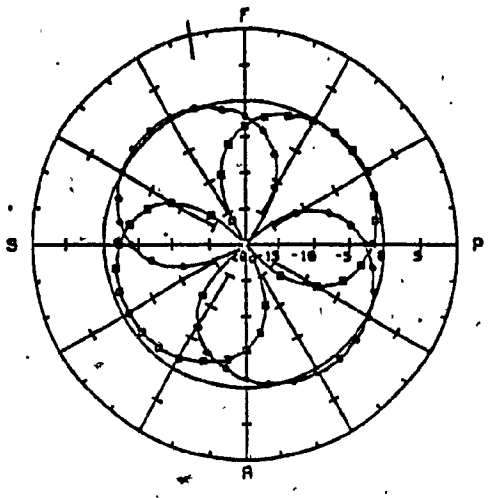

$\theta = 0^0$

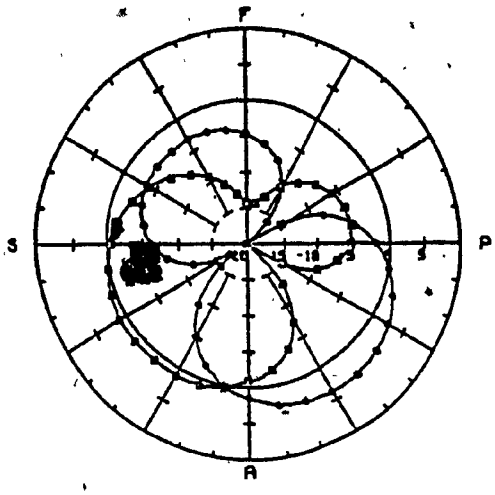

$\theta = 25^0$

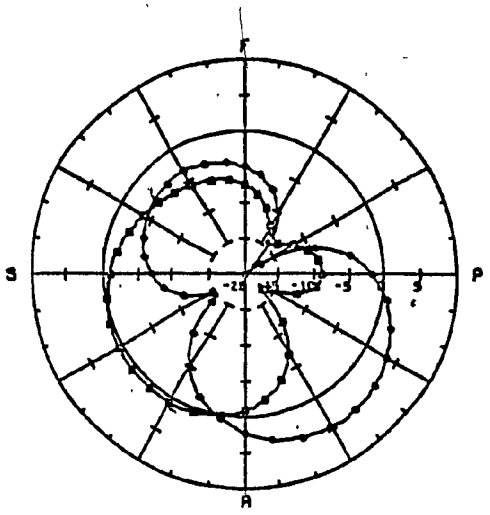

$\theta = 37^0$

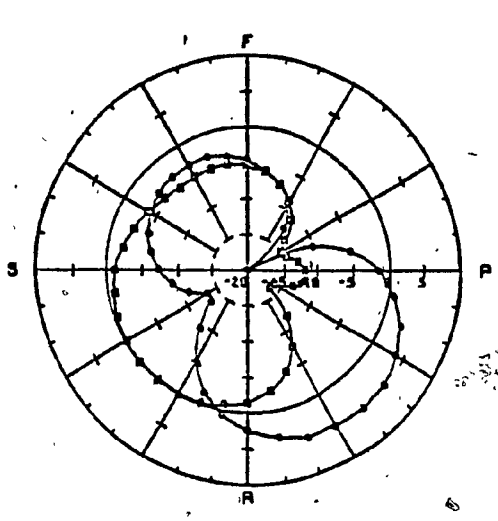

$\theta = 45^0$

Fig. 3.4 Tranline antenna measured conical patterns at 12 MHz for both polarizations, E_θ ⊏——⊐ and E_ϕ ○——○. Isotropic level is indicated as a solid circle, dB-scale.

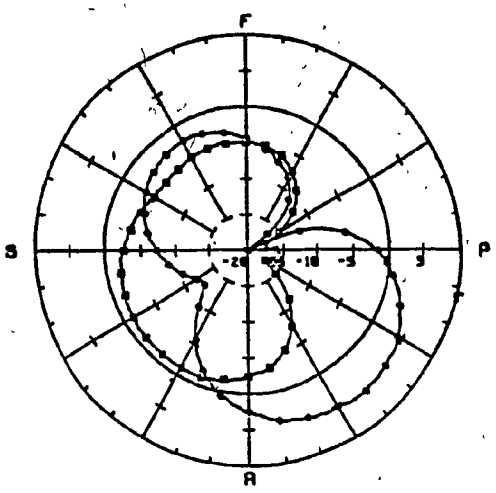

$\theta = 53^0$

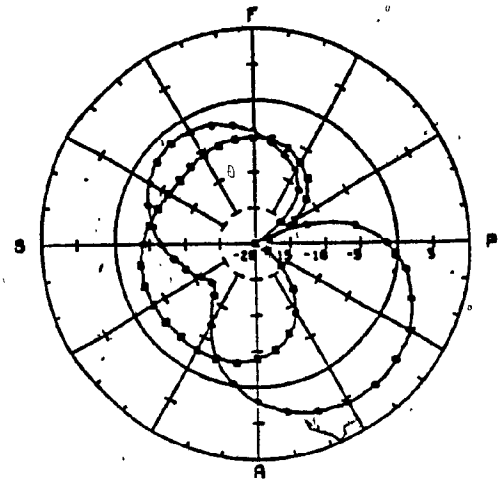

$\theta = 60^0$

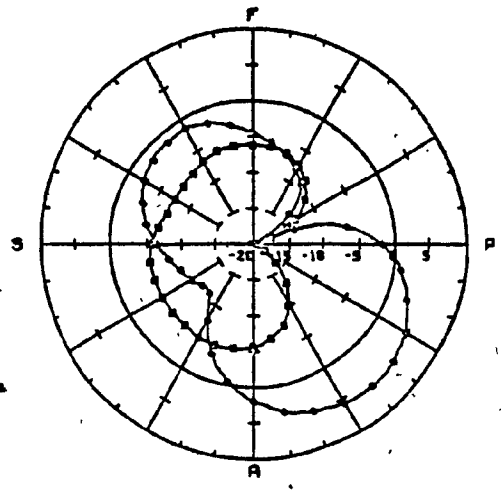

$\theta = 66^0$

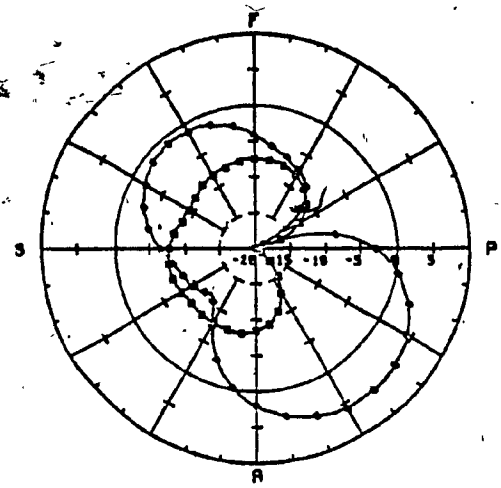

$\theta = 72^0$

Fig. 3.4 (cont'd)

Tranline antenna measured conical patterns at 12 MHz, for both polarizations E_θ ▫——▫ and E_ϕ o——o .
Isotropic level is indicated as a solid circle, dB-scale.

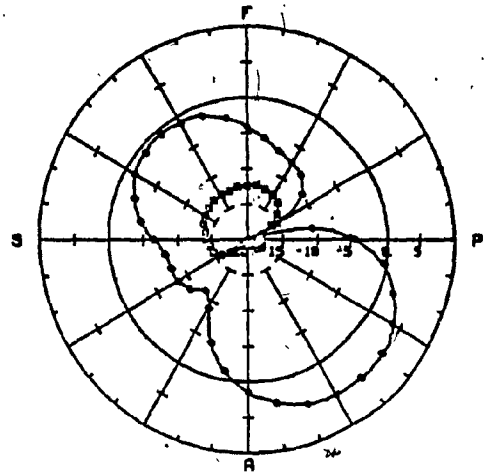

$\theta = 84^{o}$

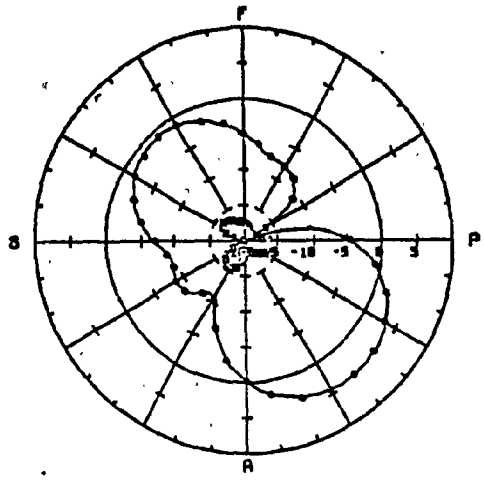

$\theta = 90^{o}$

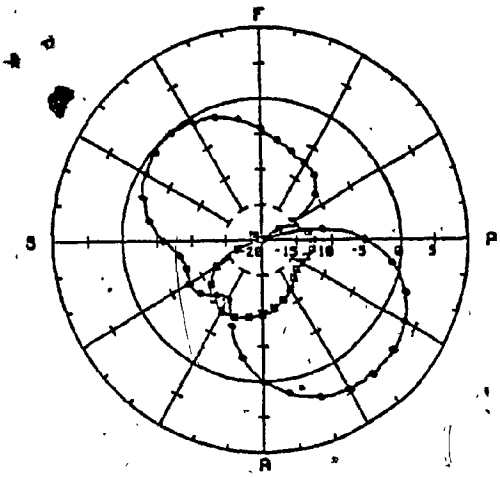

$\theta = 96^{o}$

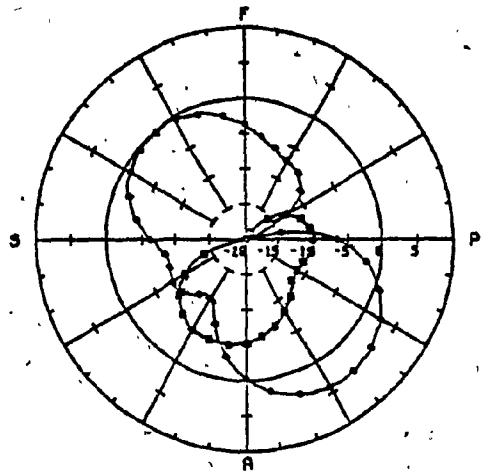

$\theta = 102^{o}$

Fig. 3.4 (cont'd)

Tranline antenna measured conical patterns at 12 MHz for both polarizations E_θ □——□ and E_ϕ o——o. Isotropic level is indicated as a solid circle, dB-scale.

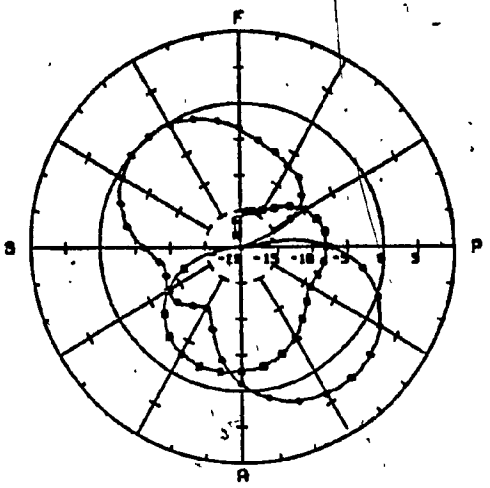

$\theta = 108^{0}$

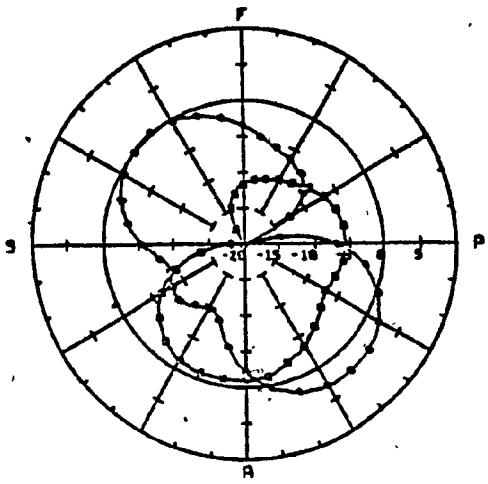

$\theta = 114^{0}$

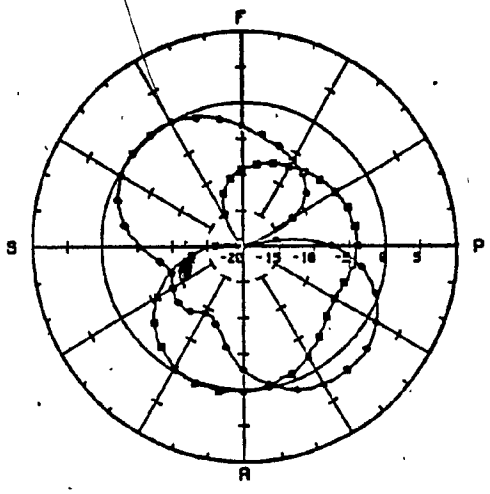

$\theta = 120^{0}$

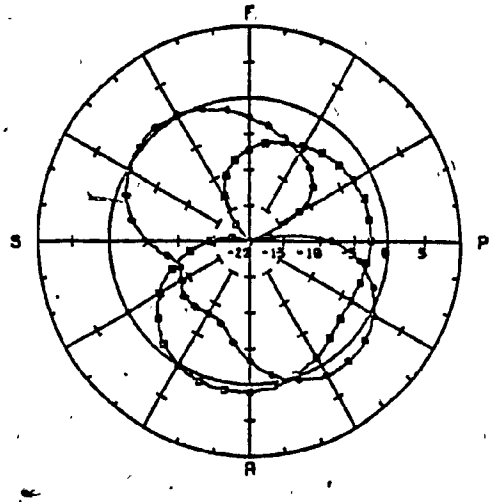

$\theta = 127^{0}$

Fig. 3.4 (cont'd)

Tranline antenna measured conical patterns at 12 MHz for both polarizations E_θ □——□ and E_ϕ o——o .
Isotropic level is indicated as a solid circle, dB-scale.

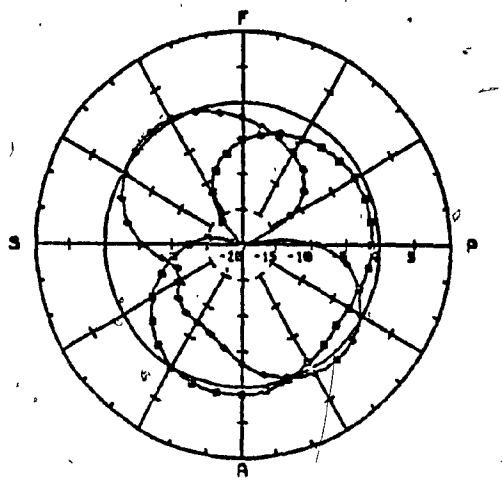

$\theta = 135^{o}$

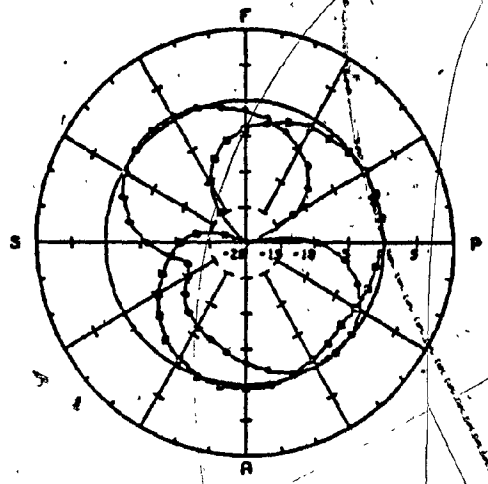

$\theta = 143^{o}$

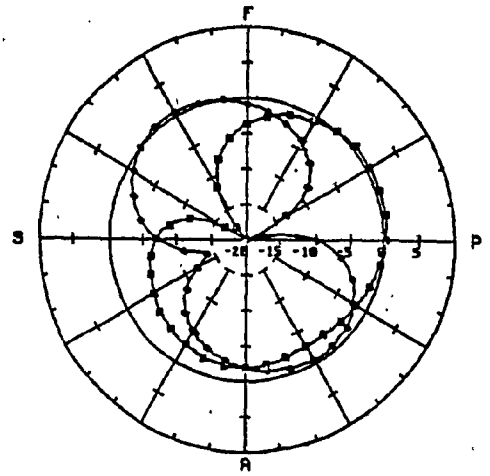

$\theta = 155^{o}$

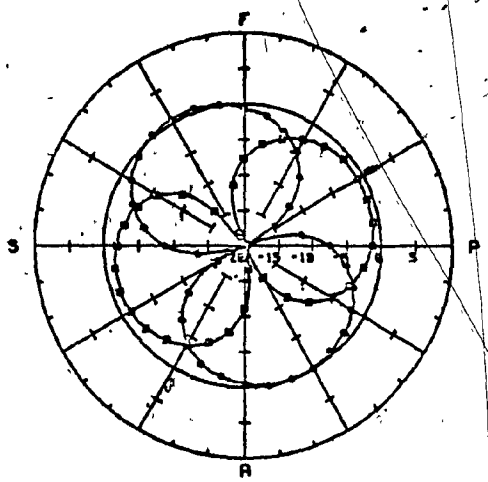

$\theta = 180^{o}$

Fig. 3.4 (cont'd)

Tranline antenna measured conical patterns at 12 MHz, for both polarizations E_θ o——o and E_ϕ o——o .
Isotropic level is indicated as a solid circle, dB-scale.

3.4.3 Radiation Pattern Efficiency

Section 3.1 introduced the requirements for adequate communication from a helicopter using an HF antenna, namely that as much power as possible be radiated in the vertical component in the sector $60 < \theta < 120$ degrees. Granger [17] defined an assessment parameter called radiation pattern efficiency (η_p) which is given by the ratio of the power radiated in both E_θ and E_ϕ in the solid angle between theta equal 60 and theta equal 120 degrees to the total power radiated by the antenna. This can be expressed as

$$\eta_p = \frac{\int_0^{2\pi}\int_{60}^{120}\left(|E_\theta|^2+|E_\phi|^2\right)\sin\theta\, d\theta\, d\phi}{\int_0^{2\pi}\int_0^{\pi}\left(|E_\theta|^2+|E_\phi|^2\right)\sin\theta\, d\theta\, d\phi} \times 100$$

A Fortran program called "ISOLEV" was written by the author and calculates the pattern efficiency from the full set of measured patterns at each frequency for the Tranline antenna. The radiation pattern efficiency is plotted as a function of frequency and is shown in Fig.3.5. The curve varies between 40 and 60 percent, with a maximum at 8.1 and 28 MHz. The minimum level of 40% occurs at 6 MHz. This method examines the relative power radiated in the desired sector, but it places no emphasis on the polarization type, although it is desired that strong radiation in the vertical component be present. Therefore

another parameter is needed which would evaluate the relative power contained in E-theta component.

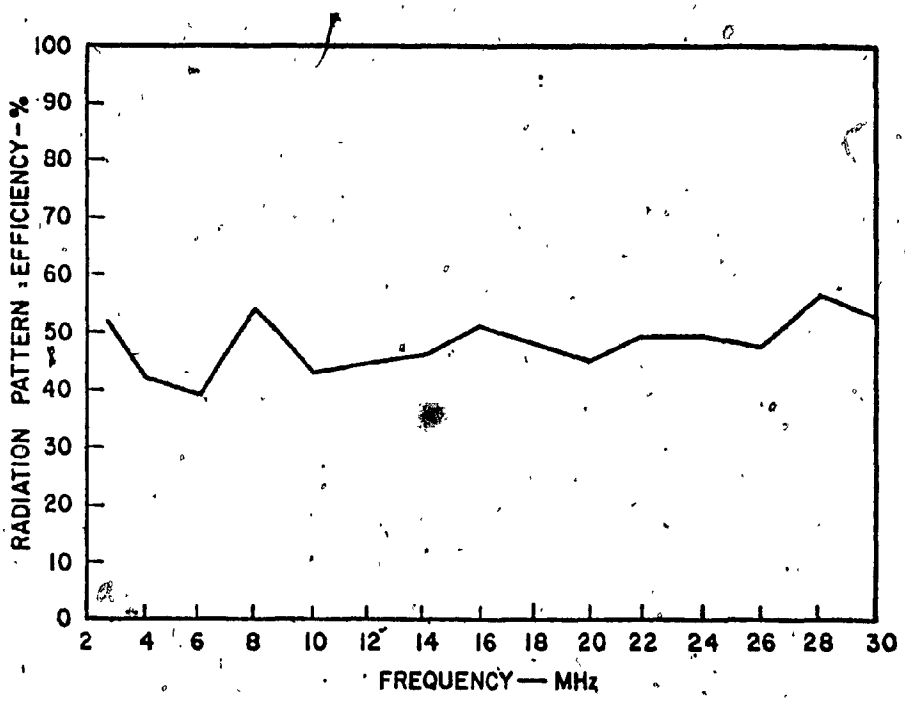

Fig. 3.5 Tranline antenna radiation pattern efficiency (ηp) as a function of frequency, obtained from measured patterns

3.4.4 Relative Power Contained in E-theta

When considering the ground wave mode of propagation, emphasis is put on maximizing the radiated power in the vertical component. Therefore an assessment parameter can be defined [16] as the ratio of the power radiated in the vertical component E_θ to the total power radiated by the antenna, and is denoted by

"percent E-theta" ($\%E_\theta$). This is given by

$$\%E_\theta = \frac{\int_0^{2\pi}\int_0^{\pi} |E_\theta|^2 \sin\theta \, d\theta \, d\phi}{\int_0^{2\pi}\int_0^{\pi} (|E_\theta|^2 + |E_\phi|^2) \sin\theta \, d\theta \, d\phi} \times 100$$

For the Tranline antenna, $\%E_\theta$ is plotted as a function of frequency in Fig. 3.6. The figure shows that the radiation patterns have only about 30% of power radiated into the vertical polarization at the lower end of the HF band, with a peak of about 60% at 8.1 MHz. Above 20 MHz the power radiated in the vertical component rises from about 38% to 60% near 30 MHz, and so at these frequencies the antenna is more effective. The percent E_θ parameter is a meaningful tool in evaluating the HF helicopter antenna performance because it quantifies the power radiated into the desired field component, and allows quantitative comparison among different antenna designs.

A similar parameter to percent E-theta was introduced by Kubina [10] and is defined as the ratio of the power contained in E_θ between theta equal 60 and theta equal 120 degrees to the total power radiated by the antenna, and will be denoted by "useful percent E_θ " or ($\%E_\theta^*$). This given by

$$\%E_\theta^* = \frac{\int_0^{2\pi}\int_{60}^{120} |E_\theta|^2 \sin\theta \, d\theta \, d\phi}{\int_0^{2\pi}\int_0^{\pi} (|E_\theta|^2 + |E_\phi|^2) \sin\theta \, d\theta \, d\phi} \times 100$$

The useful percent E_θ for the Tranline antenna is calculated using the program "ISOLEV" and shown in Fig. 3.7 as a function of frequency. This parameter is especially useful for the evaluation of HF helicopter antennas, because it examines the two requirements: that the radiation be in the vertical component and in the desired sector. The useful percent E_θ graph is quite similar to the percent E_θ graph. A comparison of the two graphs shows that much of the power radiated in the frequency range from 2 to 20 MHz is radiated in the less useful directions, (with the exception of frequencies around 8.1 MHz), because the percent E_θ is about 30% and the useful percent E_θ is only 5%. However at high HF frequencies the useful percent E_θ curve rises to values about 20 percent, and suggests that at these frequencies enough power is radiated into the desired sector in the vertical component. At 12 MHz the useful percent E-theta parameter is 6.5 percent. Thus the power contained in the vertical component in the sector for $60 < \theta < 120$ degrees is about 7 dB below that contained in the horizontal component for the same sector of angles. This is quite different from the 20 dB difference suggested by the H/V ratio parameter. Thus overall the percent E_θ and useful percent E_θ curves show that a large portion of the radiated power of the Tranline antenna goes into the horizontal component, and further that of the power radiated into the vertical component, only very little is radiated into the desired sector.

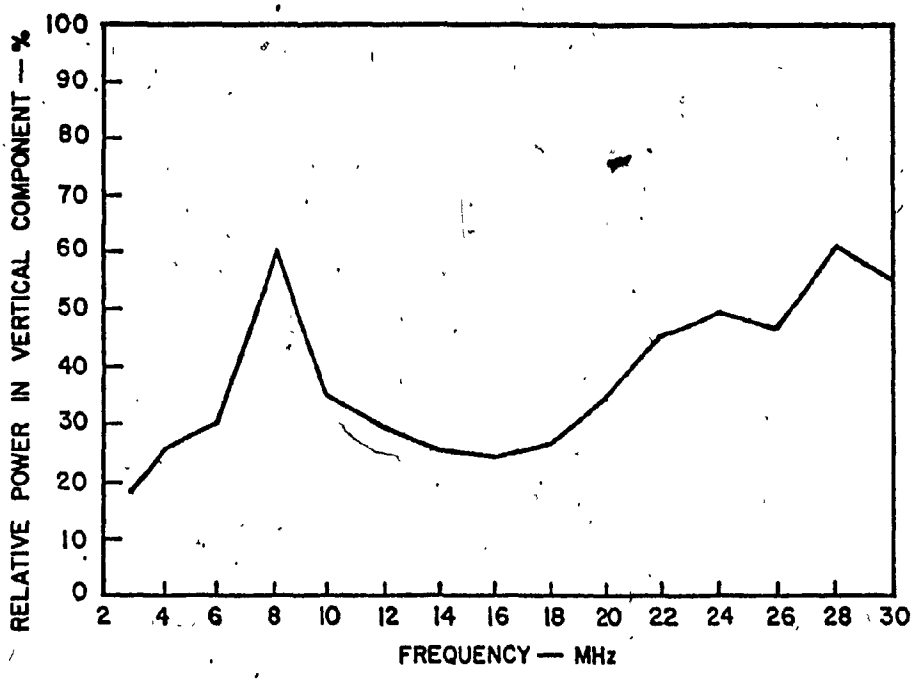

Fig. 3.6 Tranline antenna relative power contained in E_θ ($\%E_\theta$) as function of frequency, obtained from measured patterns

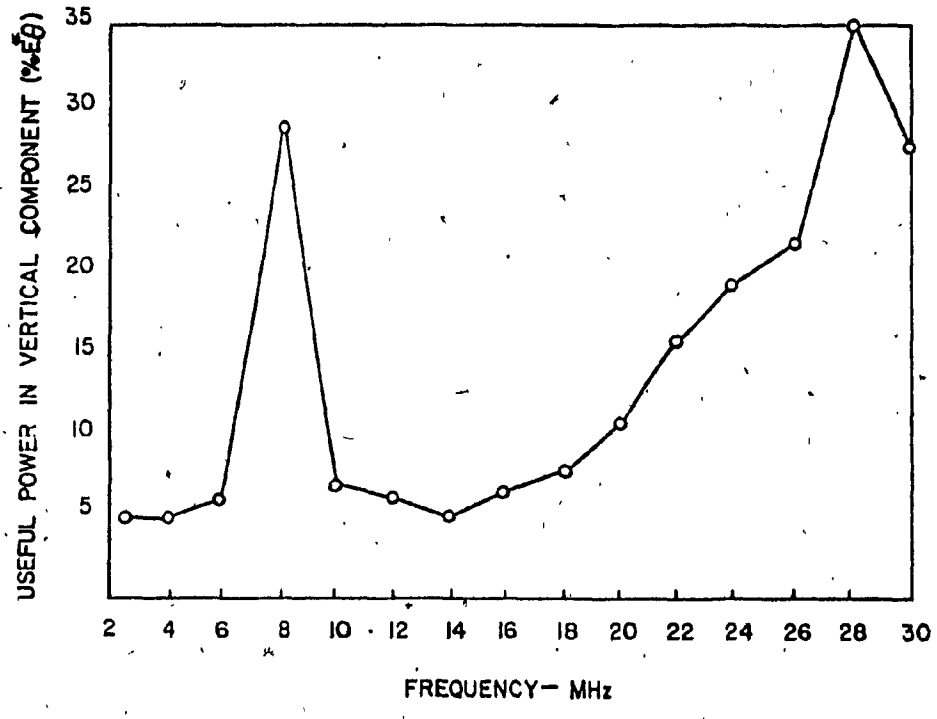

Fig. 3.7 Tranline antenna useful power contained in E_θ ($\%E_\theta^*$) as function of frequency; obtained from measured patterns

3.5 Comparative Evaluation

The Tranline antenna is a possible alternative to the old wire antennas commonly in use, and it is also similar to loop antennas under study at the Royal Aircraft Establishment, Farnborough. In order to assess its performance relative to these antennas, a comparative evaluation is made in this section. The comparison is based on the performance criteria discussed in the previous section and is a quantitative comparison of the relative values of the parameters for the various antennas.

3.5.1 Tranline Antenna VS Wire Antenna

A full set of measured patterns for five wire antennas mounted on the Sea-King model of Fig. 2.1 was obtained in 1964 at Canadair [2]. The location of each antenna is shown in Fig. 3.8, and a relative evaluation of these five antennas was carried out in 1972 by Kubina [10]. It was recommended at the time that wire antenna "E", located at the port side of the helicopter is a suitable choice among the five antennas that were investigated. The evaluation of these wire antennas was based on different performance criteria than those described above. The comparison between the Tranline antenna and the wire antenna "E" will be carried out using the radiation pattern efficiency and the relative power contained in the vertical

component E-theta given by "percent E-theta" and "useful percent E-theta".

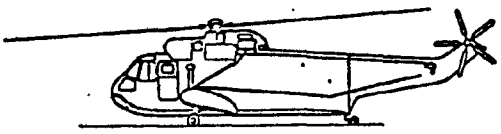

ANTENNA A

Total Length = 46 ft.

	STA	W.L.	Height
FP	343.2	192	---
ST1	310	163	10"
ST2	218	---	10"
ST3	435	---	10"
ST4	625	142	10"

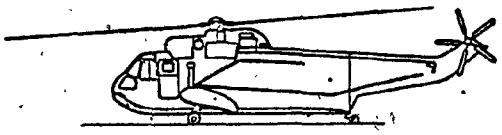

ANTENNAS B AND C

Total Length = 51 ft.

	STA	W.L.	Height	
			B	C
FP	405	162	---	---
ST1	310	163	10"	10"
ST2	218	163	10"	10"
ST3	435	113	10"	21/2'
ST4	625	142	10"	4'

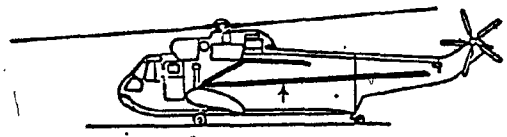

ANTENNA E

Total Length = 51 ft.

	STA	W.L.	Height
FP	405	162	---
ST1	310	163	10"
ST2	237	---	10"
ST3	435	130	21/2'
ST4	625	142	4'

Legend: FP = Feedpoint
ST1 = Stand-off #1 etc.
STA Aircraft coordinates:
W.L. Station, waterline, in inches

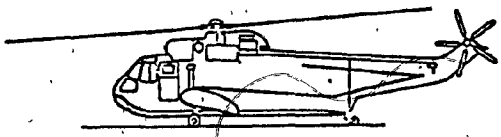

ANTENNA D

Total Length = 53 ft.

	STA	W.L.	Height
FP	405	162	---
ST1	625	142	4'
ST2	435	113	21/2'
ST3	218	---	10"

Fig. 3.8 After Kubina[10], five wire antennas mounted on the CHSS-2 Sea-King helicopter

Fig. 3.9 presents the pattern efficiency (η_p), the percent E-theta (%E_θ), and the useful percent E-theta (%E_θ) for the Tranline antenna and the wire antenna "E". In Fig. 3.9(a) η_p is plotted as a function of frequency from 2 to 12 MHz. The graph shows that η_p is comparable for both antennas. The Tranline antenna has larger radiation pattern efficiency in the frequency range from 2 to 4 MHz, and from 7 to 9 MHz, with a resonance equal to 54 percent occurring around 8 MHz. The radiation pattern efficiency of the wire antenna is larger in the frequency range from 4 to 7 MHz and from 9 to 12 MHz, with a resonance value η_p equal to 53 percent occurring aroud 10 MHz. Fig. 3.9(b) shows percent E-theta plotted as a function of frequency for both antennas. At 2 MHz the Tranline antenna radiates about 15 percent of its total power into the vertical component E-theta, whereas the wire antenna radiates about 18 percent more power or 33 percent of its total power into the E-theta component. The maximum power contained in E-theta for a %E_θ is about 60 percent and occurs at 8 MHz for the Tranline antenna compared to 10 MHz for the wire antenna "E". Finally Fig. 3.9(c) shows the useful power in E-theta or %E_θ^* as a function of frequency for both antennas. This figure leads to the same conclusion as the previous one. However the resonance value of %E_θ is about 29 percent for the Tranline antenna compared to 34 percent for wire antenna "E".

The pattern analysis presented above for both antennas, using these assessment parameters, leads the reader to believe that wire antenna "E" would have better communication

performance than the Tranline antenna. However as described in Chapter 1, each antenna has a different type of coupler, which effects the performance of the communication system. The wire antenna coupling unit efficiency is equal to 0.264 at 2 MHz [10], whereas the Tranline antenna coupling unit efficiency is estimated to be between 0.8 and 0.9 [29] at 2 MHz. Thus for a given transmitter power, the Tranline antenna radiates about 4 times more power than the wire antenna. So for similar performance by the two antennas at the lower end of the HF band, the wire antennna must have a useful percent E-theta 4 times larger than that obtained by the Tranline antenna.

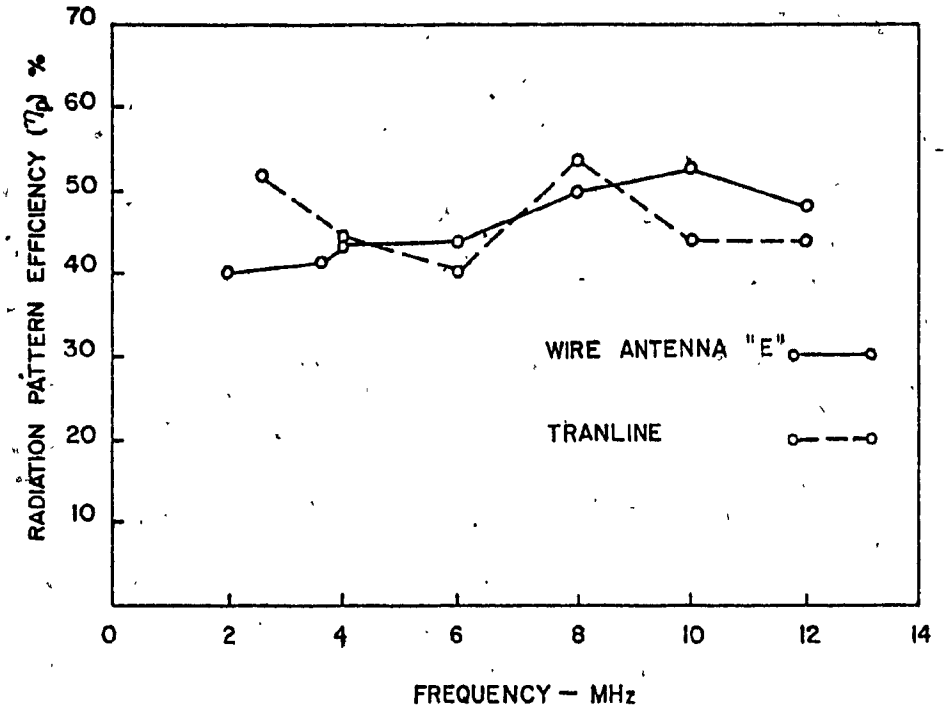

Fig. 3.9(a) Radiation patter efficiency for both Tranline and wire antenna "E" as a function of frequency

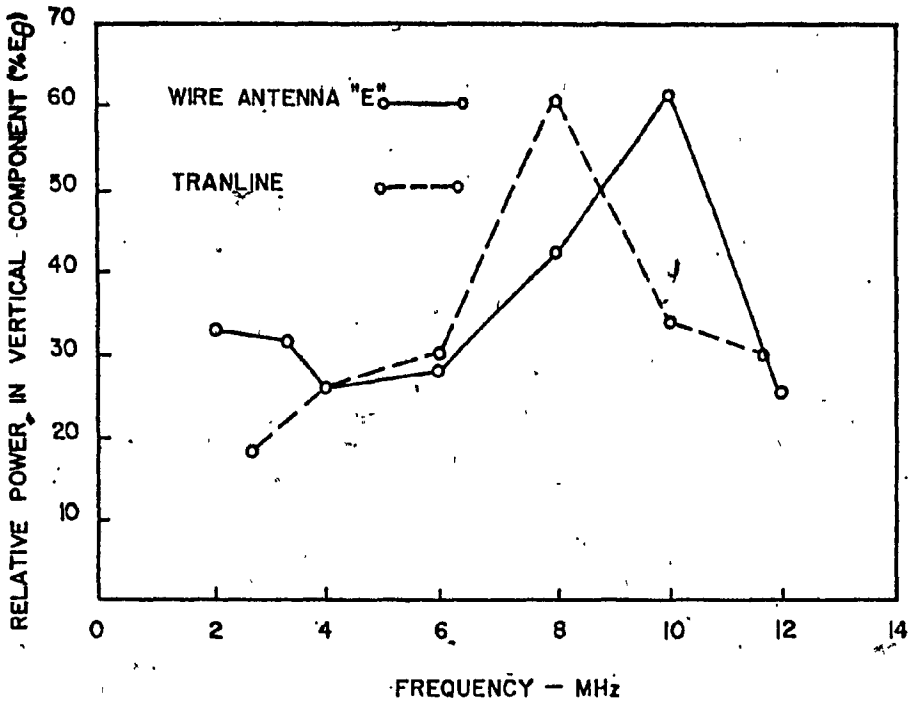

Fig. 3.9(b) Relative power contained in E_θ ($\%E_\theta$) for both the Tranline and wire antenna "E" as a function of frequency

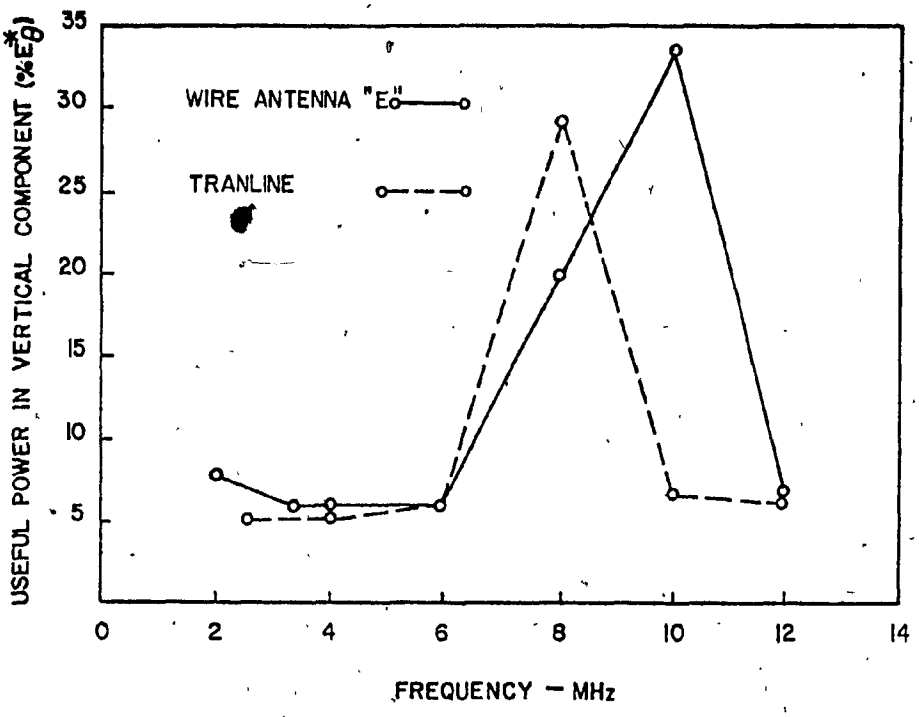

Fig. 3.9(c) Useful power contained in E_θ ($\%E^*_\theta$) for both the Tranline and wire antenna "E" as a function of frequency

However Fig. 3.9(c) shows that the wire antenna has useful percent E-theta equal to 8% compared to 5% for the Tranline antenna, this suggests that the Tranline antenna has a better performance at 2 MHz. At higher frequencies the coupling unit efficiencies for both antennas become comparable, as do their assessment parameters.

3.5.2 Tranline Antenna VS RAE Loop Position

In June 1979, radiation patterns of an HF loop antenna mounted on a Sea-king model, shown in Fig. 3.10, were measured using a vertical range at RAE Farnborough [28]. The data available to the author was limited to those azimuth patterns included in the RAE report [28]. A comparison between the Tranline antenna and the loop antenna using H/V ratio is shown in Fig. 3.11. The loop antenna is superior at all frequencies except between 4 and 7 MHz. This is because a vertical loop is a better radiator of the vertical component than is a horizontal antenna such as the Tranline antenna. Because the H/V ratio is based only on the azimuth plane pattern, this evaluation could be misleading. A comparison based on the radiation pattern efficiency and useful radiated power can not be made because not enough measured data was available. However when numerical techniques are considered later in Chapter 5, such data will be generated for comparison purposes.

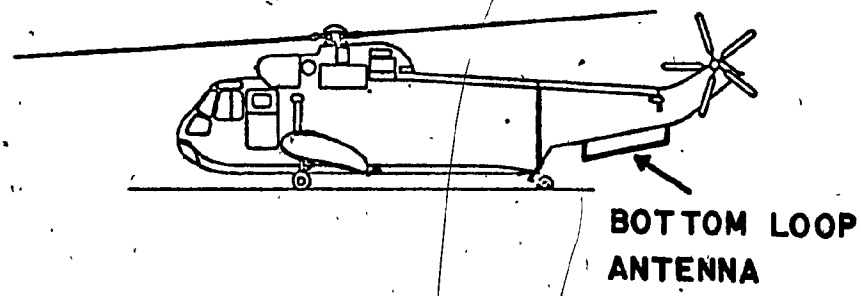

Fig. 3.10 Bottom loop antenna mounted on the Sea-King helicopter

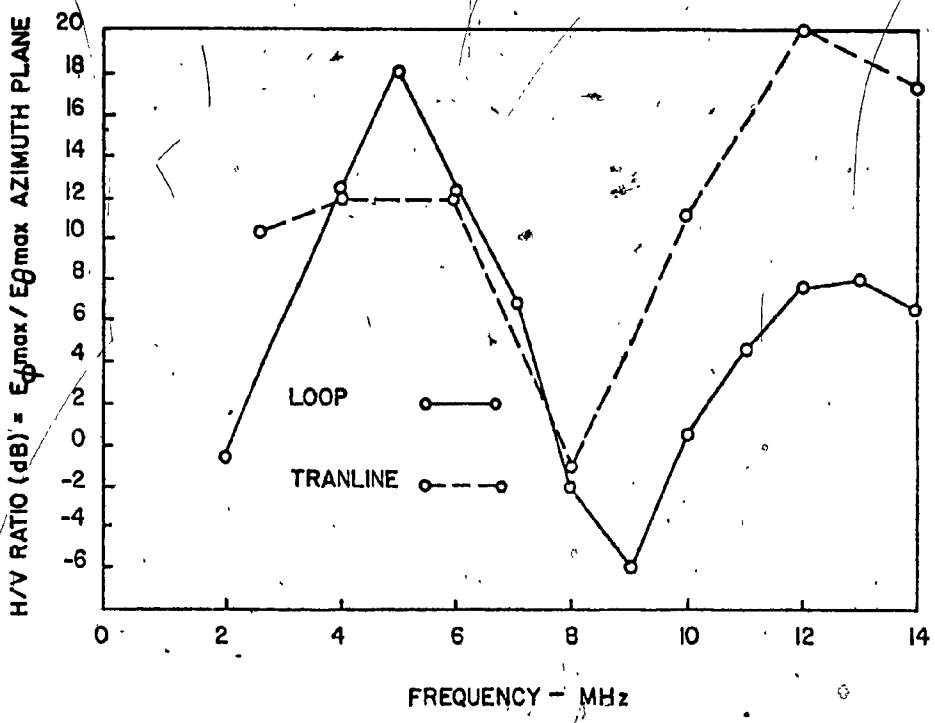

Fig. 3.11 H/V ratio for both the Tranline and bottom loop antenna as a function of frequency

3.6. Effects of the Rotor Blade Position

The performance of a helicopter antenna can be strongly influenced by the rotor blade position at frequencies where the blades form a portion of an electrical path that is resonant. Earlier radiation pattern measurement of an HF wire antenna mounted on the Sea-King scale model [3] have shown that the rotor blades have a considerable effect on the performance of the communication system, at 8.5 MHz where the pattern amplitude varies by as much as 6 dB. In order to appreciate whether or not a similar pattern degradation occurs with the Tranline antenna, the principal plane patterns were measured at 6.0, 8.1, and 10.0 MHz for the backward rotor blade position, which is shown in Fig. 2.7. The azimuth plane patterns at the three frequencies with backward position are compared in Fig. 3.12 with those included in Appendix A for the forward blade position.

The rotor blade position causes the amplitude of the Tranline radiation pattern to change at 8.1 MHz by approximately 2 dB. At 10 MHz, the E_θ pattern shows a 5 dB amplitude variation, together with some pattern shape degradation. The rotor blade modulation could have a serious effects on the communication system at those frequencies where the radiation patterns changes radically. The difficulty arises when trying to tune the Tranline antenna at frequencies between 8 and 10 MHz; the seriousness of the modulation would depend on the characteristics of the antenna coupling unit.

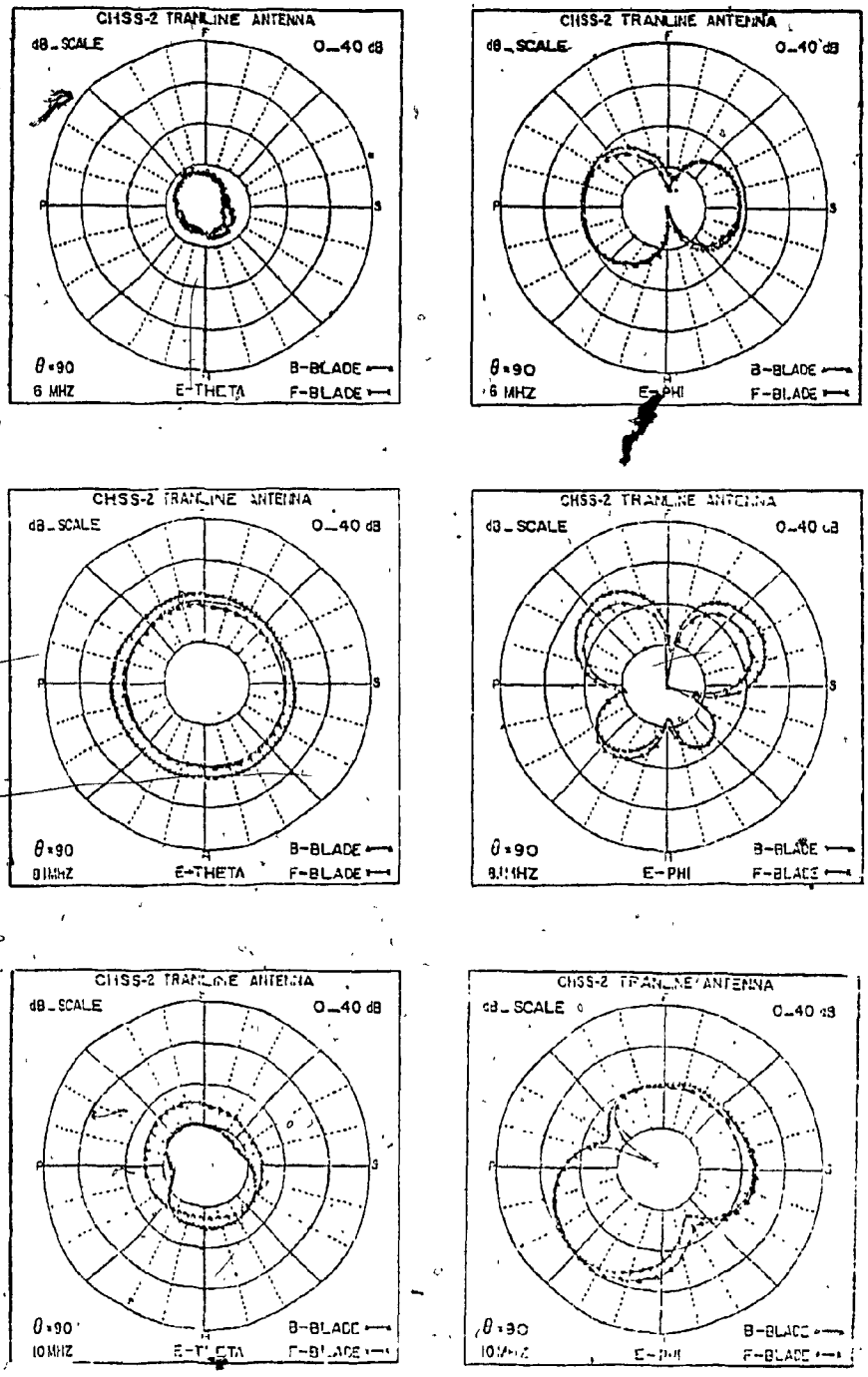

Fig. 3.12 Effect of the rotor blade position on the Tranline antenna radiation patterns at 6, 8.1 and 10 MHz. Azimuth plane only for both polarizations E_θ and E_ϕ

3.7 Summary

This chapter has presented several methods used to evaluate an HF antenna mounted on a helicopter, namely the isotropic level, H/V ratio, the radiation pattern efficiency and the relative power contained in the vertical component, E-theta. In each case the radiation patterns of the Tranline antenna were investigated. The isotropic level method has shown qualilatively that the Tranline antenna in the location tested is a weak radiator in the vertical component at the lower end of the HF band. The H/V ratio does not give a complete evaluation of the Tranline antenna, simply because it is based only on the azimuth pattern. When the Tranline antenna was evaluated using the radiation pattern efficiency it was found that about 50 percent of the total power was radiated in the useful sector of angles $60<\theta<120$ degrees in both polarizations. The most effective methods for evaluating an HF helicopter antenna are those related to the amount of power radiated in the vertical component. Both the percent E-theta and useful percent E-theta showed that the Tranline antenna radiates poorly at the lower end of the HF band, where percent E-theta is less than 30% and the useful percent E-theta is about 5%.

Since measured data of HF antennas similar to the Tranline were available, a comparative evaluation had been most helpful in understanding the characteristics of the Tranline antenna. Although percent E-theta and useful percent E-theta showed that

the Tranline antenna radiates weakly in the vertical component, such results are acceptable when compared to those obtained from wire antenna "E". Using the H/V ratio method the Tranline antenna was compared with a vertical loop antenna measured at RAE. However since a full set of data was not available to compare the radiation pattern efficiency and the relative power radiated in E-theta for both antennas, no complete conclusion was made. The rotor blade position has shown serious effects on the radiation patterns at frequencies between 8 and 10 MHz. The pattern amplitude changes by approximately 2 dB at 8.1 MHz and at 10 MHz the E-theta pattern shows a 5 dB amplitude variation. The rotor blade position had shown similar effects on the wire antenna considered earlier. Since on a pattern basis, the Tranline antenna will perform poorly at the lower end of the HF band, an alternative position to the present one is considered later in this thesis.

The next chapter describes the numerical modelling techniques, and the use of interactive graphics in the modelling and evaluation of HF aircraft antennas.

CHAPTER 4

COMPUTER AIDED ANALYSIS

4.1 Introduction

Chapters 2 and 3 have shown that the evaluation of an HF aircraft antenna requires the measurement of set of radiation patterns, and their integration to evaluate the "assessment parameters". Such measurements are difficult and time consuming, especially since data is needed at many frequencies. Direct measurement is cumbersome if a study of the performance of the HF antenna as a function of one of its design parameters, such as its location on the fuselage, is to be carried out. The performance evaluation requires the measurements of the full set of radiation patterns at all the frequencies. Such a study is more readily carried out using the computer modelling techniques described in this and the next chapter. A computer model of the aircraft with the HF antenna in a particular location is developed such that it reproduces the measured patterns. This "validated" model can then be used to study the effects on the antenna's performance of changes in the antenna position or in other parameters of the antenna. The computer model also

provides a complete map of the RF current flowing on the aircraft. This current distribution provides complete insight into the lobes and nulls in the radiation patterns, and also exhibits the modes of current flow which are associated with each resonance of the aircraft. Such information is available by direct measurement only with great difficulty and is not often attempted [30],[31]. The computer model provides the RF current map at all frequencies.

The theoretical basis for the Numerical Electromagnetics Code (NEC) [32] computer program, the solution techniques used, and the capabilities of the program for developing and analyzing computer models of aircraft are described in this chapter. The numerical modelling of aircraft antennas is usually carried out with the aid of an interactive computer graphics system [33]. Such a system provides the capability for the immediate analysis of the radiation patterns and the RF current distribution which results from a particular computer model. This use of computer graphics in developing the topology of a computer model of an aircraft and in validating the model by comparison with measured results is described in this chapter.

4.2 Theoretical Basis and Solution Methods of NEC

The Numerical Electromagnetic Code (NEC) is a computer program used for determining the current distribution on structures which are made up of wires or surfaces or a combination of wires and surfaces, in free space or over a

perfect ground plane [32]. For example, Fig 4.1(a) shows a cylinder which in general carries two components of surface current density which are functions of position over the surface of a cylinder. The surface patch representation results in the faceted model of Fig 4.1(b), where the NEC program finds the values of two orthogonal surface current density components at the center of each patch. The NEC computer code is capable of analyzing complex interconnections of straight wires, and so can readily model wire antennas such as dipoles, arrays of dipoles, yagi antennas, and other structures. Richmond (1966) [8] introduced the concept of a "wire-grid" model of a surface, and so the wire antenna analysis capability of the NEC code can be used to represent the cylinder of Fig 4.1(a) by wire-grid of Fig 4.1(c). There the computer program determines the RF current flowing axially along each wire of the grid. The results of the program are expected to be the correct currents for the physical wire-grid representation of the cylinder. The ability of the wire-grid to represent the solid cylinder is a physical modelling problem that has been investigated by Thiele (1972) [34] and Wolde-Ghiorgis (1972) [35].

A different boundary condition is enforced for a solid conducting surface approximated by flat facets and for an antenna constructed of wires. For the wire antenna, the boundary condition states that the total electric field in the axial direction along the wire must be zero. Thus at any point on the wire

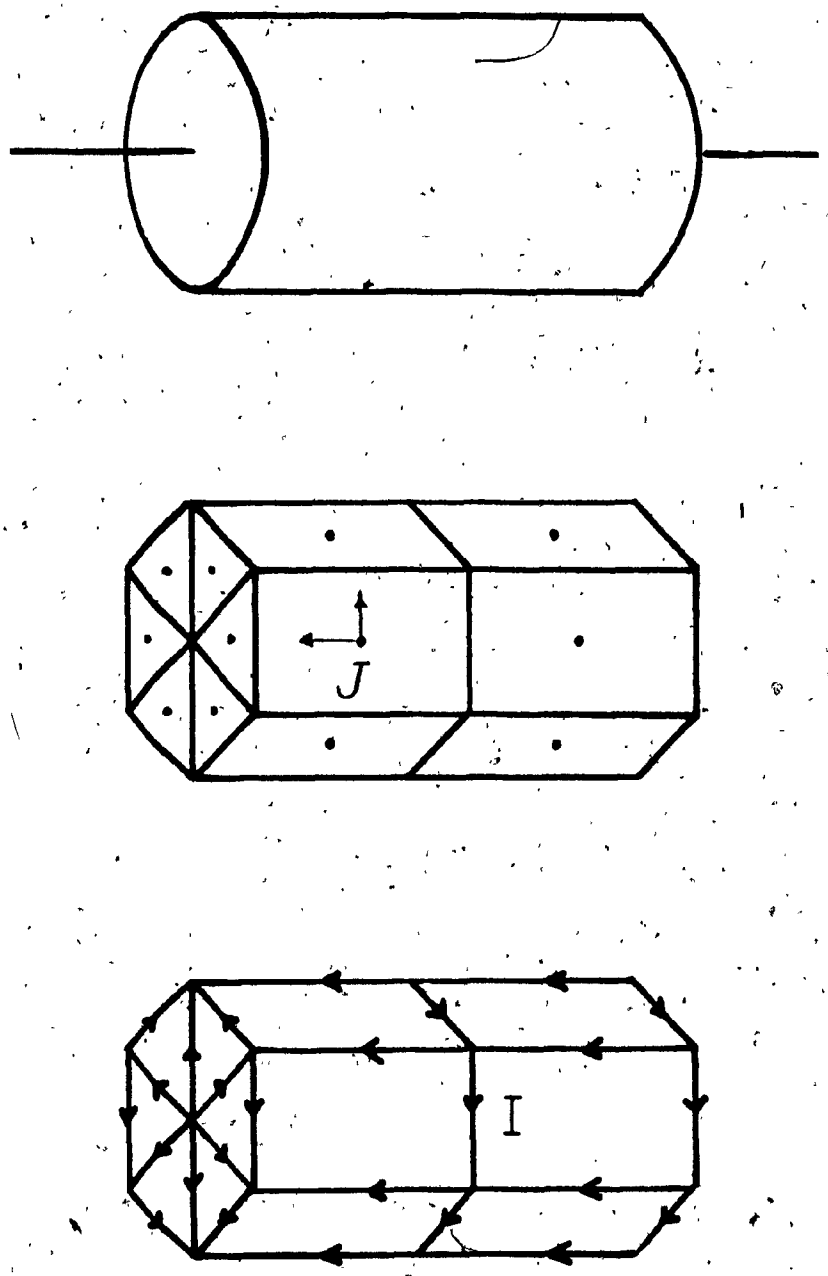

Fig. 4.1 Cylinder representation, (a) actual cylinder, (b) surface patch representation, (c) wire grid representation

$$\hat{s} \cdot [\, \bar{E}^I(\bar{r}) + \bar{E}^S(\bar{r}) \,] = 0 \quad \ldots\ldots\ldots\ldots\ldots(1)$$

where $\hat{s}$ is the axial unit vector for the wire at the observation point given by position vector $\bar{r}$. $\bar{E}^I$ and $\bar{E}^S$ are the excitation field and the scattered field or secondary field, which is due to the currents flowing on the wires of the antenna. NEC uses the Electric Field Integral Equation (EFIE) to state the boundary condition for a number of wires, NW, in terms of the current induced on the wire, thus [32]

$$-\hat{s} \cdot \bar{E}^I(\bar{r}) = \sum_{i=1}^{NW} \frac{-j\eta}{4\pi\beta} \int_{L_i} I_i(s'_i)\left(\beta^2 \hat{s} \cdot \hat{s}'_i - \frac{\partial^2}{\partial s\, \partial s'_i}\right) g(\bar{r}, \bar{r}'_i)\, ds'_i \quad \ldots(2)$$

where

$$\beta = \omega\sqrt{\mu_o\, \epsilon_o}$$

$$\eta = \sqrt{\mu_o / \epsilon_o}$$

The scattered field consists of the sum of the fields due to the current on each of the NW wires of the antenna. The field of the current on each of the wires is expressed as an integral along the length of the i^{th} wire. $\bar{r}$ is the point on the wire surface where the boundary condition is being enforced. $\bar{r}'_i$ is the point on the i^{th} wire axis, where s is the distance parameter along the wire axis at $\bar{r}$, s'_i is a point on the wire axis and $I_i(s'_i)$ is the complex current at s'_i. The reduced

kernel function $g(\bar{r},\bar{r}_i')$ is given by [32]

$$g(\bar{r},\bar{r}_i') = \exp(-j\beta|\bar{r}-\bar{r}_i'|) \;/\; |\bar{r}-\bar{r}_i'|$$

The integral equation (EFIE) is solved for the current on each wire $I_i(s_i)$ using the "moment method", as described below.

In the case of flat faceted approximation to a surface, the boundary condition states that the total magnetic field just inside the perfectly conducting surface must be zero. Thus for any point just inside the surface

$$\hat{n}(\bar{r}) \times [\, \bar{H}^I(\bar{r}) + \bar{H}^S(\bar{r}) \,] = 0$$

where $\bar{H}^I$ and $\bar{H}^S$ are the excitation field and the scattered field, which is due to the current density flowing on the surface. $\hat{n}(\bar{r})$ is the outward directed normal at $\bar{r}$. NEC uses the Magnetic Field Integral Equation (MFIE) to state the boundary condition in terms of the two current density components at the center of each of the NP [32] facets, thus

$$-\hat{n}(\bar{r}) \times \bar{H}^I(\bar{r}) = -1/2\bar{J}_s(\bar{r}) + \sum_{i=1}^{NP} 1/4\pi \int \hat{n}(\bar{r}) \times [\bar{J}_s(\bar{r}_i') \times \nabla' g(\bar{r},\bar{r}_i')\,] \, dA'$$

where $J_s(\bar{r})$, $J_s(\bar{r}_i')$ are the current density at $\bar{r}$ and the current density on the surface of the i^{th} facet respectively. The moment method is used to solve this integral equation.

The moment method used in NEC is well described in the

literature [32,36]. This method applies the concept of linear function spaces and linear operators to the problem. The solution proceeds by expanding the unknown current as a linear combination of basis or expansion functions, with unknown complex coefficients, defines a suitable inner product and a set of weighting functions, takes the inner product to form a matrix equation, and solves this matrix equation for the unknown complex coefficients of the current expansion. In case of wire antennas, let $\hat{s}.\bar{E}^I(\bar{r}) = e$, thus

$$L(I) = e \qquad \ldots\ldots\ldots\ldots\ldots\ldots\ldots\ldots(3)$$

where I is the unknown current and L is the linear operator, which is an integral operator in the case of Equation (2) [32]. e is the excitation or the known source. The current I can be expanded in a sum of basis functions b_j as

$$I = \sum_{j=1}^{M} \alpha_j b_j$$

A set of equations for the coefficients α_j are then obtained by taking the inner product of Equation (3) with a set of weighting functions $\{W_k\}$,

$$< W_k , L(I) > = < W_k , e >$$
$$k = 1, \ldots\ldots\ldots M$$

substituting for I yields

$$\sum_{j=1}^{M} \alpha_j < W_k , L(b_j) > = < W_k , e > \ldots\ldots\ldots\ldots(4)$$
$$k = 1, \ldots\ldots\ldots M$$

Equation (4) can be written in matrix form,

$$[Z_{kj}]\,[\alpha_j] = [E_k] \qquad \ldots\ldots\ldots\ldots\ldots\ldots\ldots\ldots(5)$$

where $Z_{kj} = \langle W_k , L(b_j) \rangle$

which can be expanded as

$$Z_{kj} = \int [\, W_k(s)\, L(b_j)\,]\,ds$$

where the development is over the portion of wire number k where the weight function is not zero, and

$$E_k = \langle W_k , e \rangle$$

$$E_k = \int [W_k(s)\, e(s)]\,ds$$

In NEC the weight functions are chosen to be a set of delta functions [32], where $W_k = \delta(\bar{r}-\bar{r}_k)$. $\{ r_k \}$ is a set of points called "match points" along the axis of each wire. This is a point sampling of the integral equation and is known as the "Collocation" or "point matching" method [32]. NEC uses "subsectional basis functions" [36], which means that each wire is divided up into equal length subsets or "segments" and the current on each segment is expressed as a sum of a constant term, sine term and a cosine term [32], of the form

$$b_j(s) = A_j + B_j \sin\beta(s-s_j) + C_j \cos\beta(s-s_j) \qquad \ldots\ldots\ldots\ldots(6)$$

where s_j is the value of s at the center of segment j. Two of the three unknowns A_j, B_j and C_j are eliminated by making the value of the current at each end of the segment equal to the current on the adjacent segment start, and by equating the charge density at the end of each segment to the charge density at the adjacent segment. The third unknown is determined by the matrix equation. At junctions where two or more wires are connected, Kirchoff's current law is applied. It states that the total current into the junction is equal to zero.

Once the current distribution on the wires is found, the radiated far field can then be computed using a simplified form of Equation (2). The simplified equation given below is valid for a large distance between the current element and the observation point. The far field equation is given by [32]

$$\bar{E}(\bar{r}) = \sum_{i=1}^{NW} \frac{j\beta\eta}{4\pi} \times \frac{\exp(-j\beta r_o)}{r_o} \int_{L_i} [(\hat{K} \cdot \bar{I}_i(s_i))\hat{K} - \bar{I}_i(s_i)] \exp(j\bar{K}.\bar{r}) ds_i \quad \ldots\ldots(7)$$

where $\bar{r}_o$ is the position of the observation point, $\hat{K}$ is a unit vector of $\bar{r}_o$, and $\bar{K} = \beta \hat{K}$.

The accuracy of the results obtained using NEC are highly dependent on the wire radius "a", and the segment length "Δ" compared to the wavelength. the results are also effected by the ratio "Δ/a". Studies carried out in Reference [32] indicate that the thin wire approximation presents an error of

less than 1% for " Δ/a " greater than 8, and for a ratio of " λ/Δ " greater than 10. For thicker segments, the extended thin wire Kernel approximation must be used. This assumes that the current is uniformly distributed around the circumference of the wire, and so, Equation (2) includes an integration around the wire. The use of the extended kernel approximation results in an error of less than 1% for " Δ/a " greater than 2 [32].

The moment method is used in NEC to solve the MFIE by transforming it into a matrix equation. Each component of the current density on each patch is regarded as being constant over the entire patch. This means that the current density can be discontinuous at the boundary for one patch to the next, and also the surface charge density could behave in a similar way at the boundary. In this sense the surface modelling is not as refined in procedure as is wire modelling. The problem of current discontinuity at the boundary can be overcome by increasing the number of patches representing the conducting surface. This requires more computation and it becomes very hard to model complicated surfaces. The value of each of the two surface current density components at the center of each patch is found by point matching in two orthogonal directions, thus generating two linear equations per patch. Each matrix entry requires two element integrations over the surface area of the patch.

In summary, the surface patch modelling can be slow in running time when compared to wire modelling, especially if the

discontinuity of current density at the patch's boundary is to be refined by increasing the number of patches. The surface patch method is not in a sufficiently well developed state to be directly useful for modelling the Sea-King helicopter. If a surface patch method was to be attempted, complex structures such as helicopters would require a combination of both patches and wires. Such a necessity arises at the joint of the drive shaft of the rotor blades to the helicopter body. Surface wire junctions are not precisely modelled with respect to the current distribution at the base of the wire [32]. The wire-grid modelling technique is more advanced. Computer results of a wire-grid model are highly accurate when compared with actual results obtained from a physical grid. Therefore the wire-grid technique is valid with wire-like antennas. In this thesis, the wire-grid modelling of the Sea-King helicopter attempts to apply the technique to such a structure in a new approach.

4.3 Radiation Pattern Calculation

While radiation patterns of a wire-grid model are obtained using NEC, it is important to compute the radiation contribution of certain sections of the wire-grid model, given the current distribution extracted from the NEC output. For example, this allows the study of the radiation contribution of the dominant segment currents. The development of a procedure capable of computing the far field patterns of a given complex current on a wire antenna allows radiation patterns to be computed in addition to those already computed by NEC. The use of such a

procedure to assess the importance of the current on a subset of segments by computing the radiation patterns with these currents only can identify the resonant modes on the model. If the resulting pattern is almost identical to the pattern with the full set of currents, then it is clear that the subset of the segments is primarily responsible for patterns, and the wires supporting these currents are the principal sections of the wire-grid model. In this way the parametric studies can be applied to those wires considered to be important as a result of knowledge based on their contribution to the radiation patterns. Such analyses are considered in chapter 5, and the following is the formulation of the far field expression.

4.3.1 Method of Evaluating the Far Field

This section describes the method for obtaining the radiation fields from the value of the RF current flowing on each segment of the wire-grid model of the aircraft. The method follows that used in [15]. The current on each segment is assumed to be constant and equal to the complex current amplitude at the segment center specified in the output of the NEC program. This differs from the method that NEC itself uses to compute far fields, in that NEC uses a sinusoidal current variation on the segment. The radiation patterns computed by the method of this section are identical to those computed directly by NEC itself, except in the deep nulls.

Fig 4.2 shows current element number k located at position

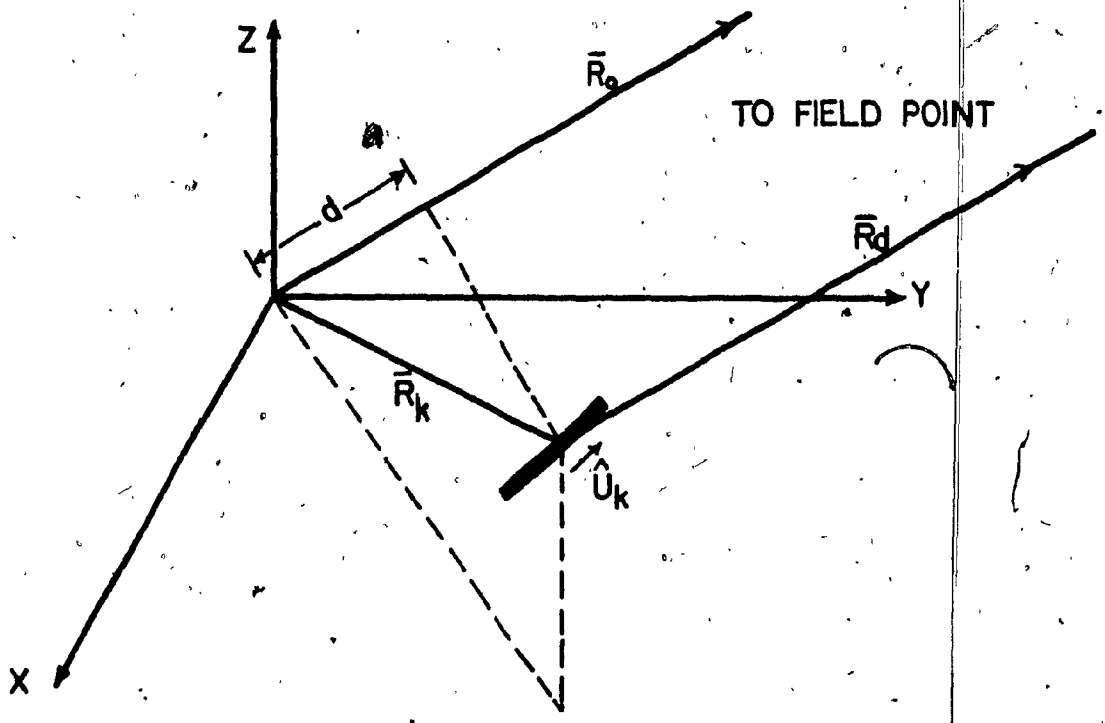

Fig. 4.2 Current element in the global coordinate system

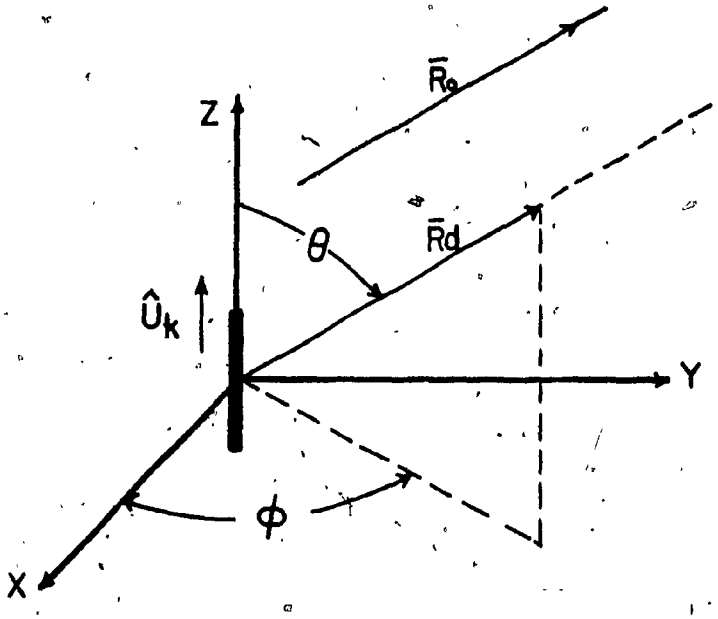

Fig. 4.3 Current element in the local coordinate system

$\bar{R}_k$ and pointing in the direction of the unit vector $\hat{U}_k$. The observation point lies at $\bar{R}_0$, and $\bar{R}_d$ is a vector from the center of the current element to the observation point. If R_0 is large, the far field of the current element may be used and is given by

$$\bar{E}_k = j\beta\eta \frac{I_k\, dl}{4\pi} \frac{\exp(-j\beta R_d)}{R_d} \sin\theta_k \hat{\theta}_k \quad \text{.....(8)}$$

where β is the free space wave number, η is the characteristics impedance of free space, I_k is the complex amplitude of the current on the k^{th} segment, dl is the length of the k^{th} segment, and θ_k and $\hat{\theta}_k$ are the spherical coordinate angle and the unit vector in the local coordinate system as shown in Fig. 4.3. Here it is assumed that the length of segment k is sufficiently short that Equation (8) can be used directly. For a segment longer than a tenth of a wavelength, Equation (8) would have to be integrated using two or more points to obtain a sufficiently accurate far field, but the segment length used in this thesis is long enough to require such integration. The far field of the full set of N segments that constitute the wire antenna is found by summing up N terms of the far field of Equation (8). It is necessary to express the local coordinate quantities θ_k and $\hat{\theta}_k$ in terms of the unit vector $\hat{U}_k$ and the global coordinate system. This geometrical conversion is described by Trueman [15] and leads to

$$\bar{E} = j\beta \sum_{k=1}^{N} \frac{I_k \, \Delta l_k}{4\pi} \left(\exp[j\beta(\bar{R}_k \cdot \hat{R}_o)]\right) \left([(\hat{U}_k \times \hat{R}_o) \times \hat{R}_o]\right) \frac{\exp(-j\beta R_o)}{R_o} \quad \ldots\ldots(9)$$

where Δl_k is the segment length.

This equation is evaluated by a computer program called EFAR1, which reads the output of the NEC program to extract the geometrical data and the segment current. The program computes the set of patterns described in Chapter 2. The results of Equation (9) have been compared with patterns computed directly with NEC, and differ only in the deep nulls. Since the nulls do not contribute significantly to the radiated power by the antenna, this small discrepancy does not affect the values of the assessment parameters which are derived from these patterns.

4.3.2 Assessment of Dominant RF Current

Equation (9) can be used for the computation of the far field radiated by a selected subset of the segments making up the helicopter model. For the Sea-King helicopter, this allows the assessment of the importance of the RF current flowing on different sections of the model. In chapter 5 this technique is used to identify the importance of the loop currents as the main

radiator at the low end of the HF band, whereas the drive shaft and the rotor blades of the helicopter model are identified as important contributers to the radiation patterns at the resonant frequency. In summary, this technique reveals the importance of the RF currents on certain parts of the computer model, and provides a better understanding of the radiation patterns.

4.4 NEC Input and Output Files

A typical NEC input file is shown in Fig 4.4, it consists of the wire-grid geometry and "control cards" [37]. Each one of the wires making up the wire-grid model is represented by the coordinates of its start and end points. The wire is identified by its "tag" number and the number of equal segments subdividing it. The input file also specifies the radius of the wire. The "control cards" which direct the NEC program to produce the desired output have many functions, namely the frequency card which specifies the frequency in megahertz, the excitation control card which specifies the antenna location by indicating the wire and the segment numbers. The type of excitation available in NEC is either a voltage or a current source or an incident wave applied to the antenna. In the case of the Sea-King helicopter models, a one volt source is used to excite the antenna. The control card which enables the program to use the Extended Kernel approximation is also specified in the NEC input file. A set of radiation pattern control cards is used to specify the pattern sampling parameters, such as conical or elevation cuts and the increment of the varying angle in

degrees. The radiation patterns specified by the Sea-King input files are those described in Section 2.3.

Executing NEC with the input file of Fig. 4.4, produces an output file containing the structure description as specified by the input, the complex current on each segment, and the radiation patterns for both E-theta and E-phi far field. NEC output file also includes the power radiated by the antenna and the antenna impedance. Reference [37] contains the outputs of some typical runs.

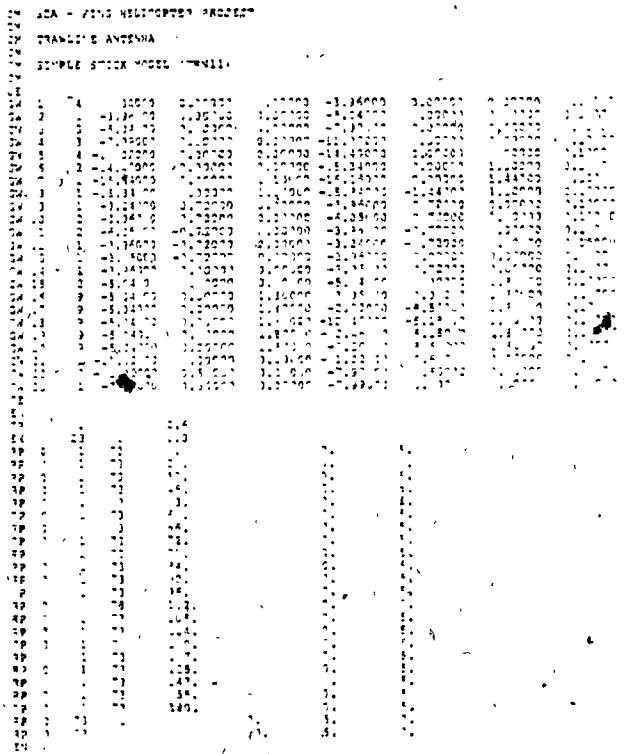

Fig. 4.4 Typical input data file used to execute the NEC program, geometry and control cards

4.5 Interactive Computer Graphics as an Analytic Tool

The CRT computer graphics on the PDP11/20 minicomputer has been programmed as an interactive tool for the effective and rapid evaluation of the currents and radiation patterns obtained from each computer model of the Sea-King helicopter. The graphics screen provides an efficient "communication link" between the computer and the antenna engineer. This section describes the programs which allow the numerical data from each computer model to be analyzed and compared with measured data in a quantitative manner.

The Concordia EMC Laboratories computer system consists of two minicomputers and a microcomputer, using RK05 removable disc packs as the principal medium of transfer for data and programs. The block diagram of Fig 4.5 shows this computer system and includes the peripheral units associated with each computer. The PDP11/20 minicomputer has a 28K word memory and three RK05 disc drives with a disc capacity of 2.2 megabytes. These discs are used to store the user programs and data files. The PDP11/20 drives a Tekronix 613 CRT storage graphics display with a hard copy unit, and this display is used extensively by the interactive graphics programs used to analyze the Sea-King helicopter models. The PDP11/20 has a dual "Dectape" magnetic tape drive and floppy disc drive which are used to create backup files of programs and data files. The PDP11/20 communicates

with the university's CDC Cyber 174 computer on a 4800 baud line using a program called "SIMTEK" [38] which simulates a TEK4014 terminal. Input data files for the NEC program can be transferred to the Cyber, on which the NEC code is executed, and then the output file is transferred back to the PDP11/20 for analysis via the 4800 baud link. Thus the data link is a vital component in the interactive evaluation of the results obtained with each computer model. In Fig 4.5, the PDP11/45 has a 28 K word memory and two RK05 disc drives, and is used to drive a Calcomp 563 plotter to make high quality line drawings of the graphics obtained on the PDP11/20. The PDP11/45 can also communicate via SIMTEK on a 4800 baud line with the Cyber. The LSI11/23 microcomputer has a 128 K word memory and two RK05 disc drives. The LSI-11 drives a Bit-Pad digitizing tablet which is used to create a computer file of measured patterns available as polar graphics. An HP storage scope can be driven as if it were the TEK-613 graphics display, which allows the LSI-11 to be used to develop graphics programs for the PDP-11/20. The LSI-11 can communicate with the Cyber via SIMTEK and a 4800 baud line. At the time of this writing, a NORPAK raster color graphics display has become available and will eventually be incorporated in the programs for the interactive evaluation of computer models.

This hardware system supports unique and flexible software for the interactive evaluation of the patterns and currents obtained from computer models of antenna systems [33]. The block diagram of Fig 4.6 shows the data files and the sequence of programs that are used to prepare a computer model, to

execute NEC to obtain the patterns and currents, and to use the interactive graphics software to evaluate the results. The procedure starts with the tabulation of the geometrical end-points coordinate of each wire making up the antenna, which is done either manually or by digitizing a "three views" drawing of the aircraft. The tabulated wire end-point coordinates and the control cards described in Section 4.4 form the input file to NEC, called "NECIN". The contents of this data file are then displayed on the CRT graphics using programs such as "MODEL", "MODDIS" and "VIEW". These model display programs allow the user to change the scale of the display and vary the angle of rotation so that different views can be obtained on the CRT. These programs have the option of numbering the wires of the model in the form of Fig.5.1. The validity of the computer model within the restriction of the NEC code is analyzed using the "WAP" program, which compares segment length to the wavelength for each wire, and checks the ratio of the segment length to the wire radius. Once the computer model has been verified by the engineer in this way, the NEC input file "NECIN" is transferred to the CDC-Cyber computer using the 4800 baud link. On the CDC Cyber computer the NEC program is executed using a "SUBMIT" batch procedure [40]. To make the data transfer of the results from the Cyber to the PDP computer efficient, only the essential data from the NEC output file is retained. The program "STRIP" reformulates the output file so that it contains only the geometry of the computer model, the frequency, the complex amplitude of the current on each segment,

the antenna impedance and the radiation patterns. This file is called "SOLN" and is much smaller in size than "NECOUT". This "SOLN" data file is transferred to the PDP system over the 4800 baud link and is stored on an RK05 disc pack. The ISOLEV program is used to read the "SOLN" data file and calculate the isotropic level from the radiation patterns, as well as the total radiated power and the assessment parameters described in Chapter 3. The quantities computed by ISOLEV are written into the "SOLN" file to obtain a modified file called "ISOLN", which is then used as an input file for the interactive evaluation programs. The current distribution is displayed on the graphics using "IDIS" and "CDDP" which show the RF current magnitude on the entire wire-grid model in the form of Fig.5.14(a-b), or on a specified group of wires from the complete model. This capability is used to identify current paths that contribute to resonance modes. The radiation patterns are displayed and compared to measured patterns for both polarization E_θ and E_ϕ. The PATCMP program which displays these patterns normalizes the field values so that equal power is radiated by both measured and computed patterns. The program has many options, namely displaying the isotropic level and the wire-grid model as a part of the pattern display as shown in Fig.5.3. The set of 23 conical patterns can also be displayed as a surface plot using the program "SURPAT". The software package described above is used in the next chapter to develop computer models of the Sea-King helicopter and the Tranline antenna.

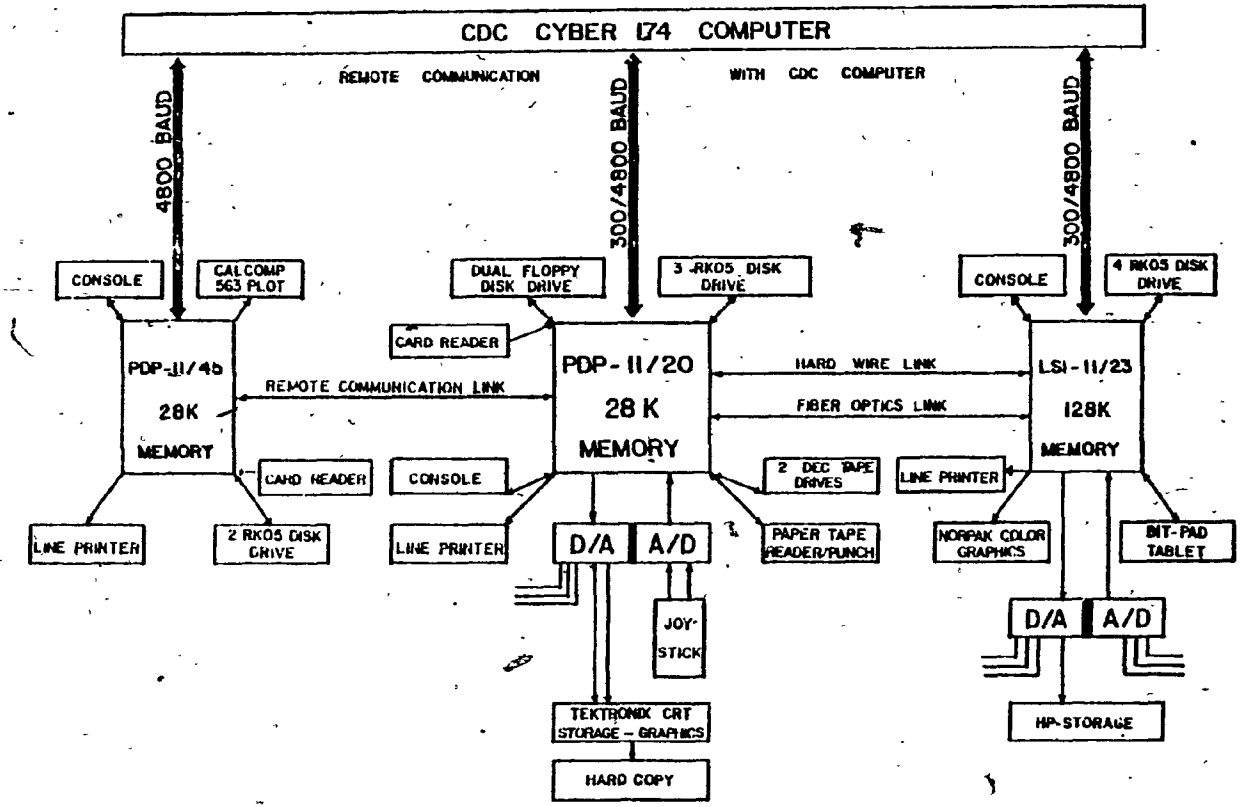

Fig. 4.5 Hard-ware configuration of the computer system used at Concordia EMC-Laboratory

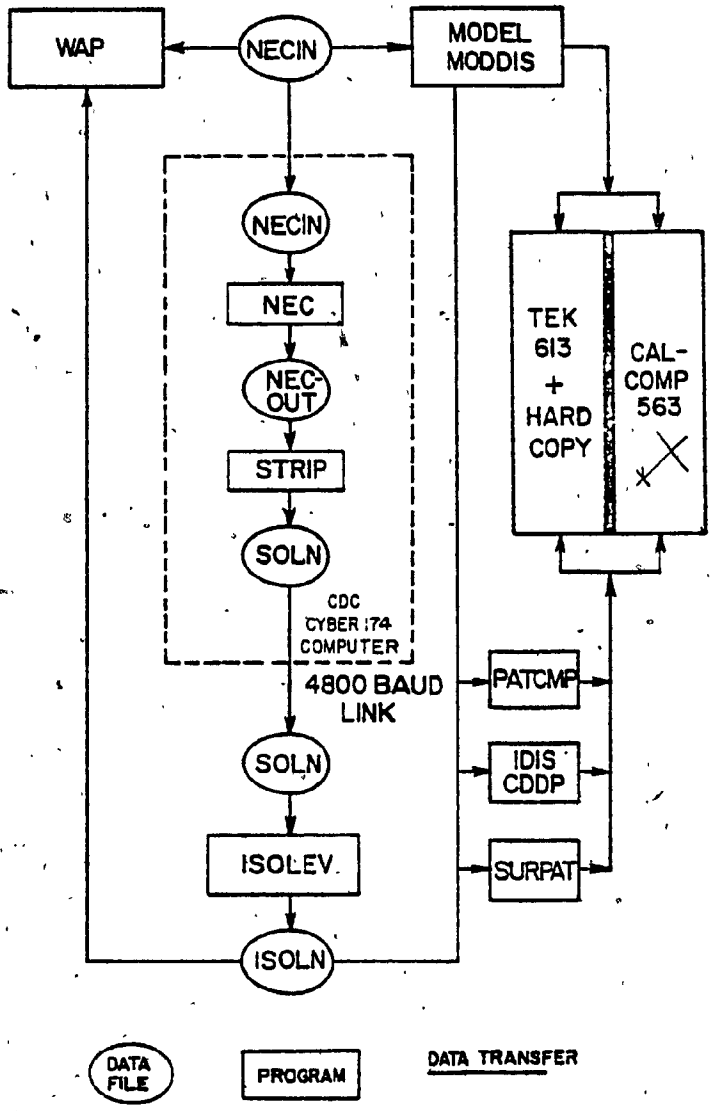

Fig. 4.6 The sequence of data files and programs that must be executed to obtain the solution and to analyze it using interactive graphics

4.6 Summary

This chapter has presented a description of the two numerical methods which can be used to solve for the current on a conducting surface, namely the flat-faceted "surface patch" model and "wire-grid" representation of the surface as a mesh of "thin wires". In each case the moment method is applied to transform an integral equation into a matrix equation. It was concluded in this chapter that the methodology for determining the current on an antenna modelled with "thin wires" is more highly developed than using the "surface patch" approximation. Therefore, wire-grid models of the Sea-King helicopter will be used in the next chapter to study the radiation characteristics of HF loop antennas mounted on it. In addition, Section 4.3 presented the method which is used to calculate the radiation patterns given the current distribution on the wire antenna. This method allows the design engineer to study the contribution of specific parts of the computer model to the radiation patterns.

The hardware and software systems used for the interactive evaluation of a computer model were presented via the block diagrams of Section 4.6. The PDP11/20 with its CRT graphics display and its remote communication link with the CDC Cyber computer make up the base for the effective and rapid evaluation of computer models. Associated with this hardware system is a software package designed for a flexible interactive evaluation of radiation patterns and current distribution on the wire-grid

model.

In the next chapter, wire-grid models of the Sea-King helicopter with the HF Tranline antenna are evaluated using the numerical techniques described in this chapter.

CHAPTER 5

WIRE GRID MODELS OF THE SEA-KING HELICOPTER

5.1 Introduction

In this chapter the performance of the Tranline antenna on the Sea-King helicopter is assessed by developing wire-grid models for this radiating system. The numerically "predicted" results for these models of the Sea-King are obtained using the NEC program. The validity of each computer model is assessed by comparing the computed radiation patterns with the measured patterns represented in Appendix(A), and by comparing the "assessment parameters" defined in Chapter 3. To construct a Sea-King helicopter wire-grid model, wires are positioned where the current distribution is suspected to be strong. The end point coordinates of each wire making up the model are manually obtained from either a scale model or a "three views" drawing of the helicopter airframe. In order for a wire-grid model to be successful, it must be "electromagnetically equivalent" to the actual helicopter, which means that it must support similar

current modes to those that exist on the surface of the helicopter. With increasing frequency, the wire-grid model needs to be geometrically more complex, whereas at low frequencies a very simple representation is adequate.

Three wire-grid models of the Sea-King helicopter are presented in this chapter, namely the simple stick model, the intermediate model and the complex model. Parametric studies are applied to the simple stick model in order to establish that certain wires of the model are mainly responsible for the radiation patterns. The frequency range over which the "simple model" is adequate is assessed. A "complex model" is presented which is valid at higher frequencies than the simple model, and which can be "tuned" to match even the resonant behaviour of the scale model of the helicopter used for measurement. Finally, various loop antennas are examined when mounted on the complex model, in comparison to the Tranline antenna at its location, and the relative performance of these loops is assessed to explore the possibility of relocating the Tranline antenna so that adequate vertical radiation at the low end of the HF band is obtained. This serves to demonstrate the usefulness of such a "wire-grid" computer model of the Sea-King helicopter.

5.2 Simple Model of the Sea-King Helicopter

Fig. 5.1 shows a simple stick model of the Sea-King helicopter which is useful for the study of the general characteristics of the Tranline antenna on the helicopter at low

HF frequencies. The fuselage is modelled by a single wire. The drive shaft of the main rotor blades, the sponsons, and the Tranline antenna located on the port side, are connected to the main fuselage wire. The fuselage wire is placed along the center line of the helicopter. This makes the drive shaft which connects the fuselage to the rotor blades 1.8m in length. The rotor blades are oriented in the forward position of Fig. 2.7. The back rotor blades are omitted for simplicity. The total number of segments making up the stick model is 78. This model is excited by a voltage source applied to wire number 23 of Fig. 5.1. This model will be referred to as "TRN11". In the following sections, the TRN11 model is tested at frequencies up to 14 MHz, although such a simple model is not expected to produce good results above 6.0 MHz. As a basis for the development of more complex models later in this chapter, the contribution of various current segments of this simple model is assessed in the following sections.

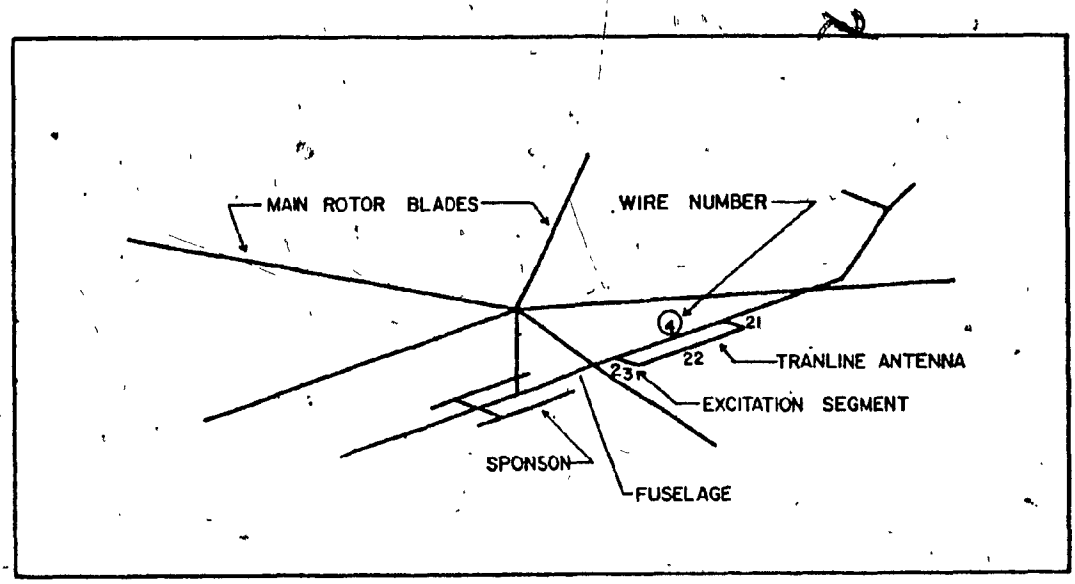

Fig. 5.1 The TRN11 simple stick model of the Sea-King helicopter, Tranline antenna mounted on the port side of the model.

5.2.1 Simple Model with Uniform Radius

The radiation patterns produced by the "TRN11" at frequencies between 2.6 and 14 MHz are obtained and analyzed in this section. A uniform radius of 0.1 m is used for all the wires making up the model as shown in Fig. 5.2. This radius makes the stick model much thinner than the surface enclosed by the actual helicopter. The ratios of wavelength to segment length and segment length to radius are calculated for frequencies between 2.6 and 8.1 MHz. The segment length to radius ratio has a minimum value of about 8. This value requires the use of the extended kernel in NEC [32], and so the extended kernel has been used throughout this chapter. The current distribution on the TRN11 model and the far field radiation patterns for both polarization E_θ and E_ϕ are obtained by execution of NEC, using the TRN11 geometry as its input data.

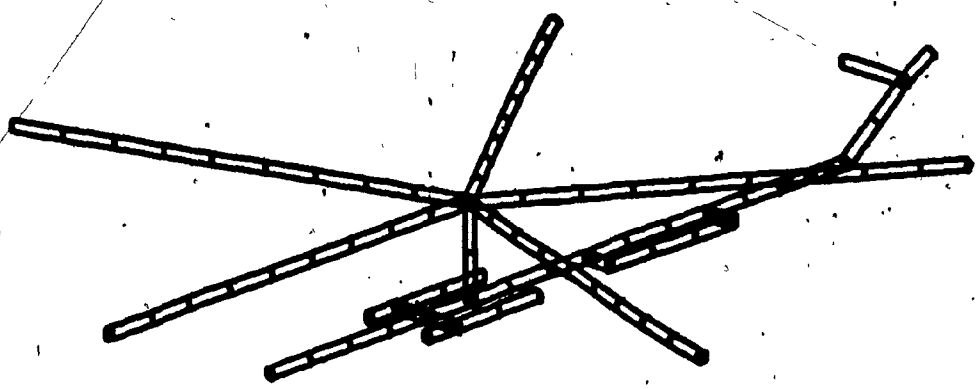

Fig. 5.2 Uniform radius representation of the TRN11 simple model of the Sea-King helicopter.

The computed radiation patterns of the TRN11 computer model with the Tranline antenna resulted in some agreement with the measured patterns at 2.6 and 4.1 MHz, very good agreement at 6.0 MHz and relatively poor agreement at 8.1 MHz and higher. Fig. 5.3 shows the azimuth pattern (theta equal to 90 degrees) at 2.6, 4.1, 6.0 and 8.1 MHz. At 2.6 MHz the measured E_θ polarization is a figure eight with minima centered toward the port and starboard. The measured E_ϕ polarization is elliptical. In contrast, the computed E_θ polarization is omnidirectional, but roughly of the same level as the measured E_θ . The computed E_ϕ is a figure eight with minima forward and aft of the helicopter, but roughly of the same level as the measured E_ϕ . The same behaviour is seen at 4.1 MHz in Fig. 5.3(b). The most important disagreement between the measured and computed patterns at 2.6 and 4.1 MHz is the presence of the null in the computed E_ϕ polarization at the forward and aft locations. The difference in level at the null location is about 9 dB at 2.6 MHz and 12 dB at 4.1 MHz. The disagreement between measured and computed patterns at this particular location is shown clearly in the elevation pattern, for phi equal to zero degrees, of Fig. 5.4 at 2.6 and 4.1 MHz. At 2.6 MHz the elevation pattern shows a measured E_ϕ polarization which is a figure eight with shallower nulls, and tilted about 10 degrees aft. The measured E_ϕ polarization is a figure eight with nulls above and below the helicopter. The computed E_ϕ polarization is a figure eight with much deeper nulls. The computed E_ϕ polarization is a figure eight but at a

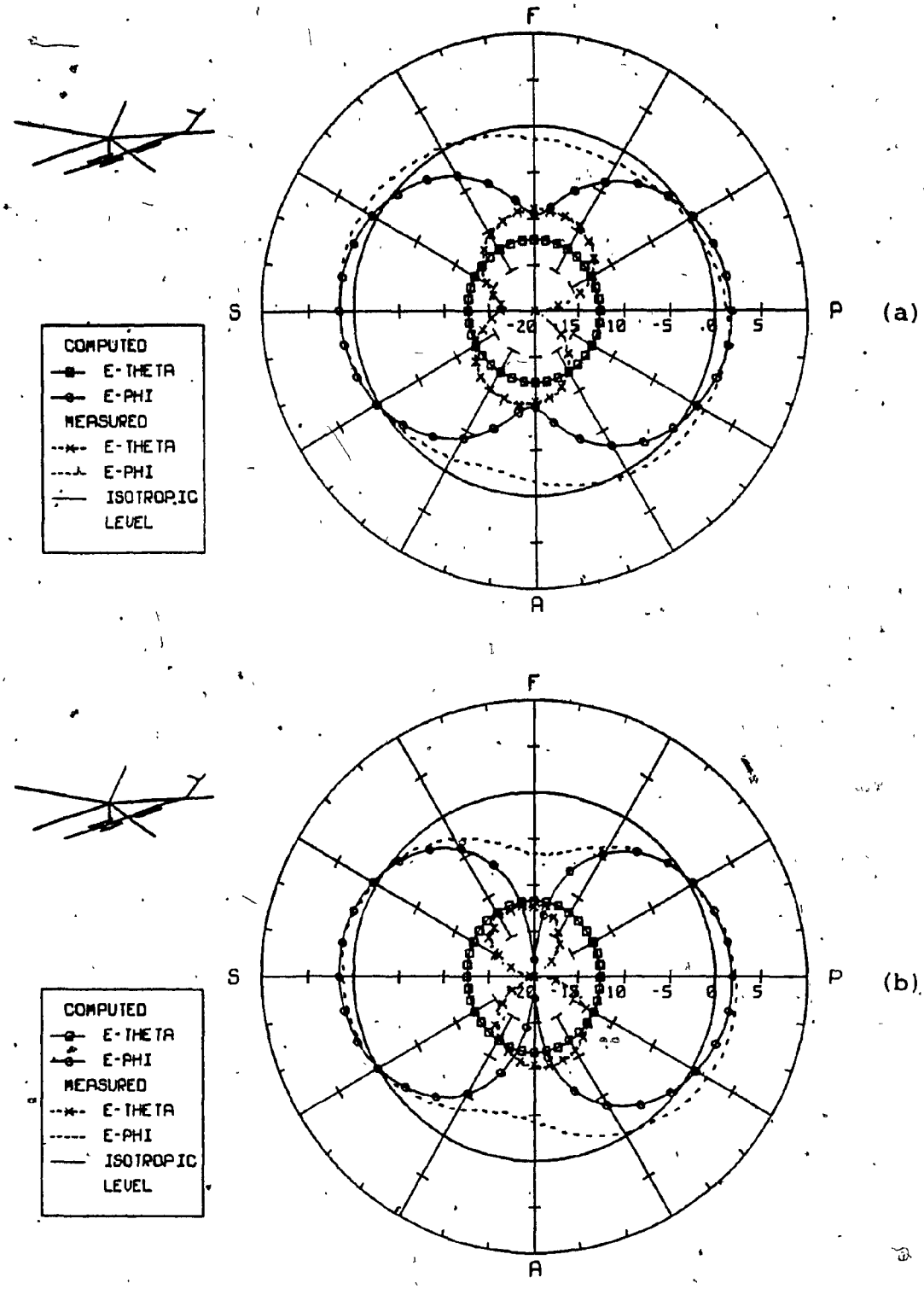

Fig. 5.3 Tranline antenna azimuth patterns obtained using the TRN11 model, compared to the measured patterns at (a) 2.6 MHz, (b) 4.1 MHz, dB-scale.

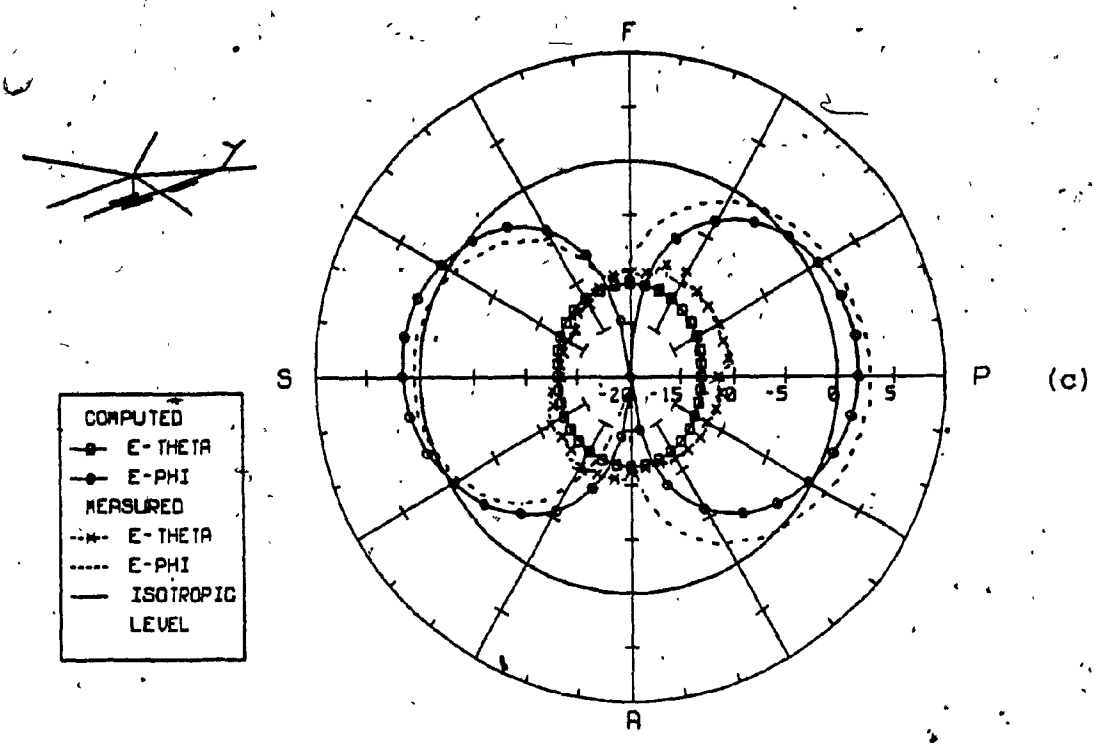

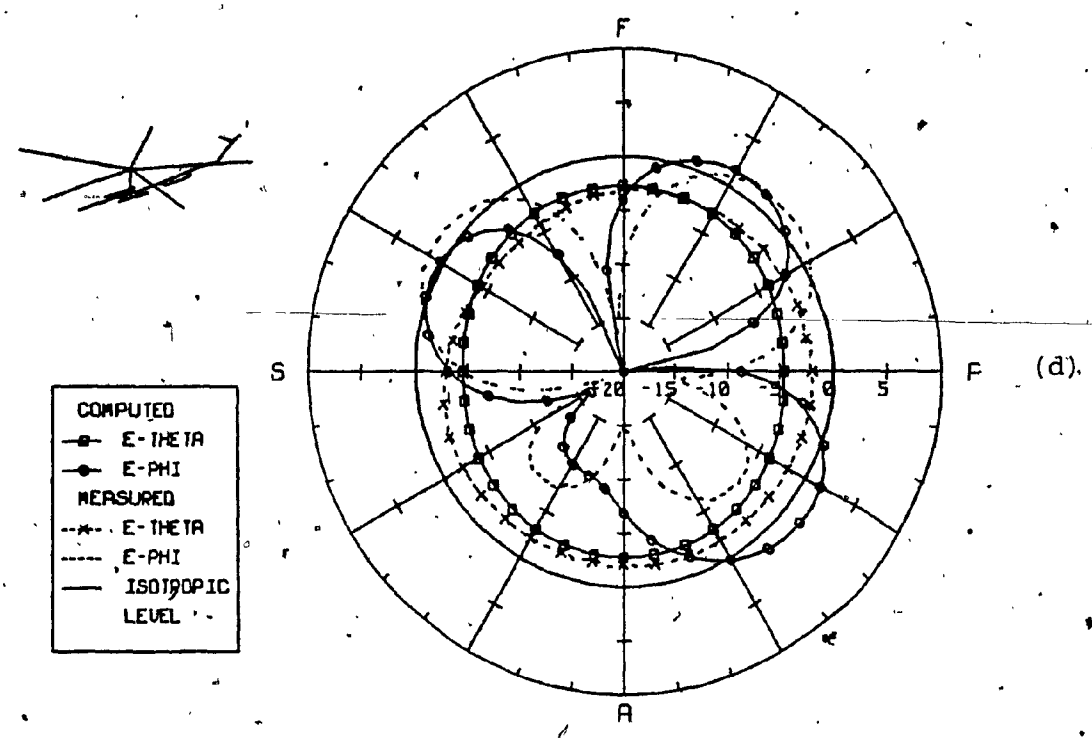

Fig. 5.3 (cont'd), Tranline antenna azimuth patterns obtained using the TRN11 model, compared to the measured patterns at (c) 6 MHz, (d) 8.1 MHz, dB-scale.

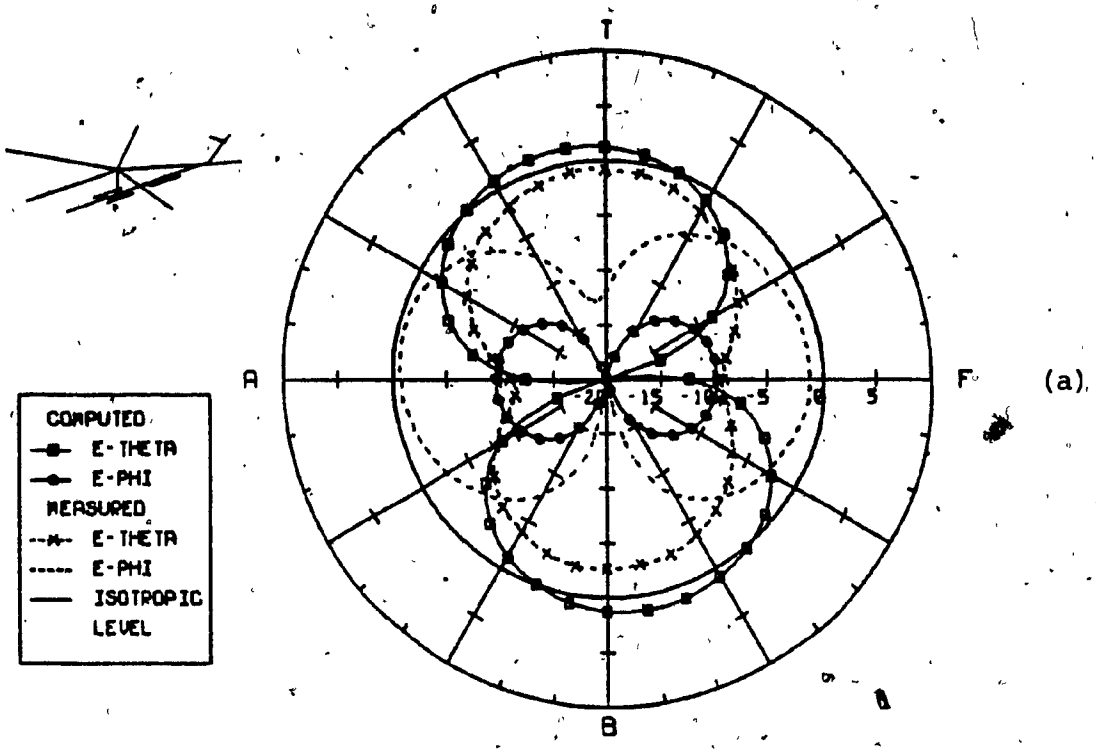

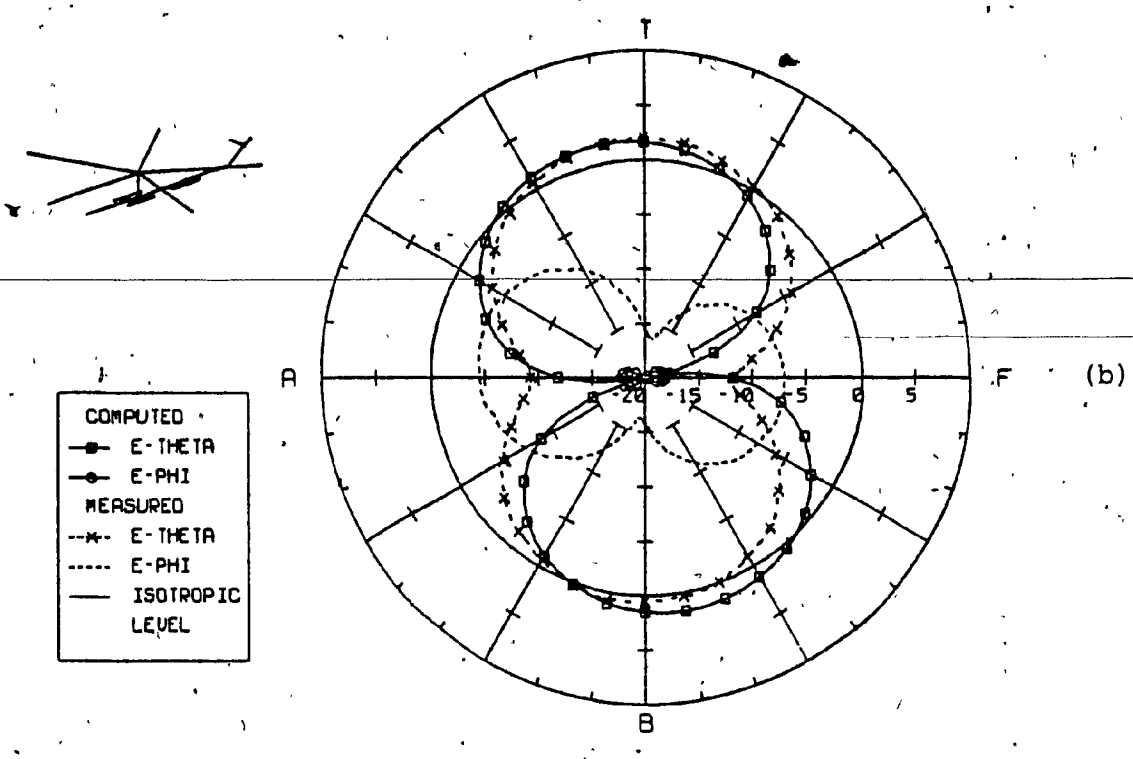

Fig. 5.4 Tranline antenna elevation patterns ($\phi = 0$) obtained using the TRN11 model, compared to the measured patterns at (a) 2.6 MHz, (b) 4.1 MHz, dB-scale.

substantially lower level than the measured pattern. The same behaviour is seen in Fig. 5.4(b) at 4.1 MHz. Thus the nulls forward and aft in the E_ϕ computed azimuth patterns of Fig. 5.3(a) and Fig. 5.3(b) correspond to the excessively low level in the E_ϕ polarization of the elevation pattern of Fig. 5.3(a) and Fig. 5.3(b). The lack of agreement in the E_θ polarization of the azimuth pattern of Fig. 5.3(a-b) is due to the simplicity of the model. TRN11 presents the drive shaft as the main radiator of the E_θ polarization in the azimuth plane, which explains the omnidirectional computed pattern instead of figure eight presented in the measured pattern. However, Fig. 5.3(c) shows that the simple model gives a good agreement at 6.0 MHz in both polarizations. The ellipitical measured pattern in the E_θ polarization is reproduced both in orientation and level by the computed pattern. The figure eight pattern in the E_ϕ polarization is also reproduced as well in both orientation and level. In Fig. 5.3(d), at 8.1 MHz the measured E_θ polarization is omnidirectional and almost reproduced by the computed pattern to within 2 dB. The measured E_ϕ polarization is a butterfly figure with the two main lobes oriented toward the nose of the helicopter. The two minor lobes are oriented toward the aft of the helicopter at a level 5 dB lower than the main lobes. The computed E_ϕ pattern reproduces the two main lobes with a 10 degree tilt toward the starboard. The rest of the computed E_ϕ pattern disagrees with the two lobe structure of the measured pattern, especially in a level difference of about 8 dB between the port and the aft of the

helicopter.

Fig. 5.5 shows the relative power contained in the vertical polarization E_θ obtained from the TRN11 radiation patterns. The figure displays both computed and measured $\%E_\theta$ values as a function of frequency. The TRN11 model radiates vertical power greater or equal to the measured values at all frequencies but 8.1 MHz. The computed $\%E_\theta$ is greater than the measured one by 9% at 2.6 MHz and 30% at 10 MHz. At 6.0 MHz both computed and measured $\%E_\theta$ are equal, which explains the good agreement in the azimuth pattern of Fig. 5.3(c). The computed $\%E_\theta$ is less than the measured one by about 12% at 8.1 MHz.

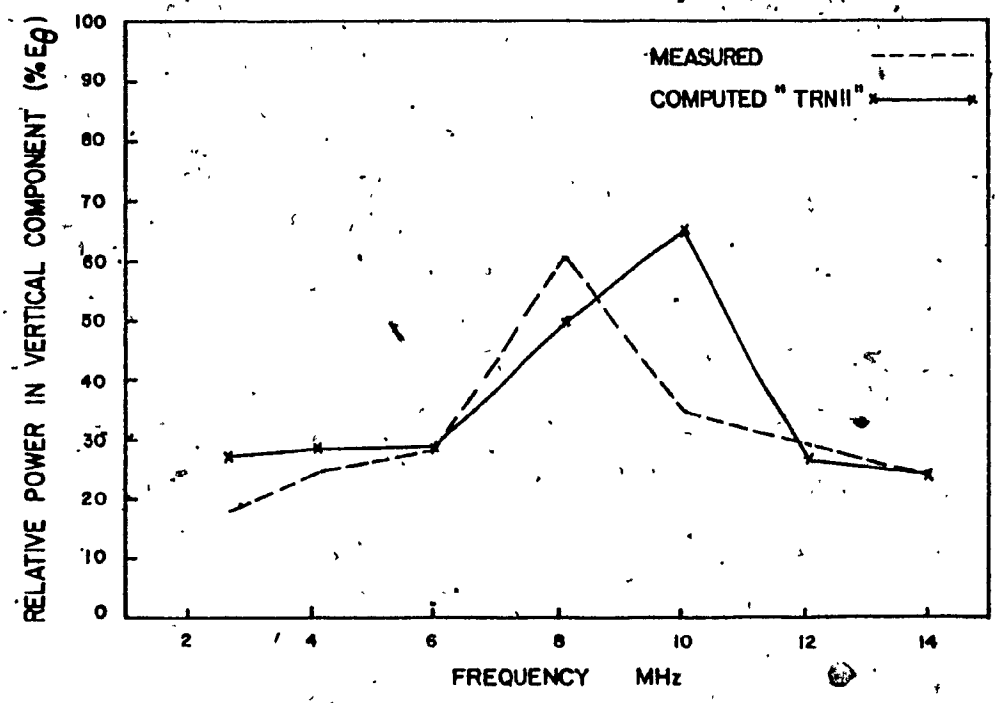

Fig. 5.5 Tranline antenna $\%E_\theta$ obtained using the TRN11, compared to the measured $\%E_\theta$ as a function of frequency.

In the next section an attempt will be made to explain the differences between the TRN11 computed patterns, and the scale model measured patterns. Such analysis is carried out by systematically varying parameters such as the fuselage radius and antenna spacing from the fuselage.

5.2.2 Parametric Studies and Simple Model

In this section the assessment parameter $\%E_\theta$ is used to determine a suitable fuselage radius for the simple model TRN11. In this approach to wire-grid parametric studies the parameter $\%E_\theta$ is computed at certain frequencies while varying a specific parameter of the model, such as the number of segments on a section of the model, the radius of a certain wire, or the location of a certain wire. In each case the computed $\%E_\theta$ is compared to the measured one.

The best wire radius for the fuselage of the TRN11 model can be chosen in this way. Fig. 5.6 shows the $\%E_\theta$ computed at 2.6 MHz for various fuselage radii. The dashed line on the diagram indicates the measured value of $\%E_\theta$, which intersects the computed curve at a radius equal to 0.3 m. Thus the wire radius for the fuselage TRN11 model should be chosen as 0.3m to match the measured $\%E_\theta$ at this frequency.

When the radiation patterns of the TRN11 model with the 0.3 m fuselage radius are examined at 2.6 MHz, an error of about 9 dB is observed in the elevation cut (phi equal to 90 degrees) in the E_ϕ polarization as shown in Fig. 5.7. This error

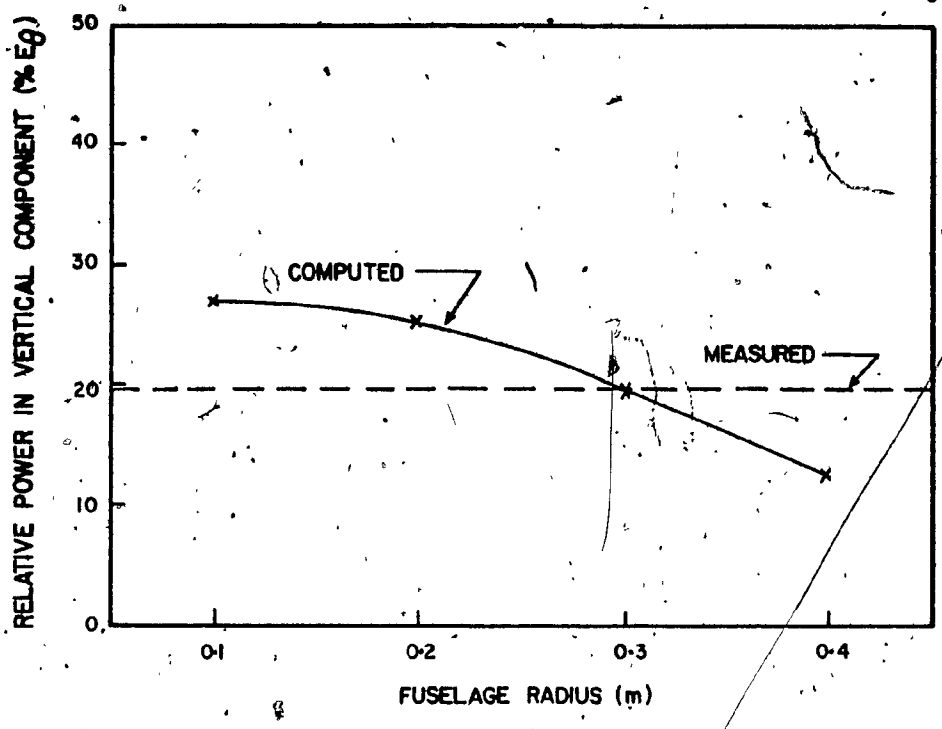

Fig. 5.6 Tranline antenna $\%E_\theta$ at 2.6 MHz, obtained using the TRN11 model as a function of fuselage radius.

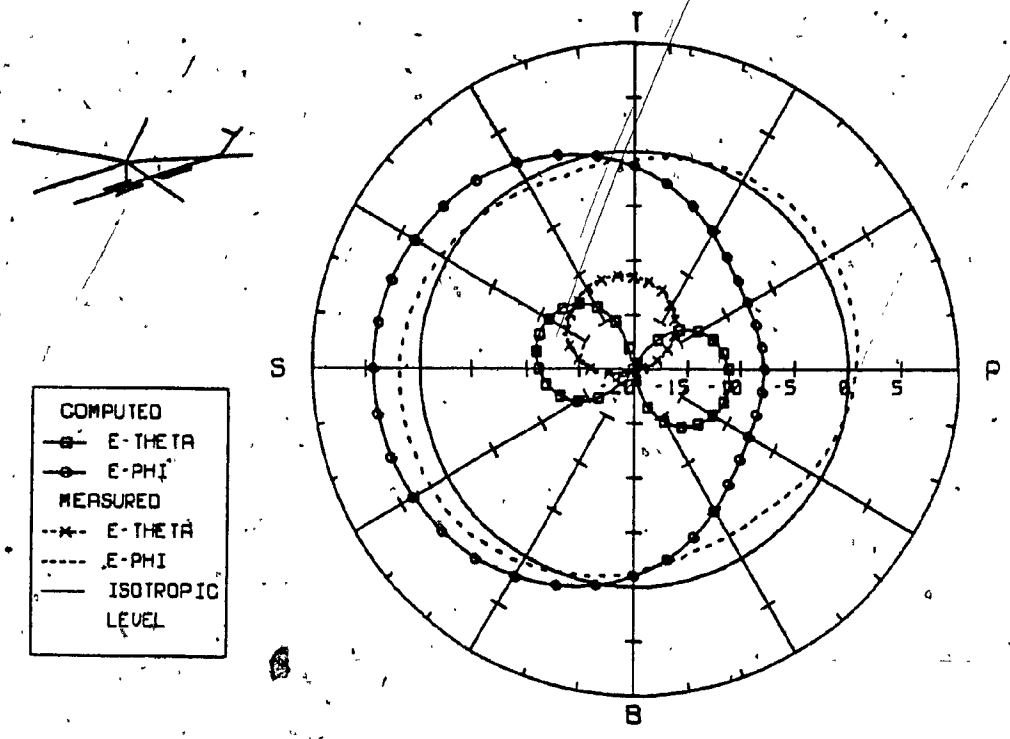

Fig. 5.7 Tranline antenna elevation pattern (ϕ=90) obtained using the TRN11 model with 0.3m fuselage radius at 2.6 MHz, compared to the measured pattern on a dB-scale.

is seen at the port side of the helicopter model which is where the antenna is located. The poor agreement is due to the close spacing of 0.6 m between the fuselage and the antenna. The methods used in the NEC program impose limitations on the closeness of the spacing of parallel wires and the manual recommends that the wires should be maintained several radii apart [32]. Recall from Section 5.2.1 that the radius of the antenna on the TRN11 model is 0.1 m. Such a radius is too thick because it is much greater than that of the actual antenna. Therefore, the first step in correcting the error discussed above is to change the antenna radius from 0.1 m to 0.01m. Using the simple model with thick fuselage radius of 0.3 m and 0.01 m for the antenna radius, a series of NEC runs were executed at 2.6 MHz for different values of the fuselage-antenna spacing. For each run the difference between the computed and the measured E_ϕ at the port side, which is theta equal to 90 degrees and phi equal to 90 degrees, was recorded, and these "error" values are plotted as a function of fuselage-antenna spacing and shown in Fig. 5.8. The curve shows that the difference between the measured E_ϕ and the computed E_ϕ is reduced from 9 dB for a separation of 0.6 m, to 0.5 dB for a separation of 1.2 m. Therefore a separation of 1.2 m was used in the subsequent runs. Fig. 5.9 shows the elevation pattern for phi equal to 90 degrees, obtained from the simple model with the 1.2 m separation between the fuselage and the antenna. The figure shows good agreement between measured and computed E_ϕ polarization, whereas poor agreement can be seen in the E_θ

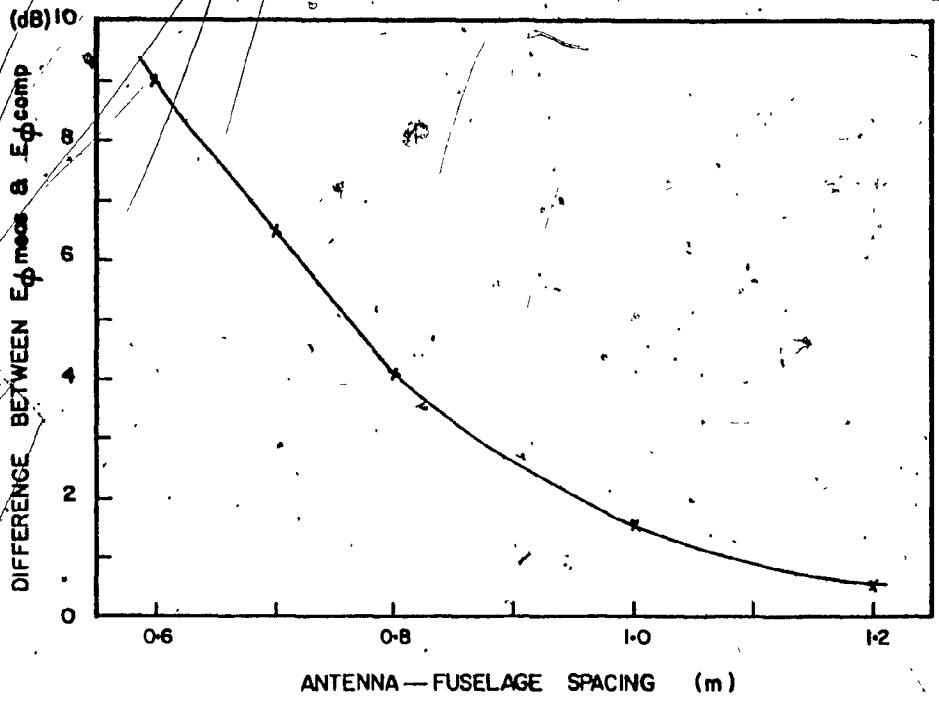

Fig. 5.8 Pattern error as a function of antenna-fuselage spacing, obtained using the TRN11 model at 2.6 MHz, Elevation pattern (ϕ=90), E_ϕ polarization.

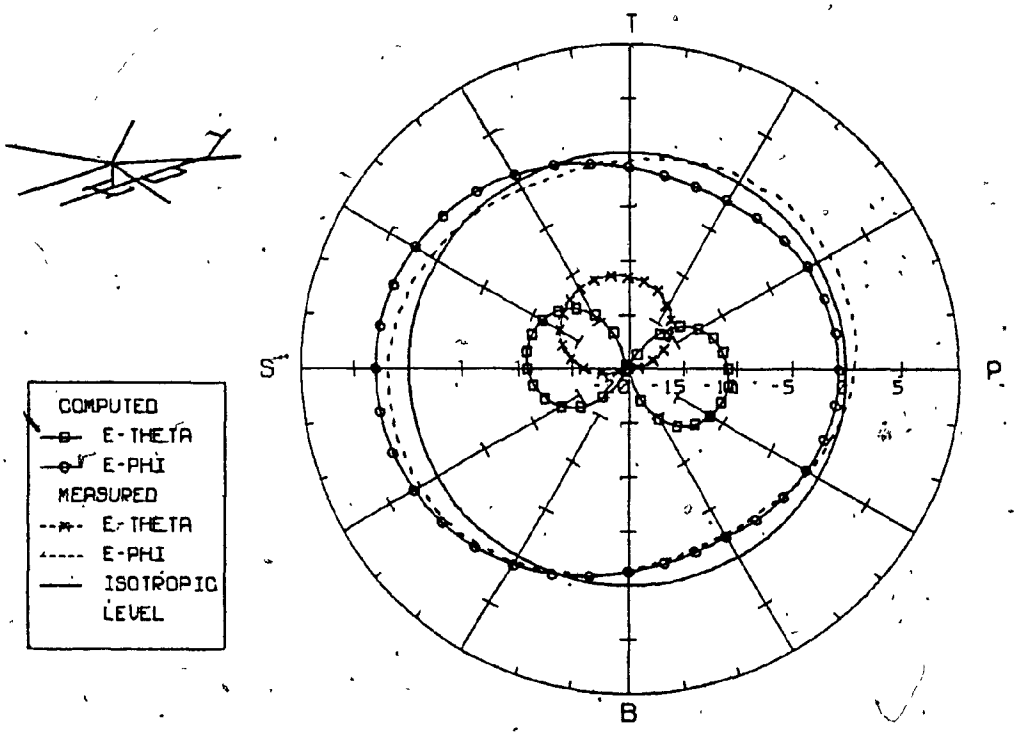

Fig. 5.9 Tranline antenna elevation pattern at 2.6 MHz obtained using the simple Sea-king model with 0.3m fuselage radius and 1.2m antenna fuselage spacing, compared to measured pattern.

polarization. This poor agreement is attributed to errors in the measured E_θ pattern since it could not be reproduced even with complex models of the Sea-King helicopter later in this chapter. The sponsons of the helicopter are modelled with wires which are parallel to the fuselage, and spaced only 0.6 m from it. This was considered too close and so was changed to 1.2 m for the reasons discussed above. The model arrived at after these tests will be referred to as TRN18 and is shown in Fig. 5.10.

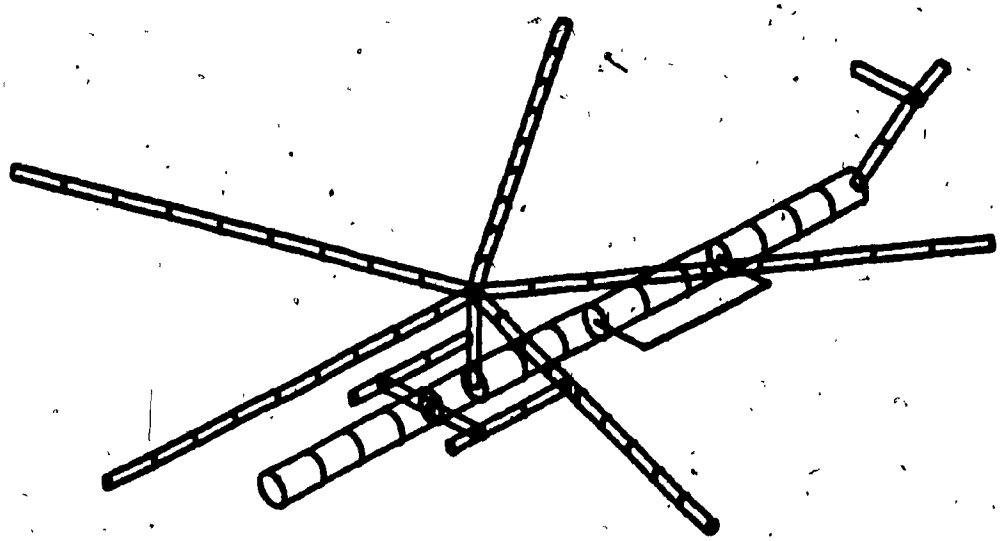

Fig. 5.10 Radius representation of the TRN18 model of the Sea-King helicopter, Tranline antenna mounted on the port side of the model.

The TRN18 model was evaluated at frequencies between 2.6 and 14 MHz. The relative power contained in E_θ is plotted as a function of frequency and shown in Fig. 5.11, where the computed $\%E_\theta$ values are joined by a dashed line, and the measured values are joined by a solid line. The figure shows that computed and measured $\%E_\theta$ correspond at all frequencies except 8.1 MHz, where the measured $\%E_\theta$ is 20 percent larger.

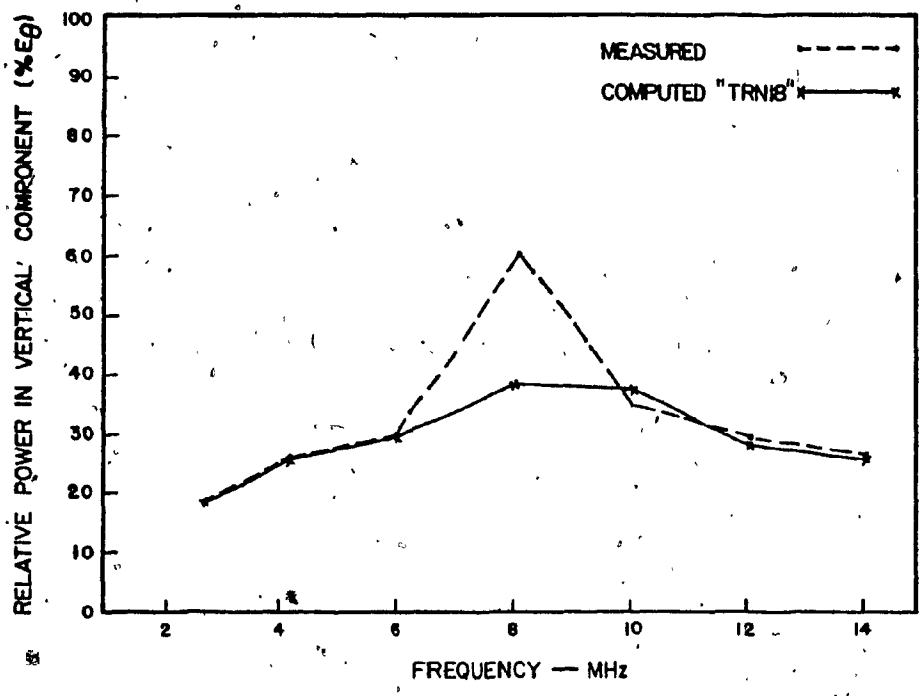

Fig. 5.11 Tranline antenna $\%E_\theta$ obtained using the TRN18 model, compared to the measured $\%E_\theta$ as a function of frequency

The azimuth radiation patterns produced using the TRN18 model are shown in Fig. 5.12(a-d), at 2.6,4.1,6.0 and 8.1 MHz. Fig. 5.12(a) shows that the measured E_ϕ polarization pattern at 2.6 MHz is reproduced by the TRN18 model. This is considered an improvement over the results obtained in Fig. 5.3(a). The computed E_θ polarization is a duplicate of that produced by the TRN11 model. The computed E_ϕ polarization at 4.1 MHz of Fig. 5.12(b) disagrees with the measured pattern at the minima by about 4 dB compared to 12 dB seen in Fig. 5.3(b). At 6.0 MHz the pattern of Fig. 5.12(c) maintains good agreement between measured and computed values in E_θ and E_ϕ. Such good agreement was produced earlier by the TRN11 model, which indicates that the helicopter is not resonant at 6.0 MHz, and therefore small changes in the wire-grid model do not greatly affect the radiation characteristics at this frequency. At 8.1 MHz Fig. 5.12(d) shows that the match between measured and computed patterns degrades in orientation and level for the E_ϕ polarization from those presented in Fig. 5.3(d). The computed E_ϕ pattern is similar in shape to the measured pattern, but is rotated by about 20 degrees in angle. The computed E_θ polarization maintains the elliptical figure but its level differs from the measured pattern by about 4 dB less. Simple models such as the TRN11 and the TRN18 model are not adequate at resonance frequencies of 8.1 MHz or higher. This frequency was identified as a resonant one from the Tranline evaluation in Chapter 3.

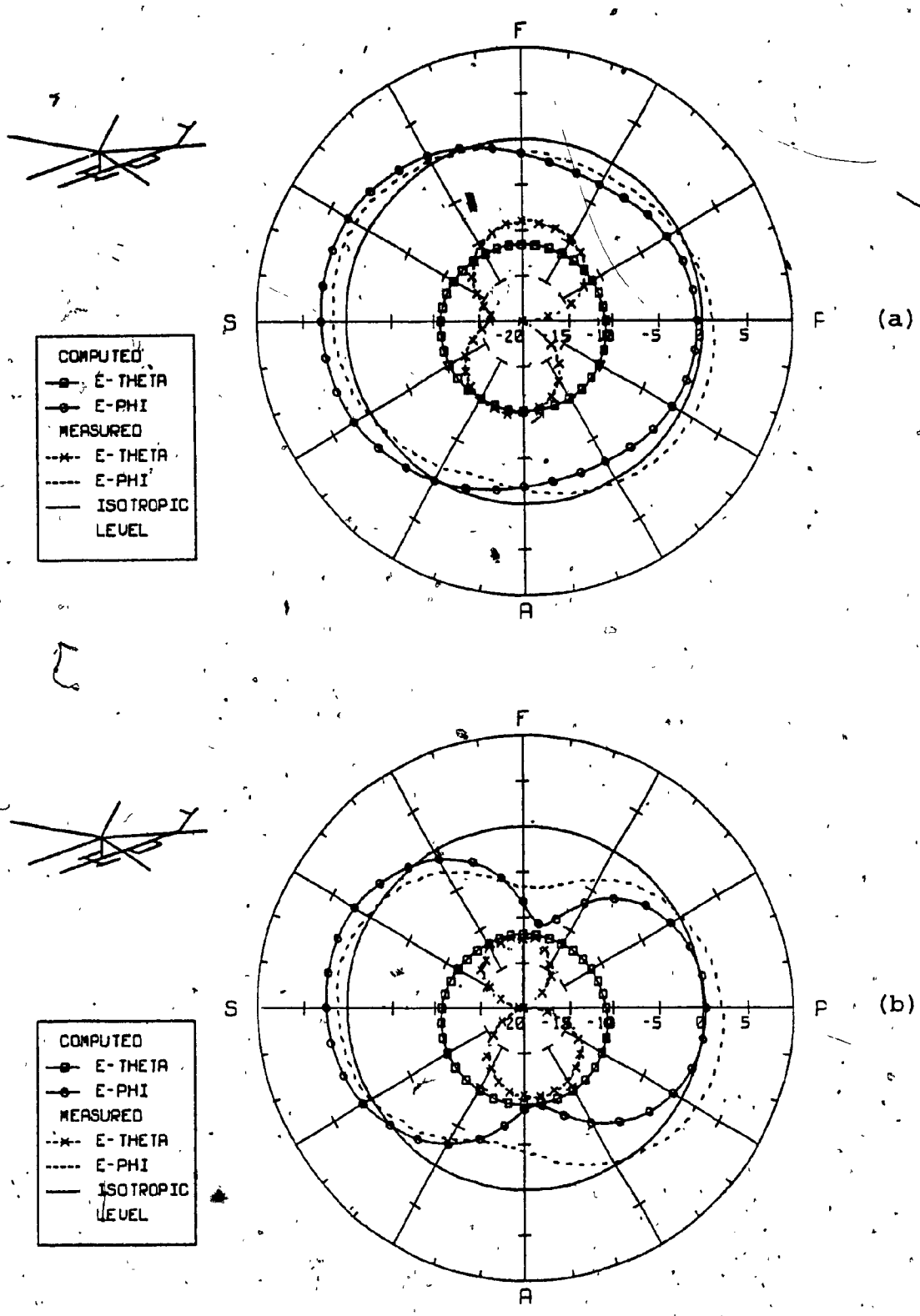

Fig. 5.12 Tranline antenna azimuth patterns obtained using the TRN18 model, compared to the measured patterns at (a) 2.6 MHz, (b) 4.1 MHz, dB-sacle.

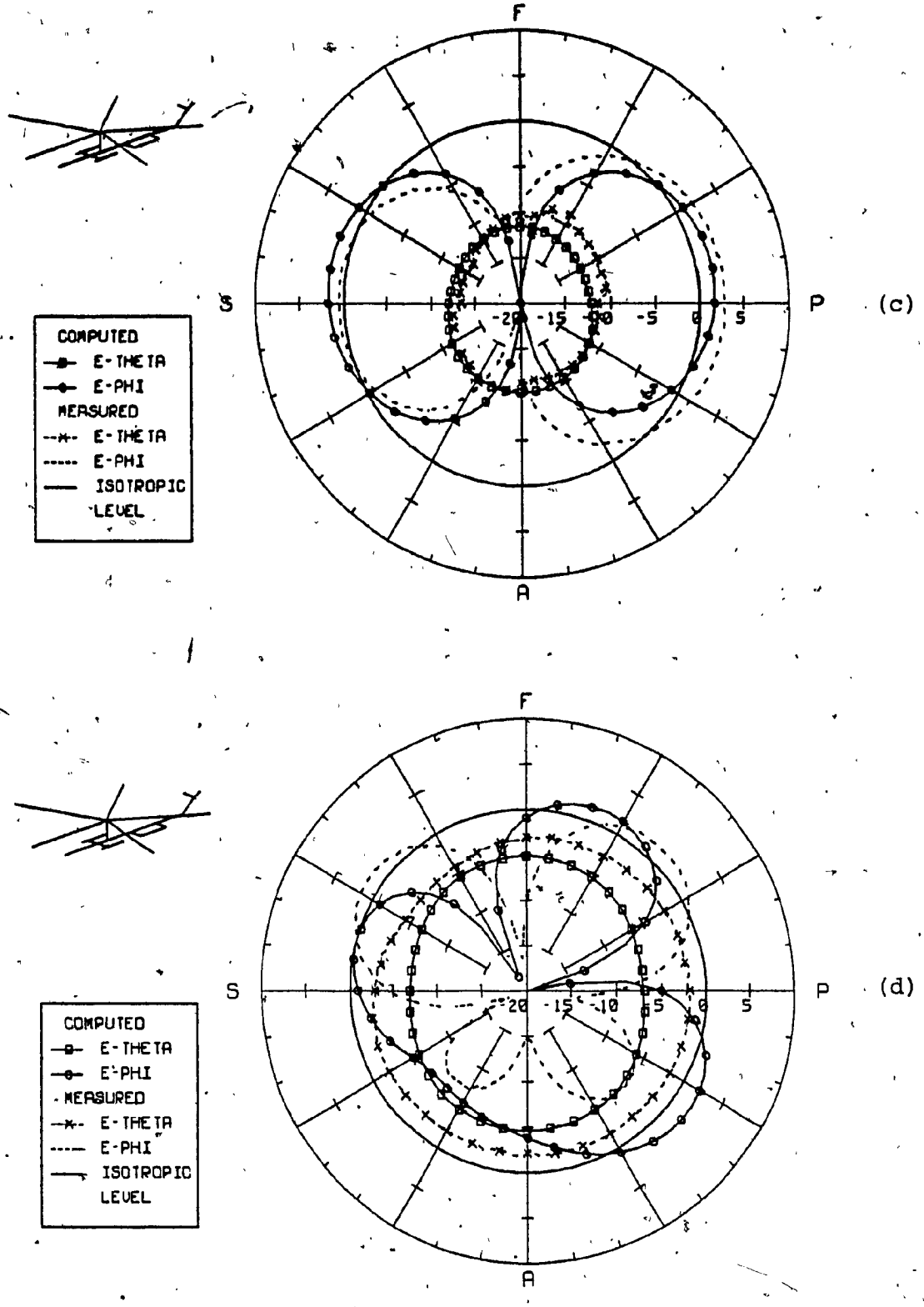

Fig. 5.12 (cont'd) Tranline antenna azimuth patterns obtained using the TRN18 model, compared to the measured patterns at (c) 6 MHz, (d) 8.1 MHz, dB-scale.

5.2.3 Comparison of Surface Plots - Measured and Computed -

Fig. 5.13 shows surface plots of complete sets of measured and computed conical radiation patterns at 2.6 MHz, for both polarizations. The plots display the theta angle on one horizontal axis and the phi angle on the other horizontal axis. The field strength of either polarization is displayed on the vertical axis. The field values are normalized such that the maximum of both polarizations at a certain frequency is set at 100 V/m. Fig. 5.13(a) shows a surface plot of the measured E_θ polarization at 2.6 MHz. The figure presents a surface with null locations at phi equal to 100 and 270 degrees. Hence all the E_θ conical patterns at 2.6 MHz have a figure eight pattern. This is clearly seen in the azimuth pattern of Fig. 5.3(a). Fig. 5.13(c) shows the surface plot of the set of conical cuts computed using the TRN11 computer model at 2.6 MHz. The surface is flat in the vicinity of theta equal to 90 degrees, which is the major difference with the measured surface of Fig. 5.13(a). This flat surface represents omnidirectional patterns which are located in the angle sector for $72 < \theta < 120$ degrees. In Fig. 5.13(e), the surface plot of the E_θ radiation patterns obtained from the TRN18 computer model is closer to the measured surface than that obtained from the TRN11 model. The main improvement in the TRN18 E_θ surface is the level of the patterns. Fig. 5.13(b) shows a surface plot of the measured E_ϕ polarization at 2.6 MHz. The display shows minima locations at

phi equal to zero and 180 degrees in the conical patterns for theta near zero and 180 degrees, but the patterns become more uniform because the surface becomes flatter for theta near 90 degrees. The computed E_ϕ polarization obtained from the TRN11 shows a surface plot with deep minima at phi equal to zero and 180 degrees as shown in Fig. 5.13(d) and this is a major difference with the measured E_ϕ surface plot. The TRN18 model shows better agreement with the measurement. Thus Fig, 5.13(f) shows that E_ϕ polarization of the TRN18 model behaves similarly to the measured plot of Fig. 5.13(b).

The surface plots of measured and computed radiation patterns at 4.1 MHz are similar to those described in Fig, 5.13(a-f), and are not presented here. The surface plots at 6.0 MHz show that the measured plots are reproduced by the computed patterns equally well using the TRN11 or the TRN18 computer model. Neither simple model is adequate at 8.1 MHz which is a resonant frequency. At 8.1 MHz the surface plots are presented later in this chapter when a complex model of the Sea-King helicopter is compared with the simple TRN18 results.

The work presented in this section indicates that numerical model optimization is effective when parametric studies are made against the assessment parameters and patterns are compared on the basis of surface plots.

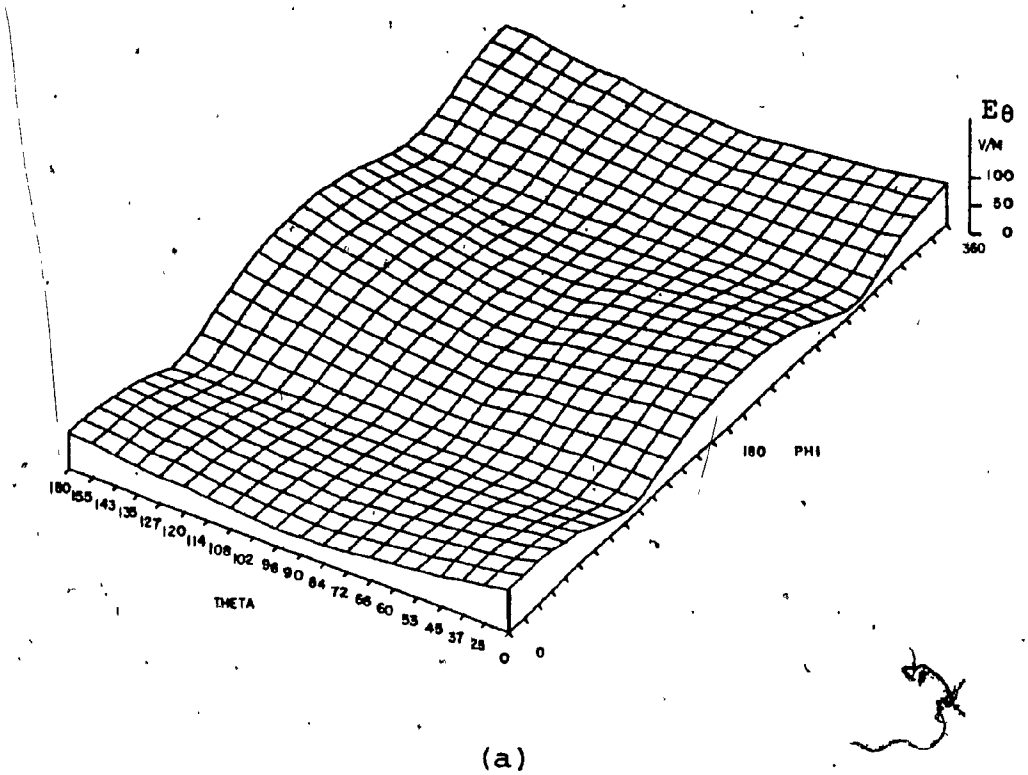

(a)

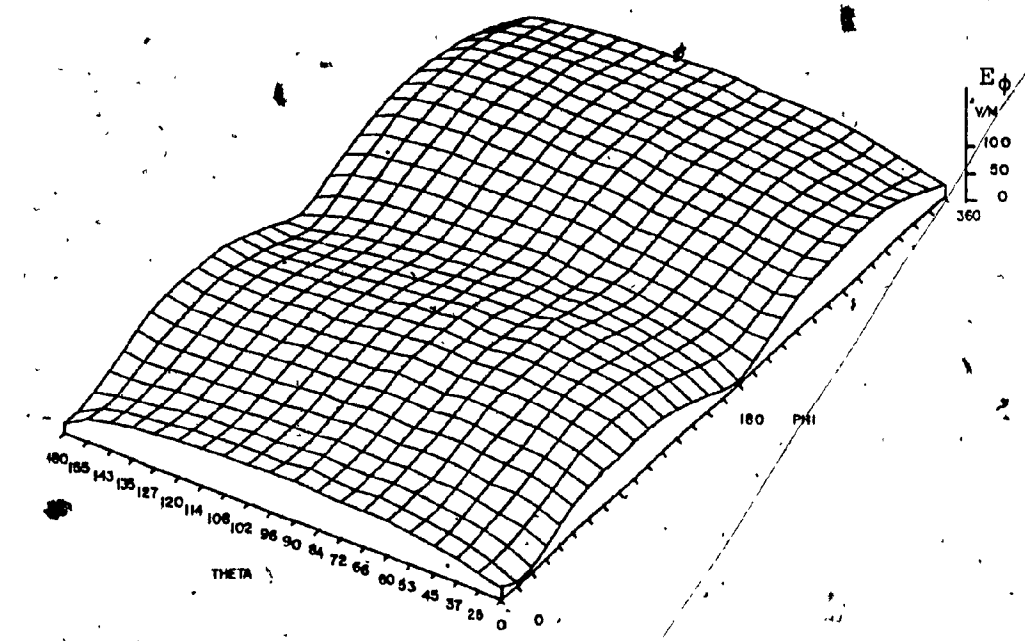

(b)

Fig. 5 .13 Tranline antenna surface plots of the measured conical patterns at 2.6 MHz, for (a) E-theta polarization, (b) E-phi polarization.

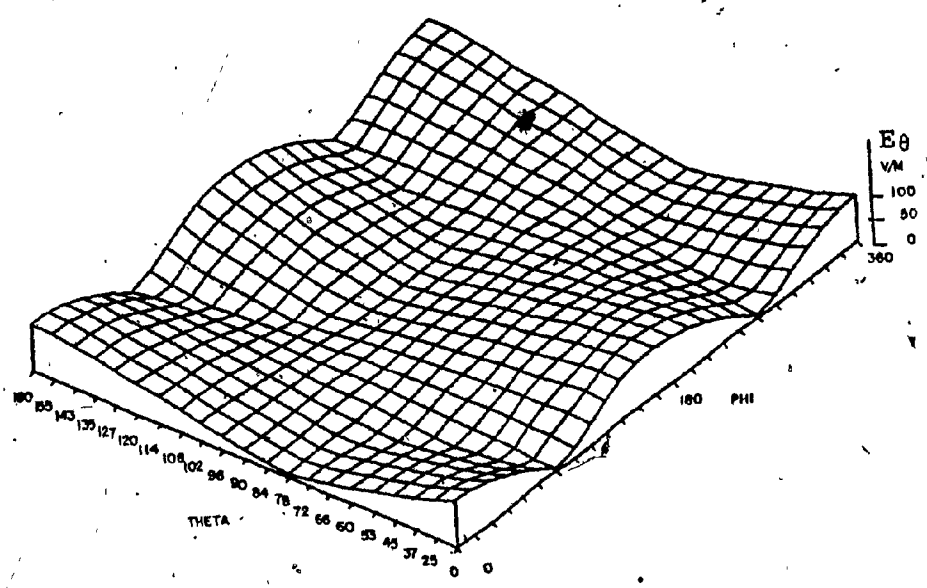

(c)

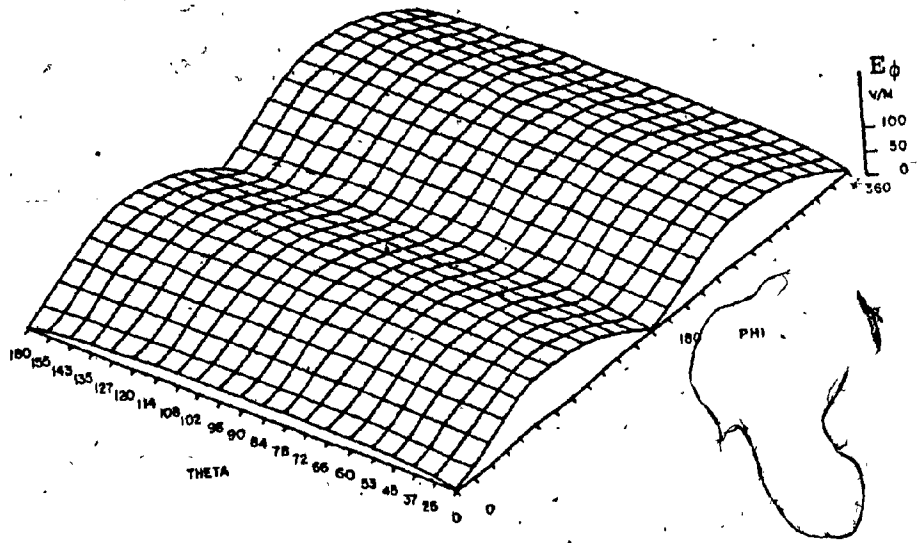

(d)

Fig. 5.13 (cont'd), Tranline antenna surface plots of the conical patterns obtained using the TRN11 model at 2.6 MHz for (c) E-theta polarization, (d) E-phi polarization.

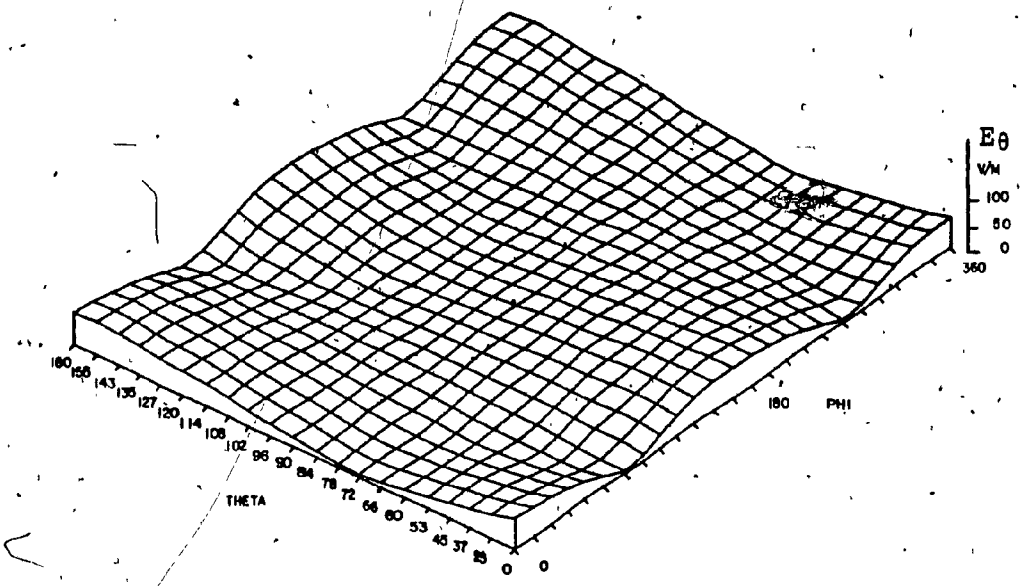

(e)

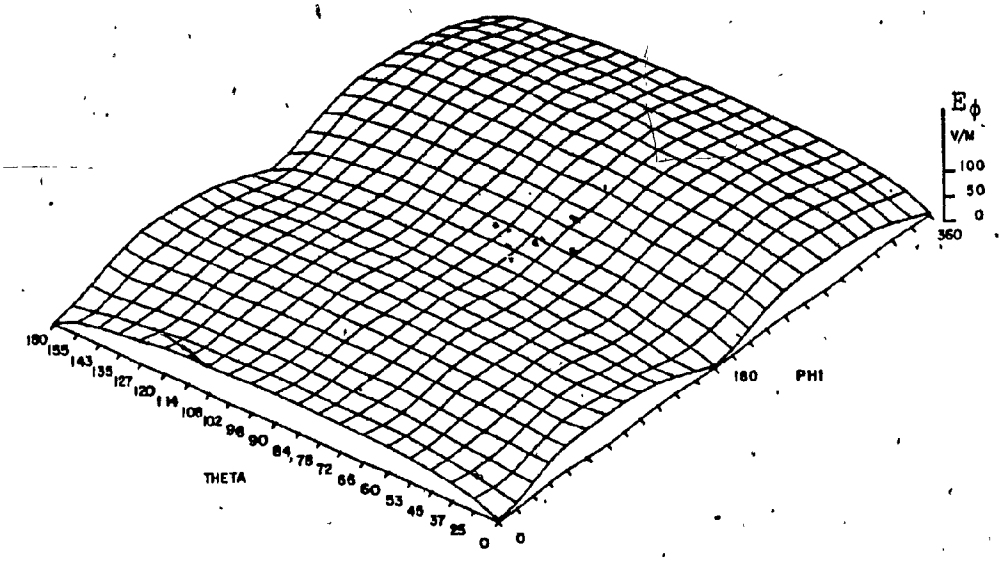

(f)

Fig. 5.13 (cont'd), Tranline antenna surface plots of the conical patterns obtained using the TRN18 model at 2.6 MHz, for (e) E-theta polarization, (f) E-phi polarization.

5.2.4 Current Distribution Analysis for the Simple Model

The lobe structure of the radiation patterns can be directly related to the current flowing on the wires of the helicopter model. Indeed it will be seen that certain wires of the model can be directly associated with the orientation of the pattern shape. Thus a vertical wire carrying a strong current radiates an omnidirectional azimuth pattern and a figure eight in elevation and this contribution can often be seen in the overall radiation pattern of the helicopter model. In addition, if such a wire is a part of a resonant path that carries a strong current, the contribution of the long wires of this path will dominate the radiation patterns. Such a path will be called a "principal radiator" or "principal current path".

The current distribution on the TRN18 model presents two interesting cases. First, at 2.6 MHz, the high current is confined to the loop formed by the wires 4, 21, 22 and 23 of Fig. 5.1, which model the Tranline antenna itself and its return path along the fuselage. Fig. 5.14(a) displays a complete picture of the magnitude of the current at the center of each segment of the "TRN18" model at 2.6 MHz. A collinear display of the complex current amplitude on this loop is shown in Fig. 5.14(b). The figure shows the magnitude of the current on a scale of 0 to 10,000 microamps, and the phase of the current where zero phase current corresponds to the direction shown by the arrows in Fig. 5.14(a). It is seen that the loop carries a constant current both in magnitude and phase on all its wires.

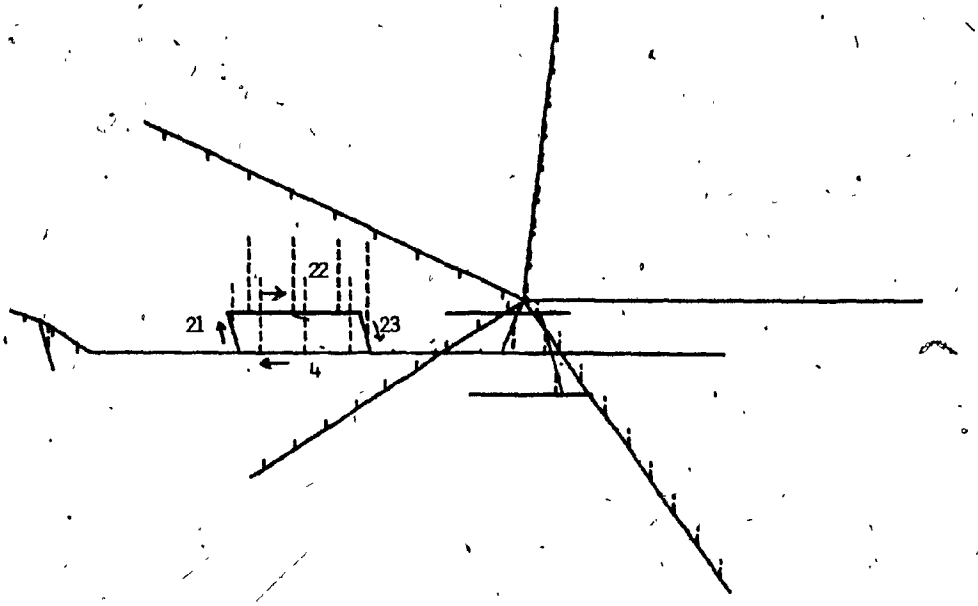

Fig. 5.14(a) Amplitude of the current distribution plotted on the TRN18 model at 2.6 MHz.

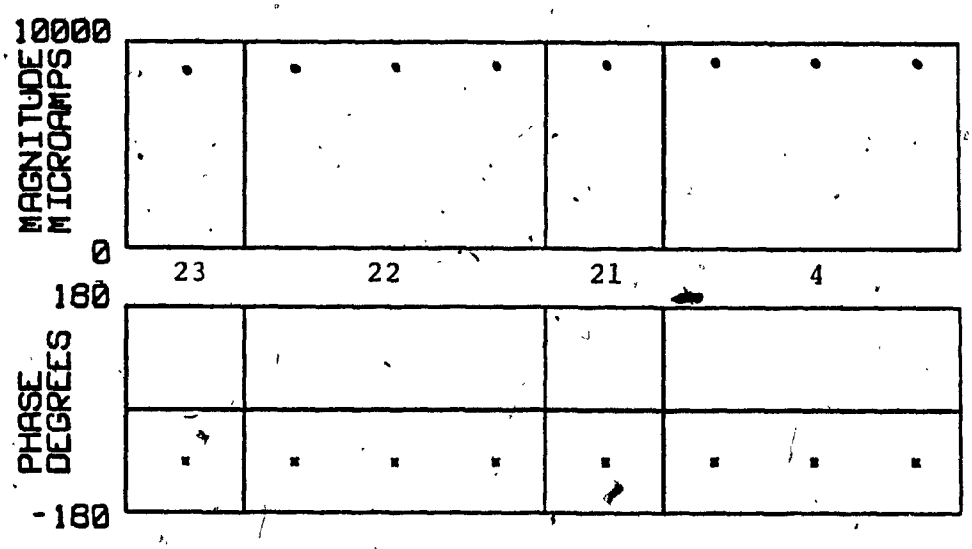

Fig. 5.14(b) Current distribution, amplitude and phase flowing on the loop formed by the Tranline antenna and its return path along the fuselage of the TRN18 model at 2.6 MHz.

The loop length is 8.5 m in the TRN18 model. Fig. 5.14(a) shows that this loop carries by far the strongest currents on the model and is the "principal radiator" at 2.6 MHz. The methods of Section 4.3 were used to compute the radiation pattern of only the wires making up the loop, and Fig. 5.15 shows the azimuth pattern of the loop alone. Note that the isotropic level is set to zero dB in all figures so that the levels of E_ϕ in Fig. 5.15 and in the patterns of the complete TRN18 model of Fig. 5.12(a) can be compared directly. A zero E_θ field strength is obtained in this pattern since the horizontal orientation of the loop makes radiation of an E_θ component vanish in the azimuth plane. Comparing Fig. 5.12(a) for

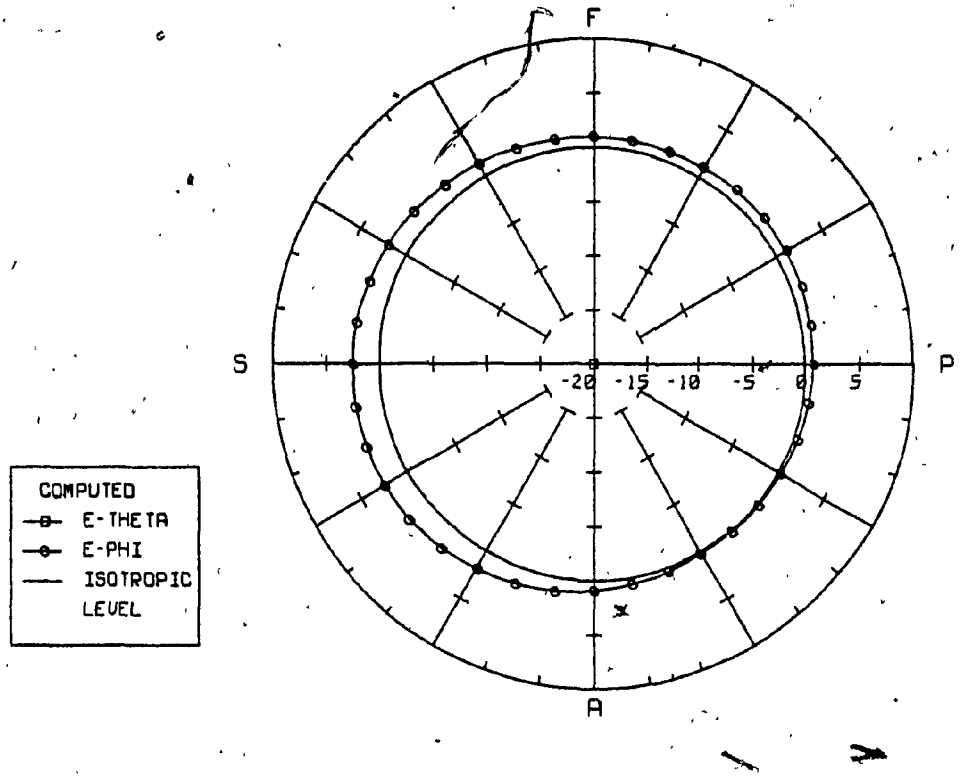

Fig. 5.15 Azimuth pattern calculated from the current flowing on the loop formed by the Tranline antenna and its return path along the fuselage of the TRN18 model at 2.6 MHz, (dB-scale).

the complete TRN18 model with the azimuth pattern of the loop alone, it is seen that the complete pattern is dominated in the E_ϕ azimuth plane. Comparing Fig. 5.12(a) for polarization by the omnidirection pattern of the loop alone. This indicates that the loop is the principal radiator at 2.6 MHz, and therefore any changes in the geometry of the loop will be clearly reflected in the radiation patterns. This was seen from the discussion of Section 5.2.2, where a large pattern change was obtained by moving the loop further from the fuselage. At 2.6 MHz, the E_θ polarization in the azimuth is produced mainly by the vertical wire of the drive shaft, this was seen in the omnidirection E_θ pattern of Fig. 5.12(a) of the TRN18 model. Although the horizontal loop does not affect the azimuth E_θ pattern directly, it was noticed that when varying the spacing between the fuselage and the antenna, the current on the drive shaft changed from about 200 microamps for a spacing of 0.6 m to 350 microamps for a spacing of 1.2m. Thus special care must be given to the loop at the low end of the HF band since it stands as the major radiator of the far field.

The second case deals with the contribution of the drive shaft and rotor blades to the far field at 8.1 MHz. Fig. 5.16(a) displays a complete picture of the magnitude of the current on each wire of the TRN18 model at 8.1 MHz. The figure shows that currents on the drive shaft and the rotor blades are stronger than those seen in Fig. 5.14(a). A collinear display of the complex current on the drive shaft and the rotor blades is shown in Fig. 5.16(b). The magnitude of the current is being

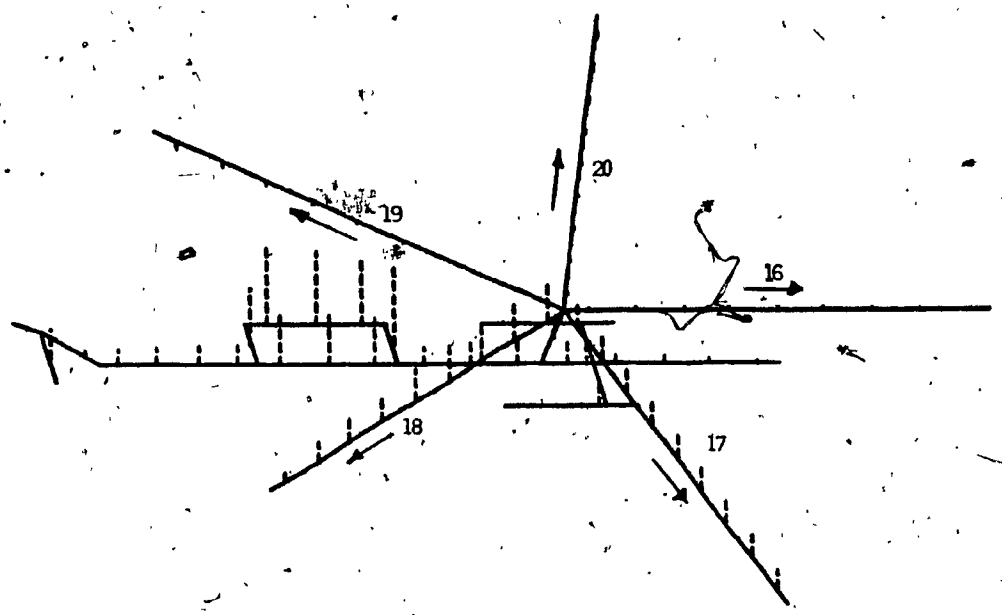

Fig. 5.16(a) Amplitude of the current distribution plotted on the TRN18 model at 8.1 MHz.

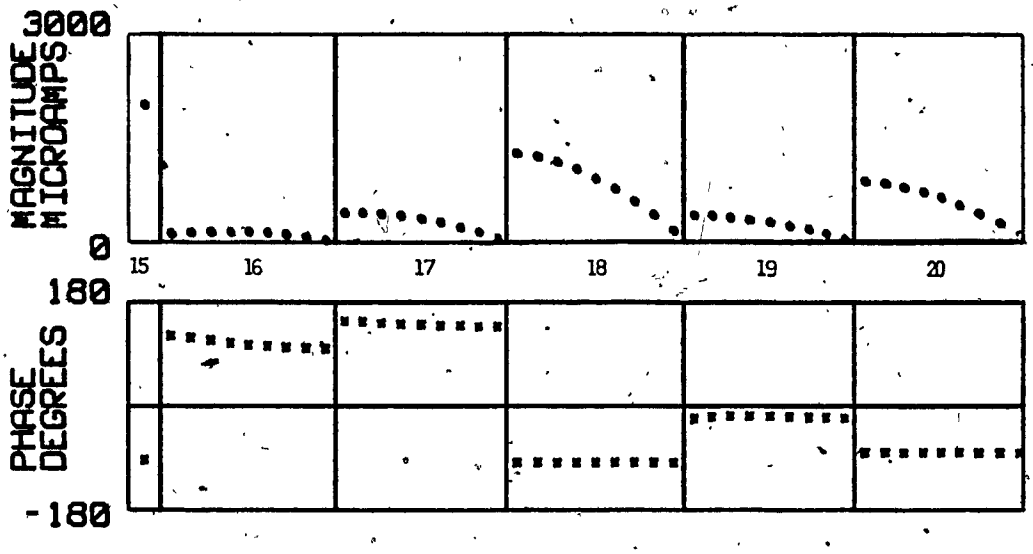

Fig. 5.16(b) Current distribution, amplitude and phase flowing on the drive-shaft and the rotor blades of the TRN18 model at 8.1 MHz.

displayed on a scale of 0 to 3000 microamps, and the zero phase current corresponds to the direction of the arrows in Fig. 5.16(a). It is seen that the current flowing on the drive shaft is about 2000 microamps at 8.1 MHz compared to 350 microamps at 2.6 MHz. Fig. 5.16(b) shows that the magnitude of the current flowing on each rotor blade is maximum at the end connected to the drive shaft and decreases sinusoidally toward the free end of the blade. Among the five blades, the lowest current magnitude is seen on the forward blade which has the same direction as the fuselage. Whereas the blade of wire number 18 has a maximum current of about 1500 microamps. The current phase on the rotor blades varies between 170 degrees and -90 degrees at 8.1 MHz compared to a constant phase of about 170 degrees at 2.6 MHz. This strong current seen on the drive shaft and the rotor blades at 8.1 MHz can influence the orientation of the radiation pattern characteristics of the TRN18 model. The azimuth radiation pattern due to the current flowing on the drive shaft and the rotor blades at 8.1 MHz is shown in Fig. 5.17. The E_θ polarization is similar to that obtained with the complete TRN18 model. The figure shows that the E_θ pattern has the same elliptical orientation presented earlier in Fig. 5.12(d). In the E_ϕ polarization Fig. 5.17 does not resemble the exact orientation of that obtained with the complete TRN18 model. However a considerable amount of far field radiation can be seen in E_ϕ polarization of Fig. 5.17. The drive shaft/rotor blades section is considered a sensitive part of the helicopter. It forms a part of a resonant path at

8.1 MHz. Thus any parametric studies at 8.1 MHz must include such a section, which would influence the radiation characteristics.

The methodical development of the simple model has been successful in many ways. It includes the method of evaluating parametric studies by the use of assessment parameter namely $\%E_\theta$. The identification of the important section of the simple model at different frequencies is the basis of further studies when more complex models are considered in this chapter. The next section will attempt to look at changes in the results when a complex model of the Sea-King helicopter is used.

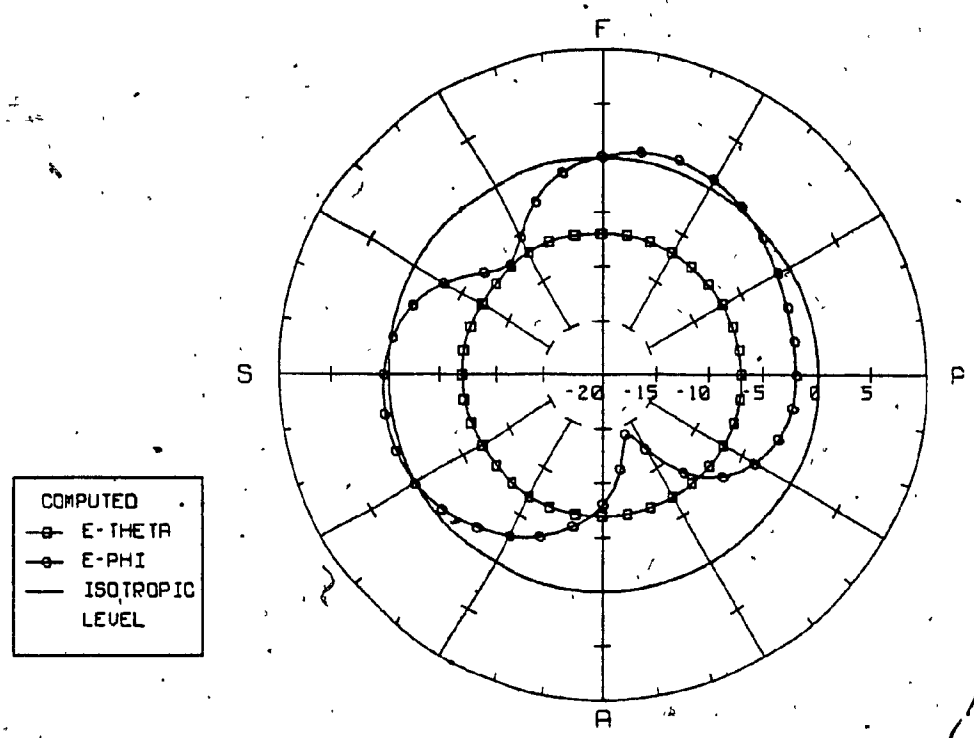

Fig. 5.17 Azimuth pattern calculated from the current flowing on the drive-shaft and the rotor blades of the TRN18 model at 8.1 MHz, (dB-scale).

5.3 Intermediate Model of the Sea-King Helicopter

Fig. 5.18 shows a wire-grid model of the Sea-King helicopter called the "TRN30" model. This section demonstrates the changes that come about when the simple "TRN18" model is increased in complexity to obtain the "TRN30" shown in this figure. It will be shown that this more complex model results in patterns that more closely reproduce the measurements at 2.6, 4.1 and 6.0 MHz, but that the agreement is not much better at 8.1 MHz in the E_ϕ polarization.

The TRN30 model is derived as follows. The fuselage is represented by rectangular grids of wires using rectangles of different sizes to model the length of the fuselage. The nose and the end of the fuselage are modelled by a four wire "pyramid" as shown in Fig. 5.18. The sponsons are represented by single wires on both sides of the fuselage. The Tranline antenna is mounted on the port side of the helicopter. The main rotor blades are oriented in the forward position of Fig. 2.7. The drive shaft which connects the main rotor blades to the fuselage is represented by a single wire of 0.6 m in length. For simplicity, the back rotor blades are not modelled. This "intermediate" model is excited by a voltage source applied to wire number 81 indicated in Fig. 5.18.

The total number of segments making up the TRN30 model is 143, which is about twice the number of segments making up the TRN18 simple model. Fig. 5.19 shows that a uniform radius of 0.1 m is used for all the wires making up the model except for the Tranline antenna where a 0.01m radius is used.

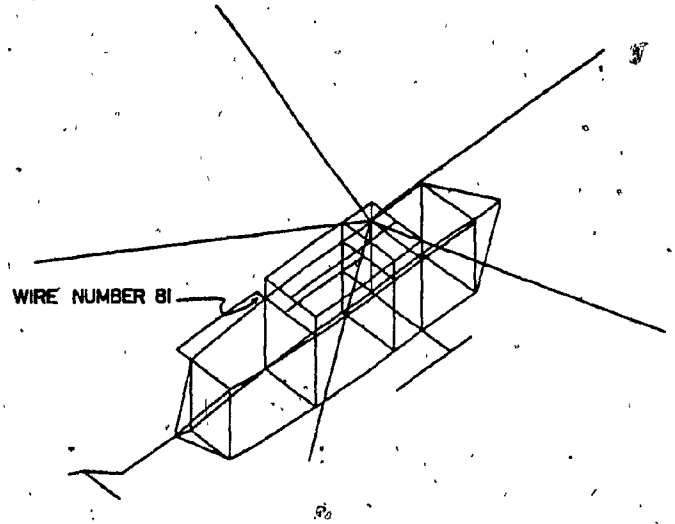

Fig. 5.18 The TRN30 intermediate model of the Sea-King helicopter, Tranline antenna mounted on the port side of the model.

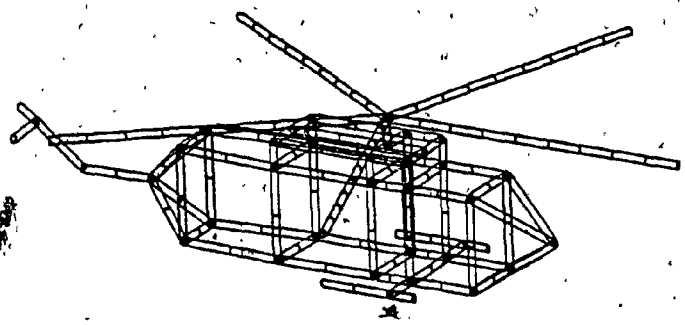

Fig. 5.19 Uniform radius representation of the TRN30 model of the Sea-King helicopter.

The purpose of the TRN30 model is to examine the changes in the radiation patterns that come about when the complexity of the model is increased over that of the TRN18 model. The TRN30 model is not a fully detailed wire-grid model of the Sea-King helicopter. It is a reasonable wire-grid approximation which models the main components of the helicopter airframe. The following is a presentation of the azimuth radiation patterns using the TRN30 at 2.6,4.1,6.0 and 8.1 MHz.

5.3.1 Radiation Patterns of the Intermediate Model

The current distribution on the TRN30 "intermediate" model of the Sea-King helicopter and the far field radiation patterns for both polarization E_θ and E_ϕ are obtained by executing NEC, using the TRN30 geometry as its data.

Fig. 5.20(a-d) shows the azimuth patterns for the theta equal to 90 degrees at 2.6, 4.1, 6.0 and 8.1 MHz. Fig. 5.20(a) displays the azimuth patterns for both the measured and the TRN30 computed patterns in both polarizations at 2.6 MHz. The computed E_ϕ pattern reproduces the elliptical measured patterns in both orientation and level. The computed E_θ has the figure eight pattern similar to the measured one, but is about 5 dB higher in level at the maximum of the pattern. The TRN18 azimuth pattern of Fig. 5.12(a) showed an omnidirectional E_θ pattern but with about the same level as the measured one. Thus the main difference between the two computer models is that the TRN30 model reproduces the figure eight in shape and orientation

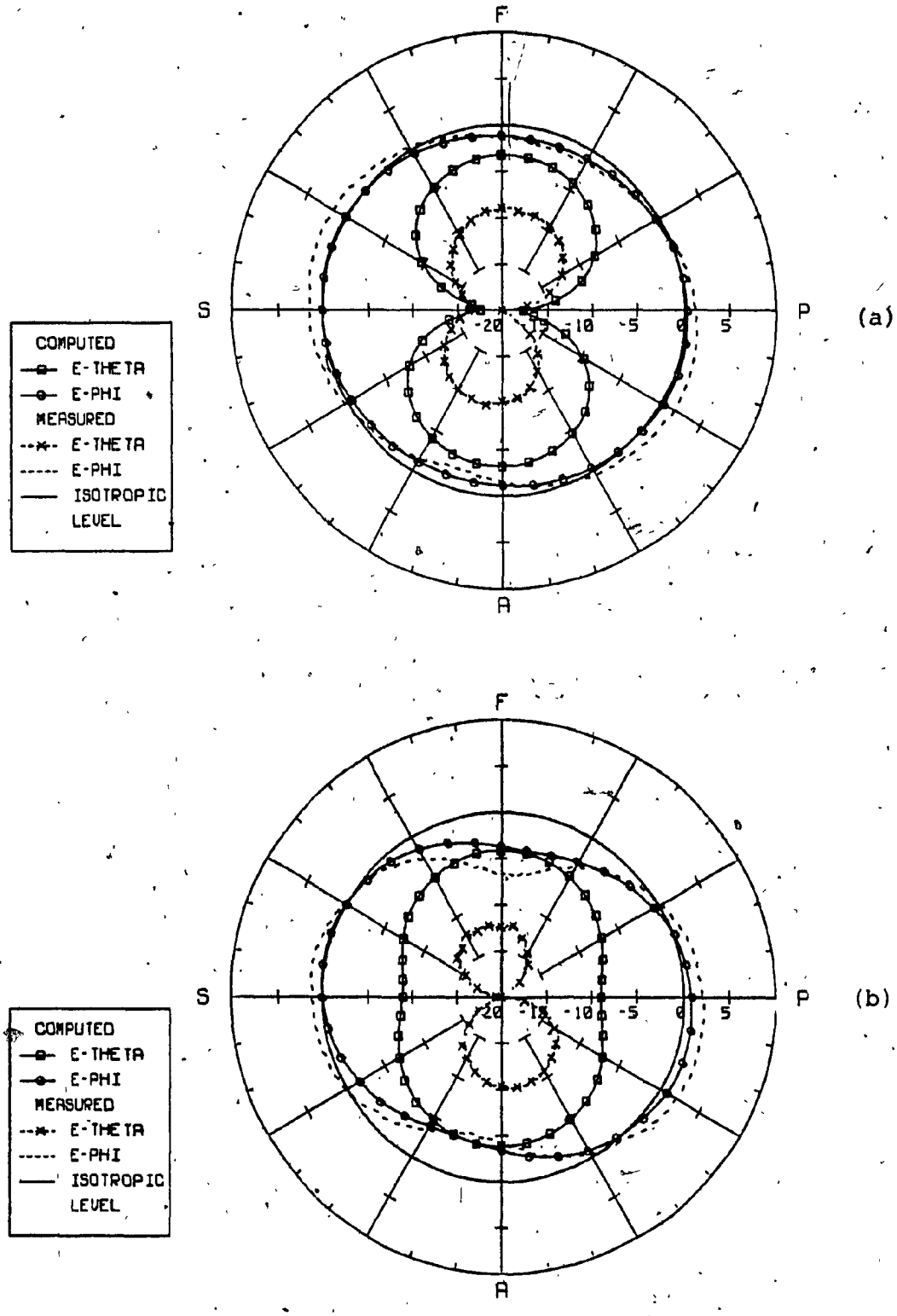

Fig. 5.20 Tranline antenna azimuth patterns obtained using the TRN30 model, compared to the measured patterns at (a) 2.6 MHz, (b) 4.1 MHz, (dB-scale).

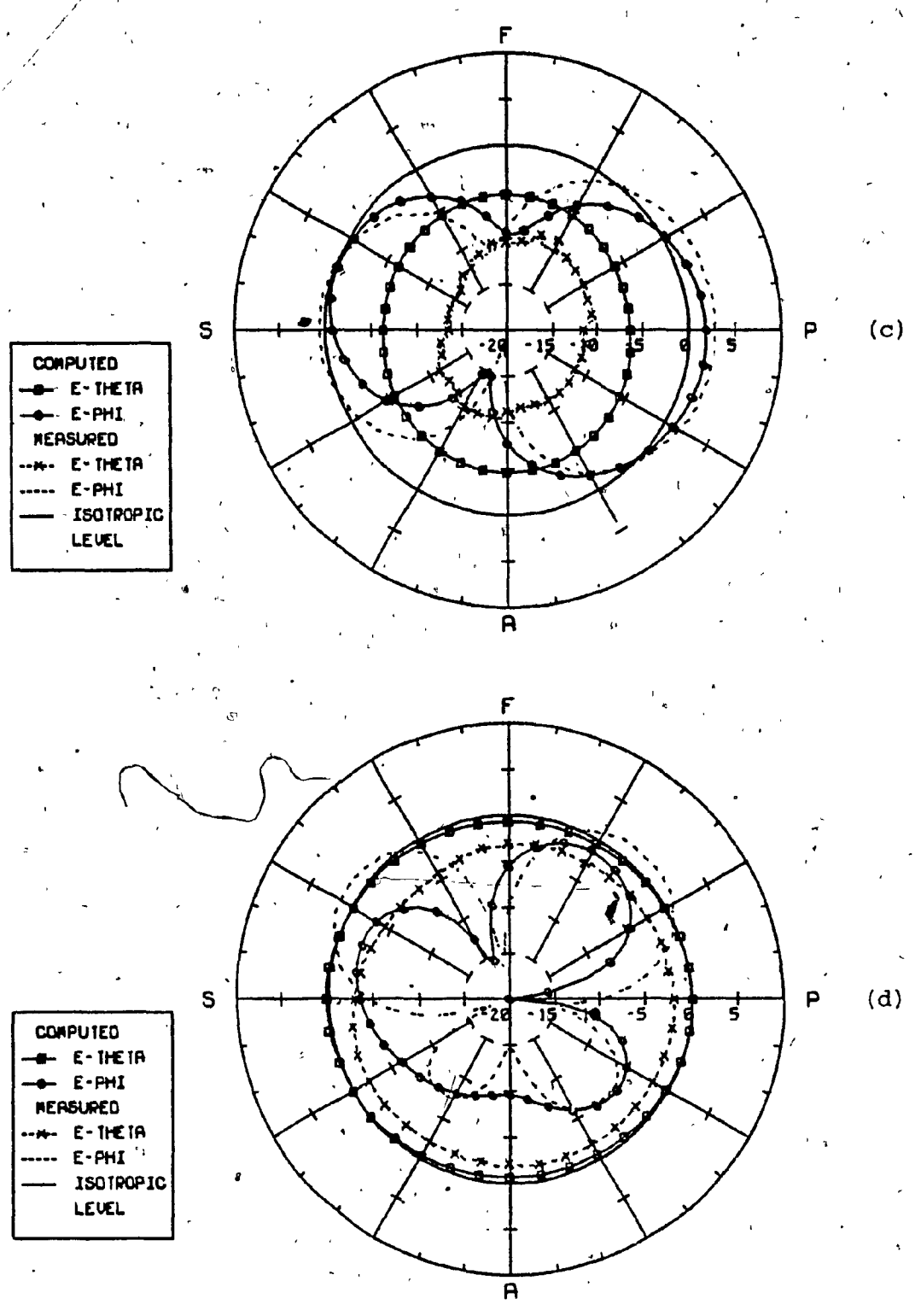

Fig. 5.20 (cont'd) Tranline antenna azimuth patterns obtained using the TRN30 model, compared to the measured patterns at (c) 6 MHz, (d) 8.1 MHz, dB-scale.

of the measured E_θ pattern, whereas the TRN18 model did not reproduce the shape but only the level. Fig. 5.20(b) compares the TRN30 computed azimuth pattern to the measured one at 4.1 MHz. This pattern behaves in a similar way to the pattern obtained at 2.6 MHz of Fig. 5.20(b). The computed E_ϕ polarization reproduces the elliptical figure of the measured pattern with good agreement in level. The computed E_θ polarization resembles the figure eight of the measured E_θ pattern but at a 7 dB higher level, and with shallower minima. At 6.0 MHz the computed E_ϕ polarization agrees with the measured pattern in terms of orientation and level as shown in Fig. 5.20(c). The computed E_θ polarization at 6.0 MHz has the same elliptical figure as the measured pattern but at a level 4 dB higher. Fig. 5.20(d) shows that at 8.1 MHz the computed E_ϕ polarization has the same level as the measured pattern but the orientation is similar to that obtained by the TRN18 simple model. The E_θ pattern at 8.1 MHz, agrees reasonably with the measurement.

Fig. 5.20 shows that high E_θ radiation is a major problem with the TRN30 computer model between 2.6 and 6.0 MHz. However, the TRN30 model reproduces the orientation of the figure eight of the measured E_θ pattern at 2.6 and 4.1 MHz. This is considered an improvement over the E_θ patterns produced by the TRN18 at these frequencies. The density of the rectangular wire grids modelling the fuselage in the TRN30 model is not sufficient to provide a reasonable path for the horizontally oriented current flow. This would account for a low radiation

level in E_ϕ, and hence it appears that the E_θ component is too strong relative to the E_ϕ component. The addition of more wires to increase the grid density results in the complex model of the next section.

5.4 Complex Model of the Sea-King Helicopter

Sections 5.2 and 5.3 of this chapter have presented models of the Sea-King helicopter of simple and intermediate complexity. In this section a detailed or "complex" model called the "TRN40" model of the helicopter is considered, as shown in Fig. 5.21. The derivation of such a complex model from the geometry of the helicopter is somewhat arbitrary because no guidelines exist to dictate the density of wires needed to represent the surface, nor where such wires should be located in the surface. It is generally accepted that adjacent wires should be closer together than one-tenth wavelength in order to be sufficiently dense in the surface [11]. In areas where the current distribution is expected to be strong, the number of wires is increased. Parts of the airframe that are made of plastic or glass fiber materials are usually assumed to be electrically transparent in the HF band and are therefore omitted from the wire-grid model structure.

The "TRN40" model of the Sea-King helicopter was developed by the Royal Aircraft Establishment (RAE), Farnborough, where it was used to study the HF wire and loop antennas. The coordinates of the wire endpoints of the model were acquired

from RAE, and in this section this model is used to study the Tranline antenna on the helicopter. This allows comparative evaluation of the Tranline antenna in the location measured and the loop antennas studied at RAE using the same TRN40 wire-grid model of the helicopter.

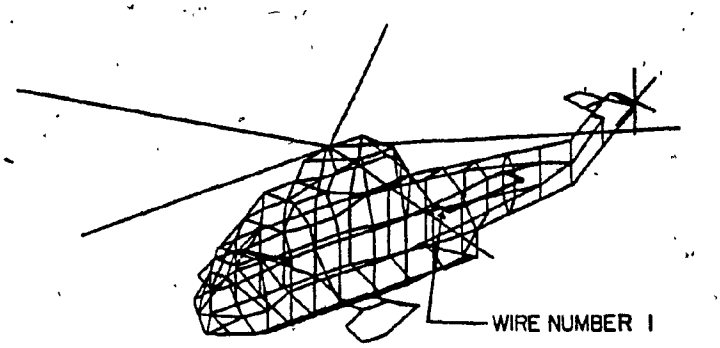

(a)

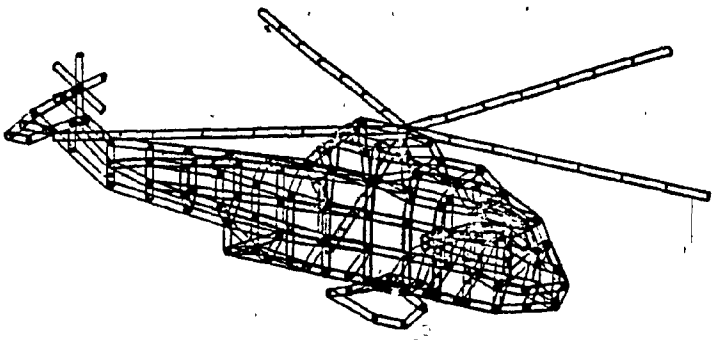

(b)

Fig. 5.21 The TRN40 complex wire-grid model of the Sea-King helicopter, (a) wire representation, (b) radius representation, Tranline antenna mounted on the port side of the model.

The TRN40 model of Fig. 5.21 consists of the following. The fuselage is modelled by ten interconnected and equally spaced vertical hexagonal or octagonal sections depending on their position along the fuselage. The nose of the helicopter is formed by joining the vertices of the front hexagon to the forward point of the model. The sponsons are modelled by a number of wires, reasonably approximating the sponsons of the actual helicopter. The tail of the helicopter is made up of two parallel wires. The back rotor blades and the horizontal stabilizer are modelled as shown in the figure. The drive shaft of the main rotor blades is connected to the middle of the wire joining section five and six of the fuselage. The main rotor blades are oriented in the forward position of Fig. 2.7. The Tranline antenna is located on the port side of the TRN40 model. This model is excited by a voltage source applied to wire number 1 indicated in Fig. 5.21. The total number of segments making up the TRN40 model is 335, all of lengths less than one tenth of the wavelength at 20 MHz. A uniform radius of 0.1 m is used for all the wires making up the TRN40 model, except for the Tranline antenna where the radius is 0.01 m.

The following reports the Tranline antenna radiation patterns in the HF band using the TRN40 complex model. The resonant behaviour of the complex model is examined.

5.4.1 Radiation Patterns of The Complex Model

The TRN40 complex model was analyzed at frequencies between 2.6 and 14 MHz, by using the NEC program to calculate the current flowing on the wires and the far field radiation patterns. Fig. 5.22 shows the azimuth patterns at 2.6, 4.1, 6.0 and 8.1 MHz for the TRN40 model in comparison with the measured patterns. Fig. 5.22(a) displays the azimuth pattern at 2.6 MHz. The computed E_ϕ polarization reproduces the elliptical figure of the measured pattern in both orientation and level. Similarly the E_θ polarization also reproduces the figure eight of the measured pattern in both orientation and level. The E_θ polarization produced by the TRN40 model at 2.6 MHz shows a definite improvement over the same pattern produced by the "simple" TRN18 model and the "intermediate" TRN30 model. The TRN30 model reproduces the figure eight in orientation only. Fig. 5.22(b) shows the azimuth pattern at 4.1 MHz. The E_ϕ polarization reproduces the measured pattern in both orientation and level. The E_θ polarization reproduces the figure eight of the measured pattern, however its level is about 2 dB higher. This is an improvement over the 7 dB difference between the "intermediate" TRN30 model's pattern and measured pattern. Very good agreement is obtained at 6.0 MHz in both polarizations as shown in Fig. 5.22(c). The figure shows that the E_θ pattern with the complex TRN40 model is about 4 dB lower than that produced by the "intermediate" TRN30 model, and similar to that produced by the "simple" TRN18 model. Fig. 5.22(d) shows the azimuth pattern at 8.1 MHz of the "complex" TRN40 model. The

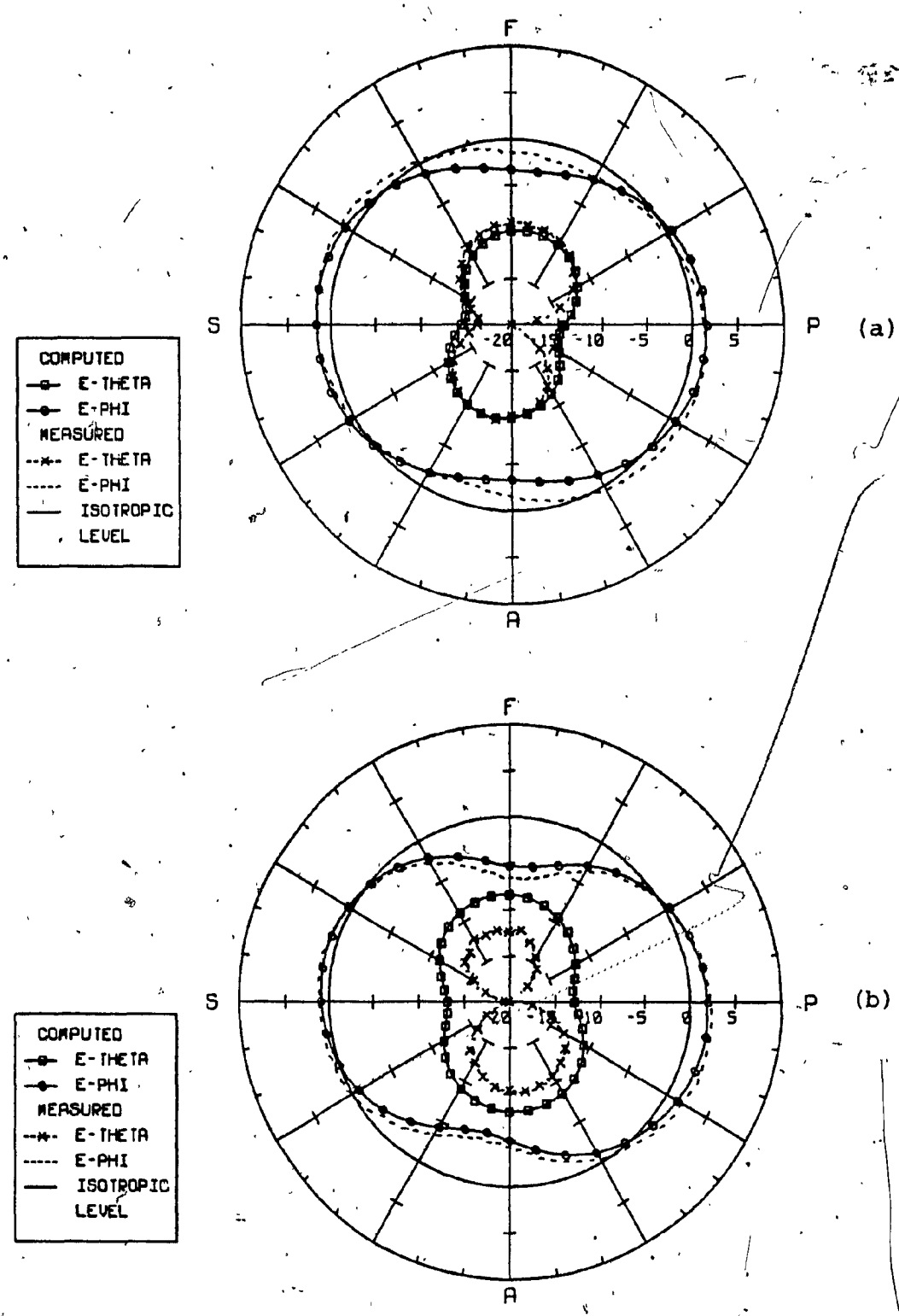

Fig. 5.22 Tranline antenna azimuth patterns obtained using the TRN40 model, compared to the measured patterns at (a) 2.6 MHz, (b) 4.1 MHz, (dB-scale).

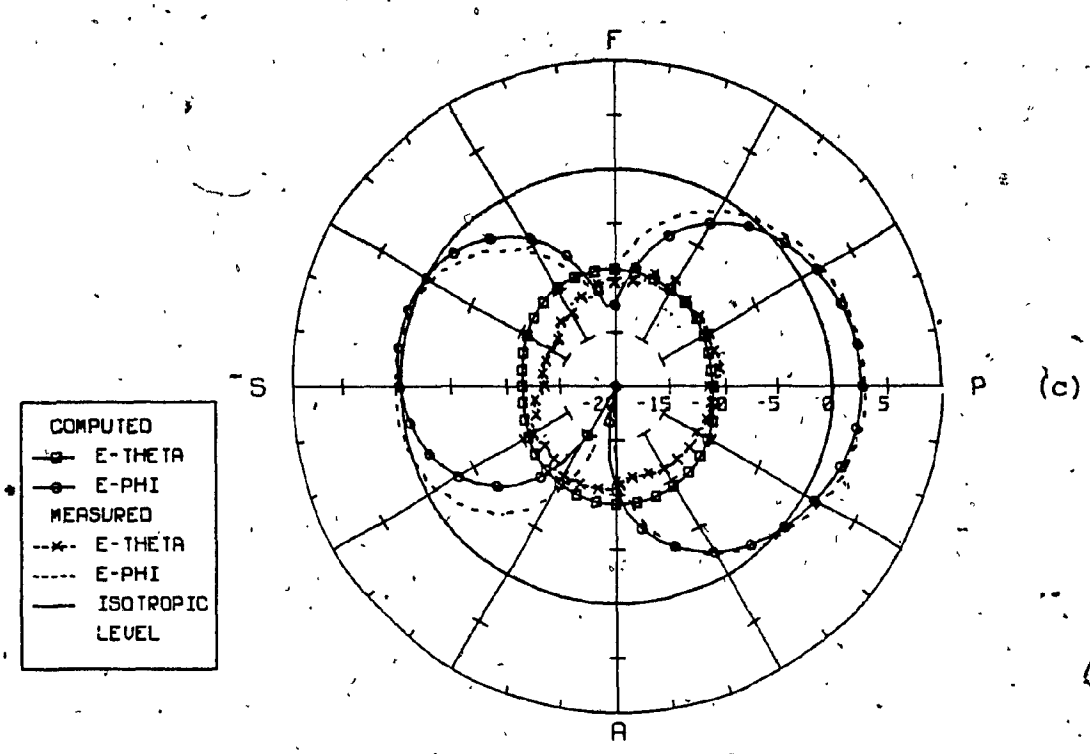

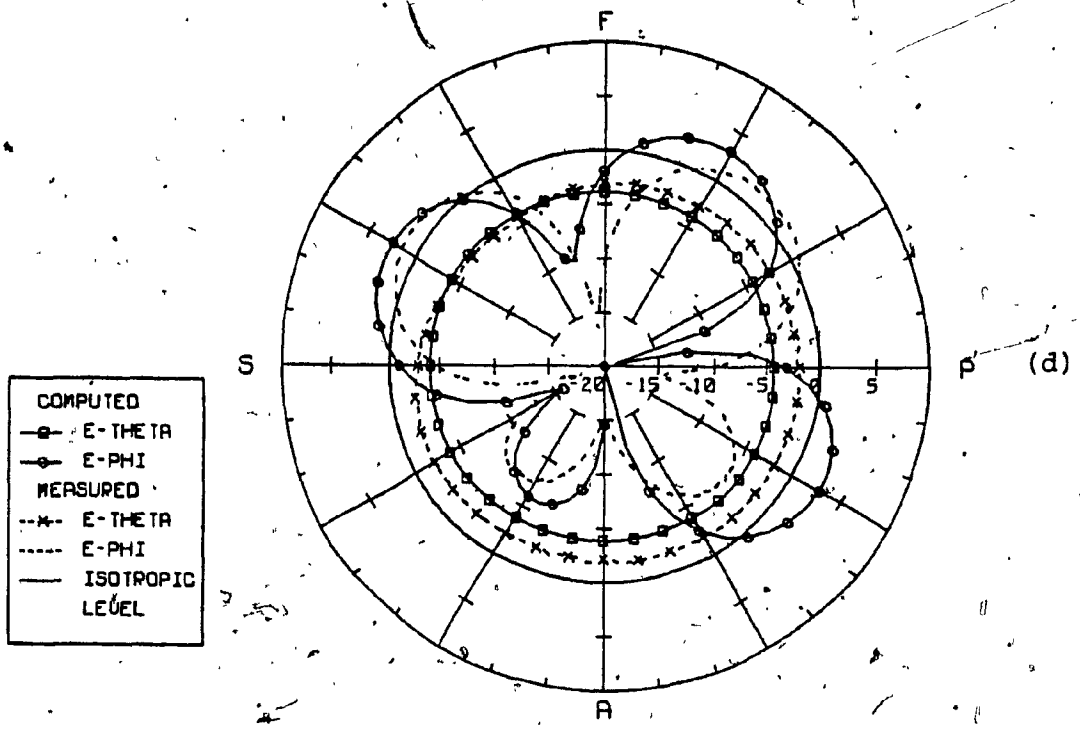

Fig. 5.22 (cont'd), Tranline antenna azimuth patterns obtained using the TRN40 model, compared to the measured patterns at (c) 6 MHz, (d) 8.1 MHz, dB-scale.

computed E_ϕ polarization reproduces the four lobes of the measured pattern with a rotation toward the starboard of about 10 degrees. The level of three lobes matches those of the measured pattern. The fourth lobe located between the port side and aft of the helicopter shows a difference of about 10 dB between the measured and computed patterns. The computed E_θ polarization reproduces the omnidirectional measured pattern in shape and level. The TRN40 results at 8.1 MHz show the best agreement with the measured patterns among all the runs of the simple and intermediate models. However, the $\%E_\theta$ curve of Fig. 5.23 shows a difference of about 19% between measured and computed values at 8.1 MHz. At other frequencies the measured and computed $\%E_\theta$ correspond to within 2%.

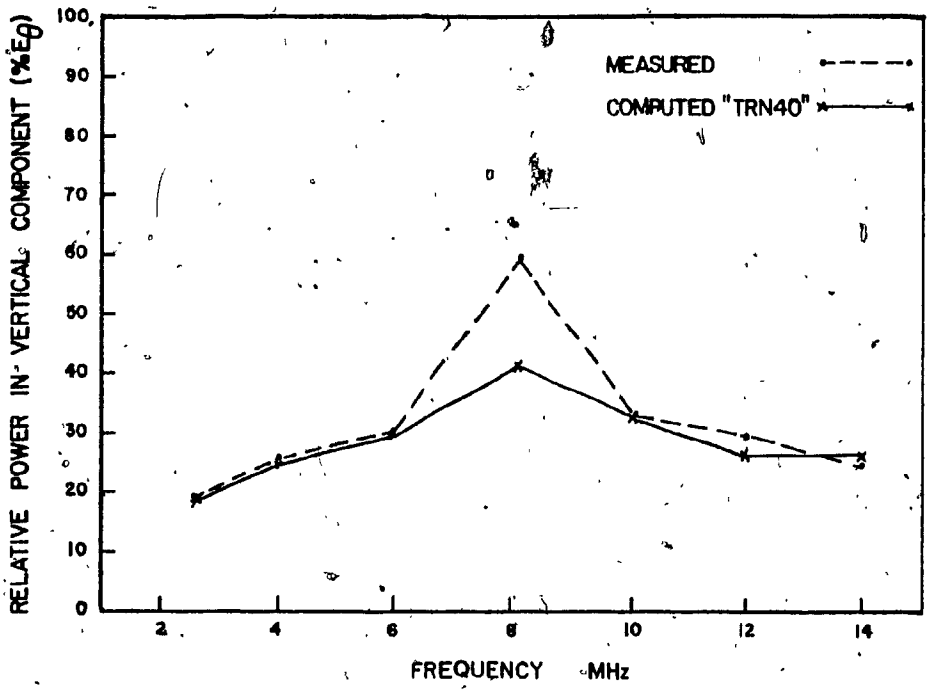

Fig. 5.23 Tranline antenna $\%E_\theta$ obtained using the TRN40 model, compared to the measured $\%E_\theta$ as a function of frequency.

Fig. 5.24 shows the surface plots of radiation patterns at 2.6 MHz using the TRN40 model. The plot of the computed E_θ polarization is shown in Fig. 5.24(a). The display corresponds to that of the measured plot of Fig. 5.13(a) except at the minima location. This minima is seen at phi equal to 75 degrees of the computed surface plot compared to phi equal to 108 degrees for the measured one. The surface produced by the complex model is a definite improvement over the surface plots obtained by the two "simple" TRN11 and TRN18 models.

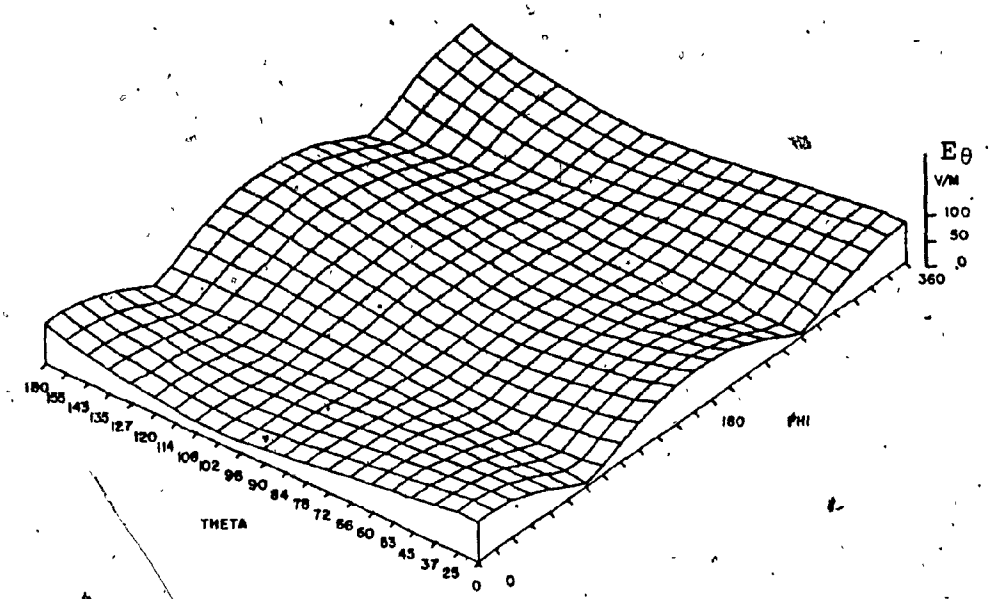

Fig. 5.24(a) Tranline antenna surface plot of the conical patterns obtained using the TRN40 model at 2.6 MHz for the E-theta polarization.

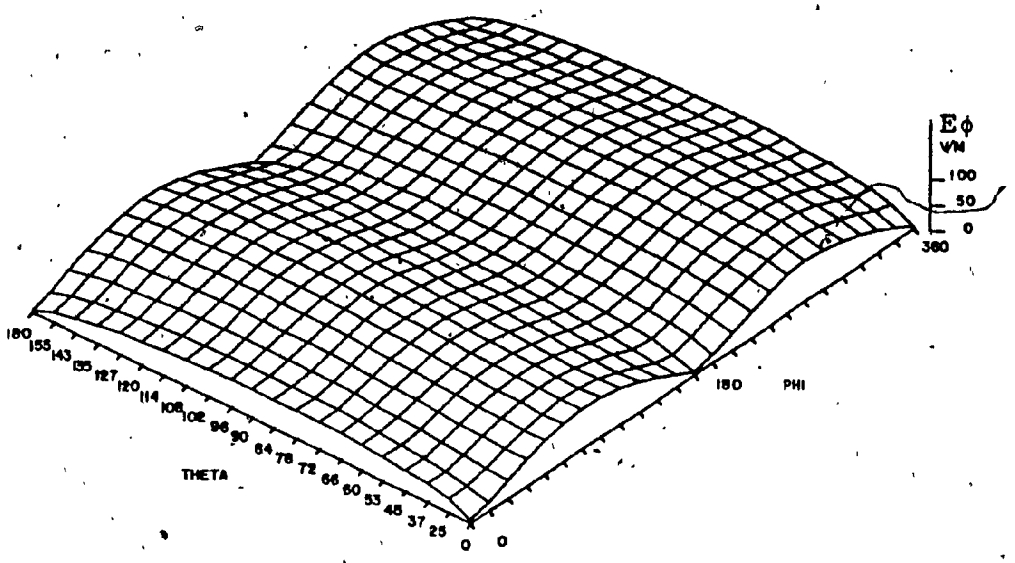

Fig. 5.24(b) Tranline antenna surface plot of the conical patterns obtained using the TRN40 model at 2.6 MHz for the E-phi polarization.

Fig. 5.24(b) shows a display of the E_ϕ surface plot at 2.6 MHz produced by the complex model. The plot corresponds to the measured surface of Fig. 5.13(b) except at the minima location where about a 12 degree shift is seen. The surface plots obtained from the complex model at 4.1 and 6.0 MHz are not shown here, but they reproduce their corresponding measured surface plots in the same manner as the surface plots of Fig. 5.24.

In the next section detailed studies of the complex "TRN40" model are considered at resonant frequencies around 8 MHz.

5.5 Resonant Behaviour of the Complex Model

In the previous section of this chapter, models of various complexity have produced reasonable to good agreement with the measured patterns at 2.6,4.1 and 6.0 MHz. It was also indicated that these computer models are resonant at frequencies in the neighbourhood of 8.1 MHz. Fig. 5.25 shows the normalized sum of the current amplitude flowing at the center of each of the seven segments of the five rotor blades of the TRN40 model, as a function of frequency. The current on the rotor blades is much stronger near 8.0 MHz than at other frequencies, indicating that the computer model is resonant near 8 MHz and that the rotor blades are part of the resonant path. The purpose of this section is to examine the resonant behaviour of the "complex"

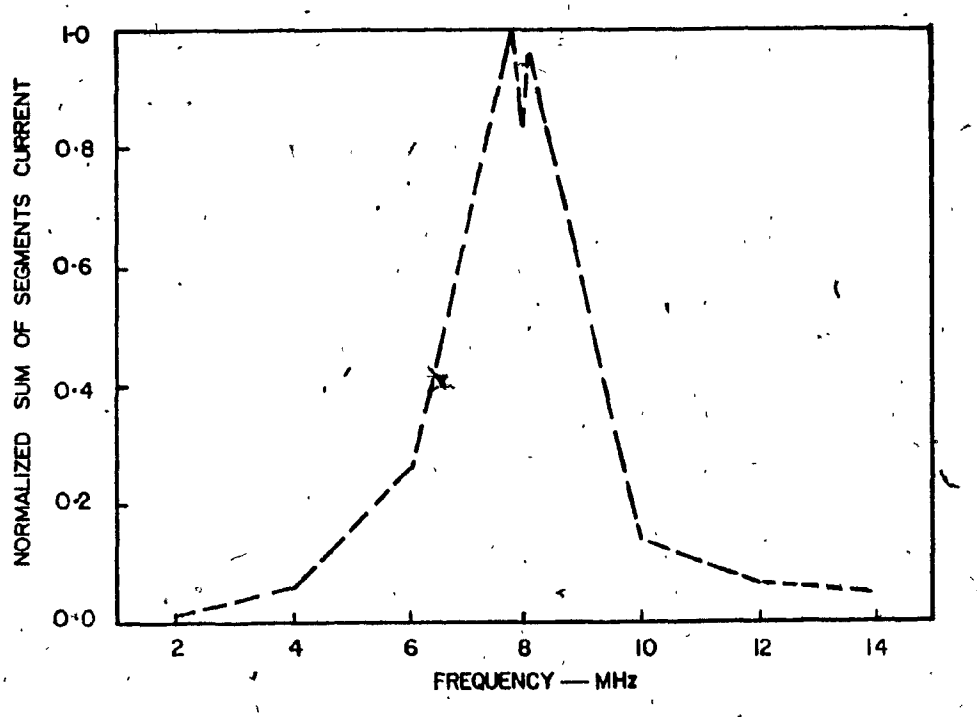

Fig. 5.25 Normalized sum of the current on the segments of the five rotor blades of the TRN40 model as a function of frequency.

TRN40 model in the vicinity of 8 MHz. The model is used with a uniform radius of 0.1 m. Little change was seen in the radiation pattern using 0.07 m or 0.15 m for the radius at 8.1 MHz. The resonant studies presented here can be divided into two parts, namely the use of the extended boundary condition, and the tuning of the TRN40 model to match the measured patterns.

5.5.1 Extended Boundary Condition

The Electric Field Integral Equation (EFIE) of chapter 4 does not have a unique solution at frequencies for which resonant modes can exist in the interior of a closed structure such as the metallic skin of the helicopter [39]. In such a case the field inside the structure does not vanish. The interior of the "complex" TRN40 model presents a cavity which might support resonating modes at 8.1 MHz. This may introduce errors in the RF current distribution which would then consist of a mixture of radiation-mode currents and cavity-mode currents. Although in theory the cavity mode current does not radiate, in practice they contaminate the numerical solution sufficiently that they must be suppressed in order to obtain satisfactory radiation patterns.

It was suspected that the difference between the measured and computed E_ϕ pattern of Fig. 5.21(d) was a result of the presence of a cavity-mode resonance in the interior of the helicopter model. Such a resonance can be suppressed by

insuring that the field inside the TRN40 model is zero. To achieve this, six diagonal wires are placed into the model's interior. These diagonal wires connect the adjacent sections of the model and they are shown as dashed lines in Fig. 5.26. The suppression of the field inside the cavity is an extension of the boundary condition from the surface of the metallic structure to its interior, and is called the "extended boundary condition".

The current distribution and the radiation patterns of the TRN40 model with these interior diagonal wires are obtained by executing the program NEC at 8.1 MHz. The results show that the diagonal element near the nose of the helicopter support very little current. The current becomes stronger on those elements which are closer to the feed point of the Tranline antenna. The maximum current seen on the diagonal elements is about one sixteenth the value of the antenna current and about one eighth of the rotor blades current. The current induced on the diagonal wires did not introduce any changes to the radiation patterns at 8.1 MHz. Fig. 5.27 shows an azimuth pattern which is a replica of that seen in Fig. 5.21(d).

Thus the application of the "extended boundary condition" does not result in any improvement at 8.1 MHz, and so the difference between the measured and computed patterns of Fig. 5.21(d) is not due to a resonant mode in the interior of the TRN40 model.

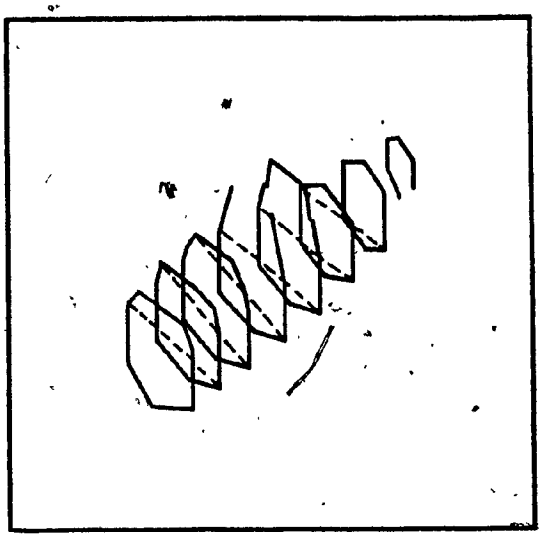

Fig. 5.26 Six diagonal wires shown as dashed lines are added to the interior of the fuselage of the TRN40 model.

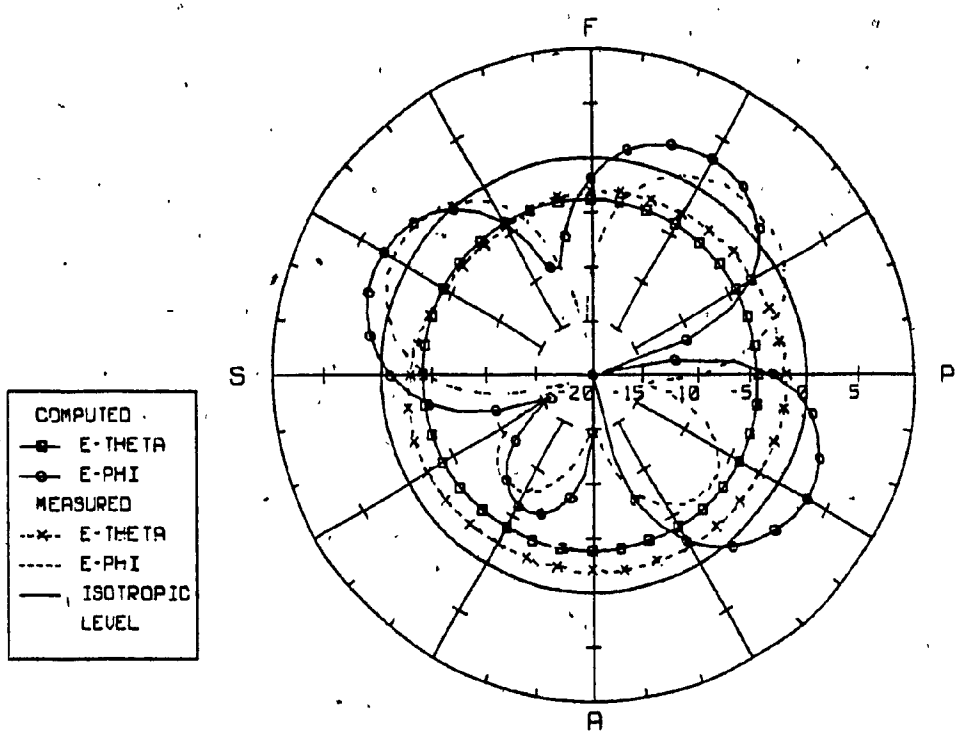

Fig. 5.27 Tranline antenna azimuth pattern obtained using the TRN40 model with diagonal wires, compared to the measured pattern at 8.1 MHz, (dB-scale).

5.5.2 Tuning the TRN40 Model

Fig. 5.25 shows the integrated current amplitude on the rotor blades as a function of frequency. The curve indicates that the rotor blades are part of a resonant-length path for RF current around 8.0 MHz. A detailed presentation of the current on the rotor blades in this resonant band is given in this section. The "complex" TRN40 model of the Sea-King helicopter is tested at 7.8, 7.9, 8.0 and 8.1 MHz, and found to be resonant at a slightly lower frequency than the measured model. The complex model is then tuned to resonate at the same frequency, and the agreement of the radiation patterns is improved.

Fig. 5.28(a) shows the current distribution flowing on the rotor blades of the TRN40 model at 8.1 MHz. The figure plots

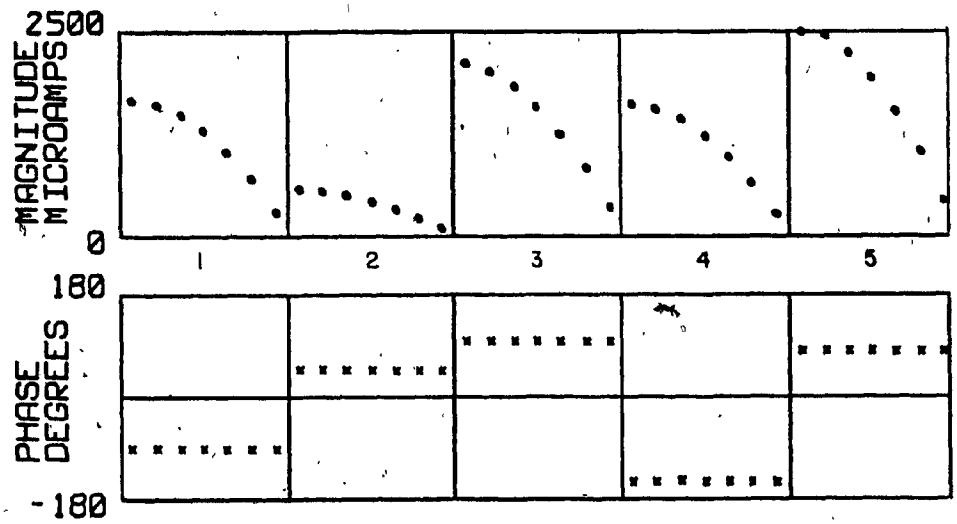

Fig. 5.28(a) Current distribution amplitude and phase, flowing on the rotor blades of the TRN40 at 8.1 MHz, (blade numbers are indicated in Fig. 5.28(b)).

the current as a function of distance along each blade starting at the shaft of the blade and proceeding toward the tip. Zero phase has the direction of flow indicated by the arrow in Fig. 5.28(b) and indicates that the maximum current occurs on blade number 5 shown in Fig. 5.28(a). This blade is oriented between the port side and forward end of the helicopter. A relatively strong current can also be seen on blade numbers 3 and 4. These blades are oriented toward aft of the helicopter. The azimuth radiation pattern for this case is shown in Fig. 5.29(a), where a 10 dB difference is observed between the computed polarization and the measured pattern in the lobe level oriented between the port side and aft of the TRN40 wire-grid model.

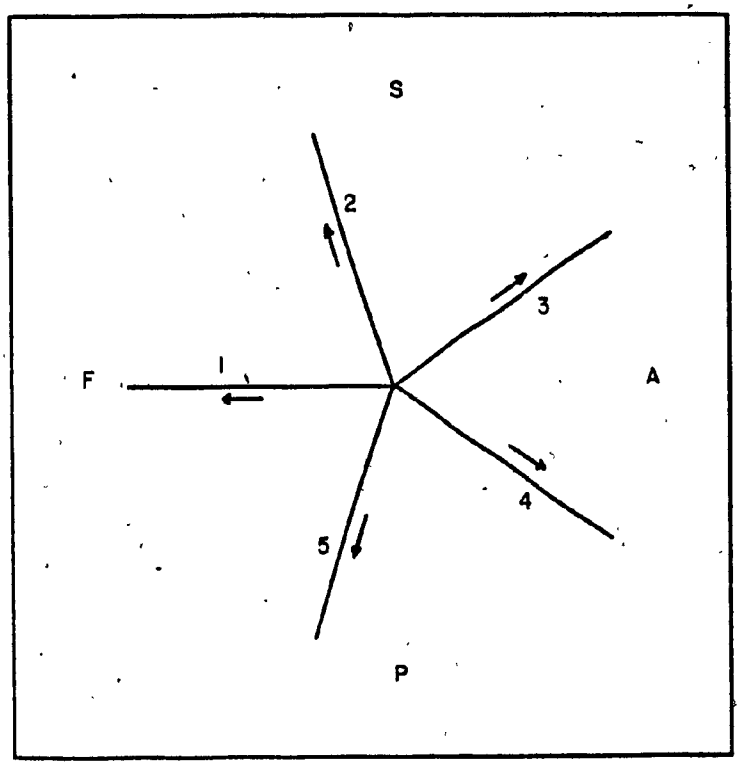

Fig. 5.28(b) Numbering of the rotor blades of the TRN40 model.

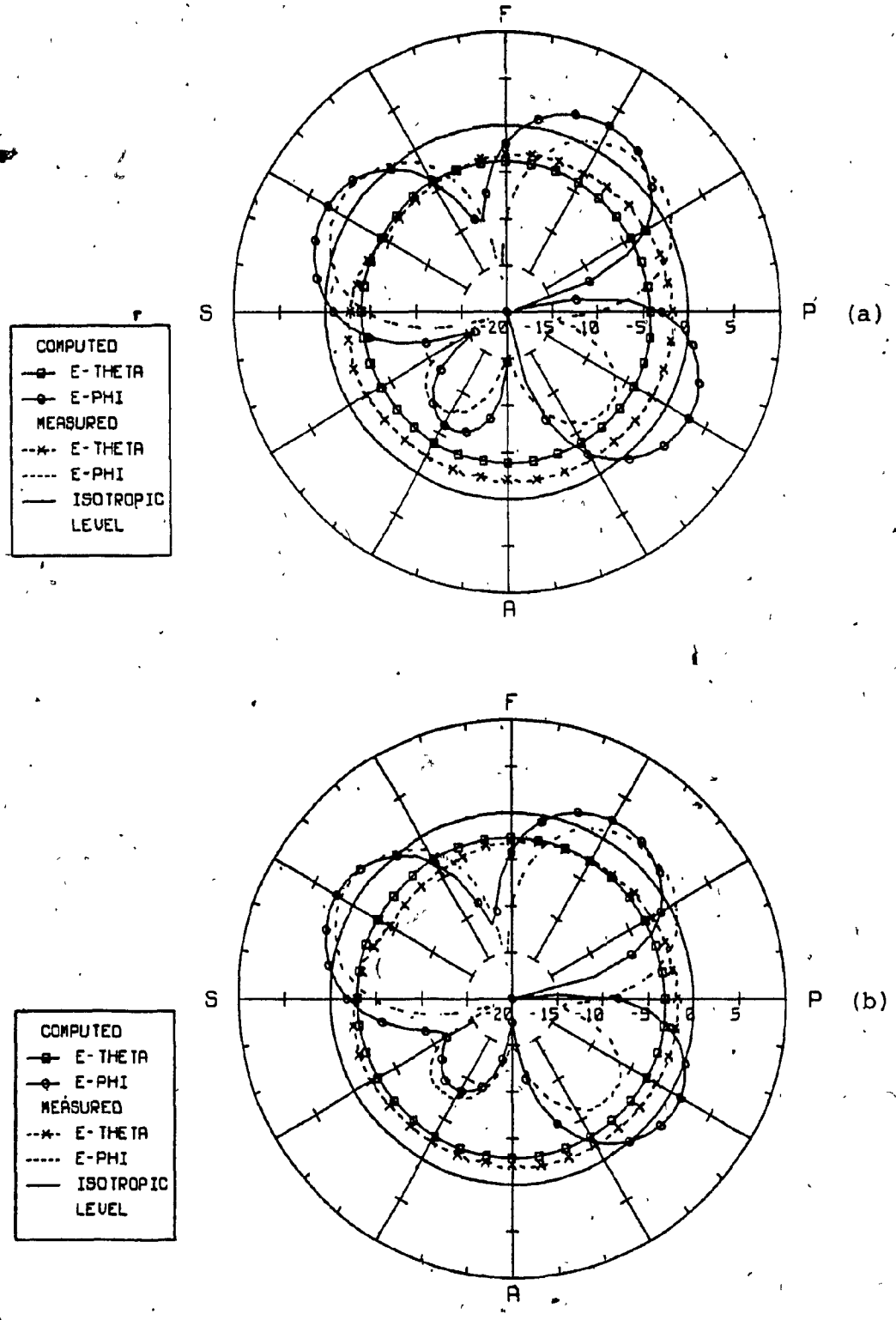

Fig. 5.29 Tranline antenna azimuth patterns obtained using the TRN40 model at (a) 8.1 MHz, (b) 8.0 MHz, as compared to the measured pattern at 8.1 MHz, (dB-scale).

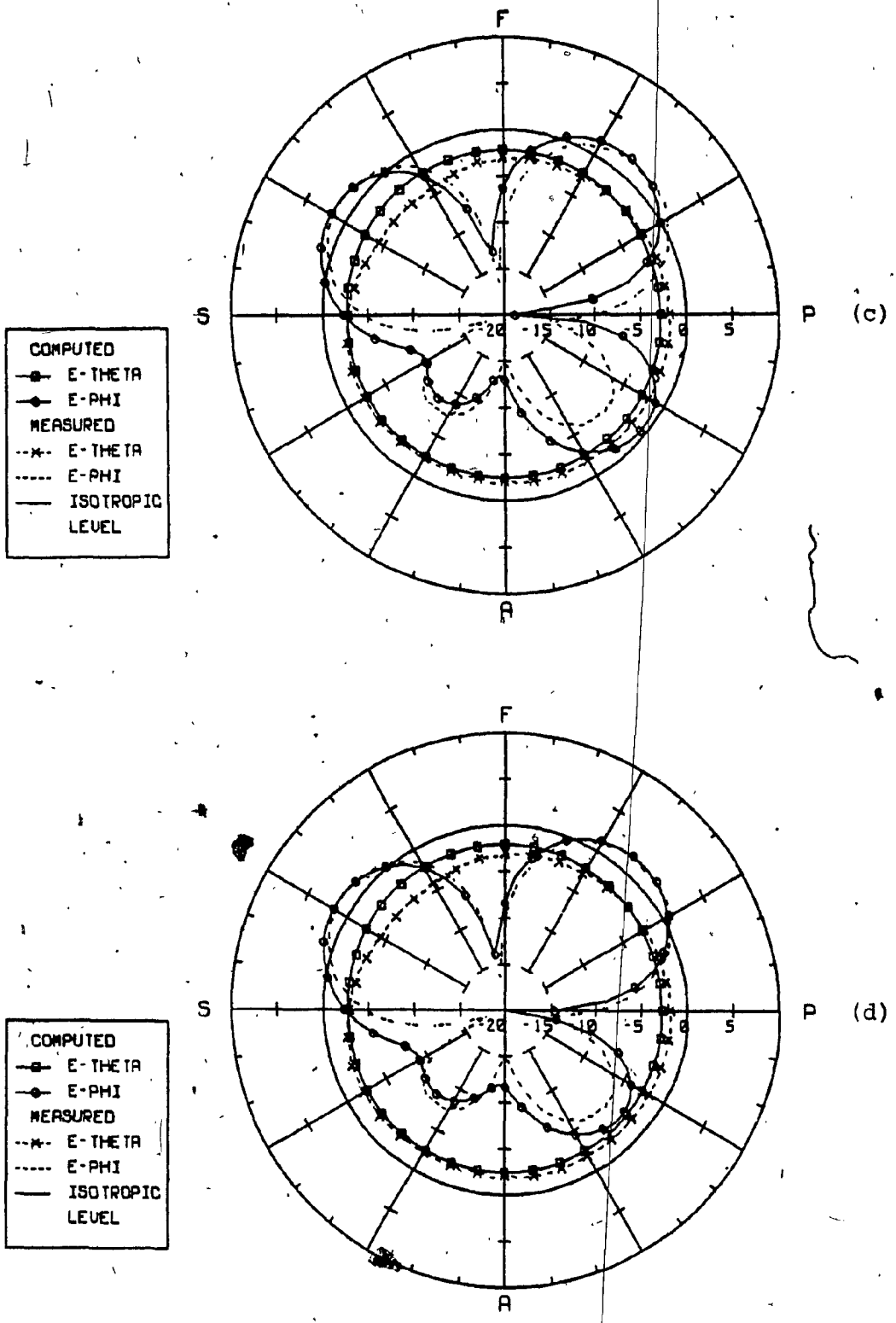

Fig. 5.29 (cont'd), Tranline antenna azimuth patterns obtained using the TRN40 model at (c) 7.9 MHz, (d) 7.8 MHz, as compared to the measured pattern at 8.1 MHz, (dB-scale).

Also the computed E_ϕ pattern showed a rotation of about 10 degrees toward the starboard side. The TRN40 model was analyzed at 8.0 and 7.9 MHz, and the RF current distribution shows that the current on blade number 5 decreases with frequency, whereas the current on blade numbers 3 and 4 increases. Fig. 5.29(b-c) shows improvement over that of Fig. 5.29(a). The difference between the computed and measured pattern at 8.1 MHz is reduced from 10 dB to about 5 dB in the lobe level described above. Also the computed pattern is rotated back toward the port side by about 5 degrees. Fig. 5.30 shows the current distribution on the rotor blades at 7.8 MHz. At this frequency the maximum current occurs on blade number 3 and also the current becomes stronger on blade number 4 with a phase change of about 40 degrees when compared to that of Fig. 5.28(b). The computed

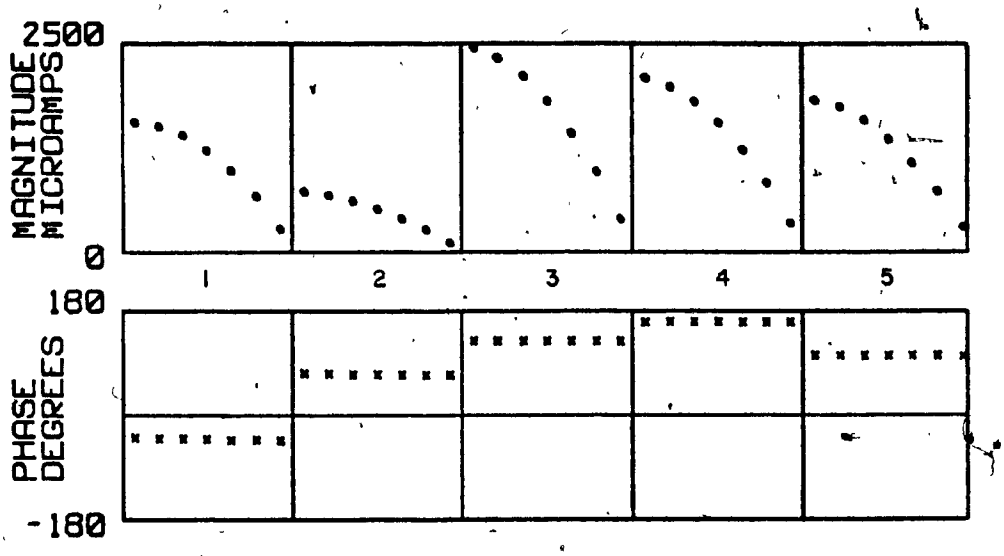

Fig. 5.30 Current distribution amplitude and phase plotted on the rotor blades of the TRN40 model at 7.8 MHz.

azimuth pattern at 7.8 MHz matches the measured pattern at 8.1 MHz, in both level and orientation except at the minima located near the starboard side, as shown in Fig. 5.29(d). The computer model agrees best at 7.8 MHz with the measured E_ϕ at 8.1 MHz. This appears to a degree that the computer model supports a resonant current mode at 7.8 MHz which is similar to that of the measurement model at 8.1 MHz. Thus the computer model needs to be "tuned" to agree with the measured model.

Section 5.2.3 showed that each rotor blade is part of a resonant path, and they contribute to the far field radiation patterns of Fig. 5.12(d). It was recommended then, that any adjustment to the model is effective when including the rotor blades. In order to make the TRN40 computer model resonate at a higher frequency than 7.8 MHz, its resonant path length should be shortened. Thus the rotor blades of the TRN40 model are shortened by 0.4 m so that the computer model resonates at 8.1 MHz, the same resonant frequency as the measured model. The tuned TRN40 model is analyzed at 8.1 MHz using the NEC program. Fig. 5.31(a) shows the current amplitude and phase on the rotor blades of the tuned model. The figure indicates that the current amplitude on each of the shortened blades is proportional to that of the corresponding blade current at 7.8 MHz, shown in Fig. 5.30. This means that the "tuned" complex model resonates at the same frequency as the measured model. Fig. 5.31(b) shows the azimuth pattern obtained using the tuned TRN40 model at 8.1 MHz. The figure shows that the computed pattern reproduces the measured pattern in both level

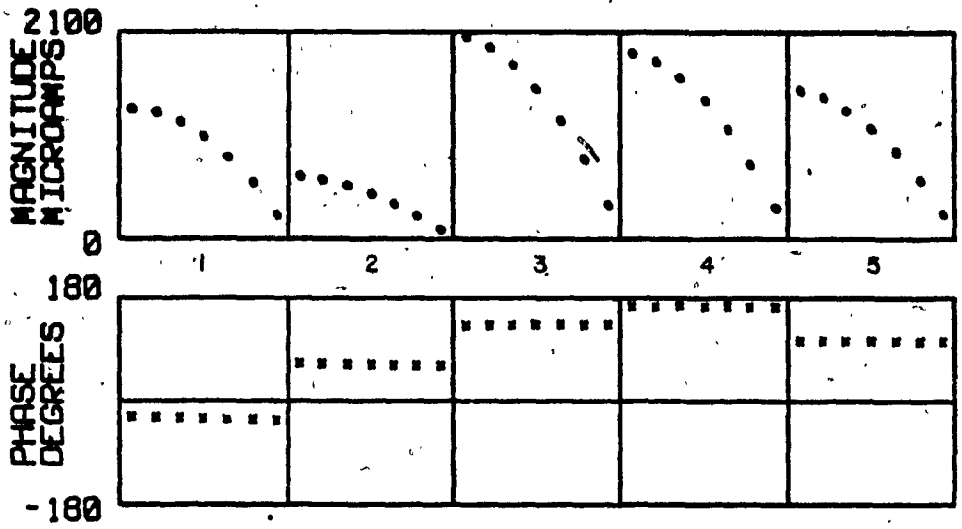

Fig. 5.31(a) Current distribution, amplitude and phase plotted on the rotor blades of the tuned TRN40 model at 8.1 MHz.

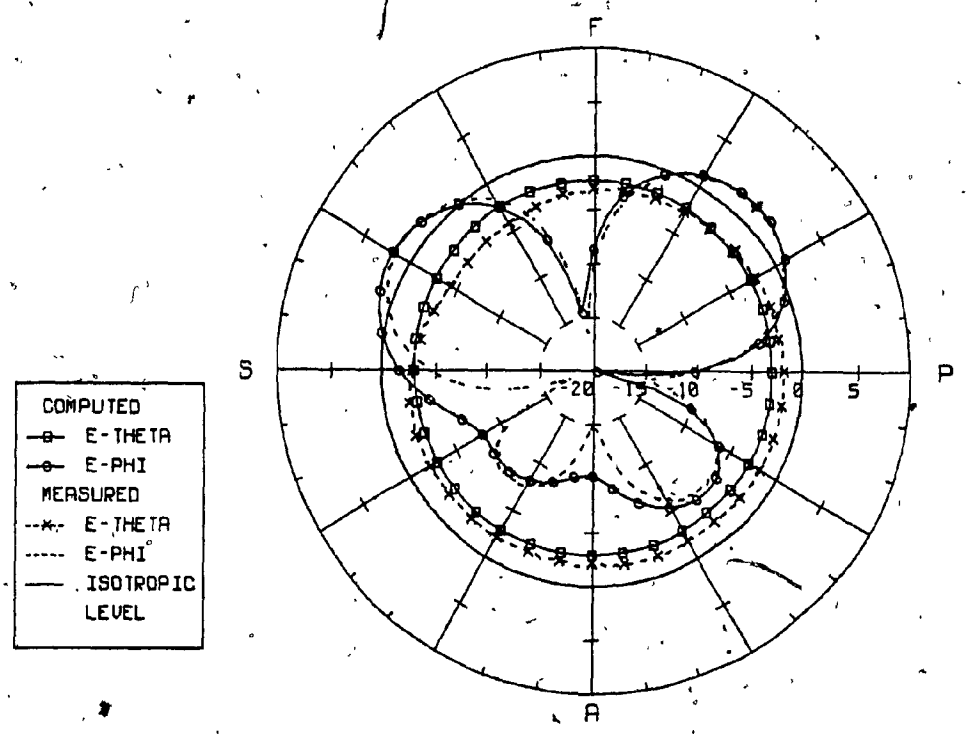

Fig. 5.31(b) Tranline antenna azimuth pattern obtained using the tuned TRN40 model, compared to the measured pattern at 8.1 MHz.

and orientation. The computed E_ϕ polarization has a shallower null between the starboard and aft of the helicopter than that seen in the measured polarization. The $\%E_\theta$ obtained at 8.1 MHz using the tuned TRN40 model is about 53% which is 7% less than measured $\%E_\theta$ seen in Fig. 3.6. Recall that Fig. 5.23 shows that "complex" TRN40 model produces a $\%E_\theta$ of about 40% at 8.1 MHz. Therefore the tuned TRN40 model achieves 13% improvement in $\%E_\theta$ at this frequency.

In summary this section has shown that the rotor blades of the helicopter are extremely important at resonant frequencies. By changing their lengths, the resonant path length is changed to become equal to that of the measured resonant path on the scale model. Consequently the computed patterns agreed with the measured patterns at the resonant frequency. A finer tuning of the TRN40 model can be obtained to produce a "perfect" agreement between the measured and computed patterns at 8.1 MHz. However further analysis or parametric studies with the complex TRN40 model are relatively expensive and do not present a tremendous advantage over the results seen in Fig. 5.31(b). The tuned TRN40 model will be considered in this thesis as a validated model and it will be used to explore the possibilities of improving the Tranline antenna's performance by relocating it at various locations along the fuselage of the helicopter.

5.5.3 Comparison of Surface Plots of Various Models

Fig. 5.32 shows surface plots of complete sets of conical radiation patterns at 8.1 MHz, both measured and computed, and for both polarizations. The display format is identical to that described in Section 5.2.2. Fig. 5.32(a) shows a surface plot of the measured E_θ polarization at 8.1 MHz. The surface represents a figure eight polar pattern at theta equal to zero degrees. The patterns gradually change to omnidirectional as theta increases up to 108 degrees. For theta more than 108 degrees the pattern becomes elliptical with the major axis aligned along the forward-aft or phi equal to 0^0 and 180^0 axis of the helicopter. Fig. 5.32(c) shows the surface plots of the computed E_θ polarization at 8.1 MHz obtained for the "simple model" called "TRN18", described in Section 5.2.2. The simple model reproduces the basic structure of the measured surface plot of Fig. 5.32(a) except at theta equal to 72 degrees, where the measured pattern has a deep null. Fig. 5.32(e) shows the surface plot of the computed E_θ polarization obtained from the tuned complex TRN40 model at 8.1 MHz. The surface is similar to that obtained with the simple model but has a level closer to the measured surface of Fig. 5.32(a). Note that the surfaces are normalized so that the total power in the measured and computed pattern is the same. The E_ϕ polarization surface plots are presented in Fig. 5.32(b), Fig. 5.32(d) and Fig. 5.32(f). Fig. 5.32(b) shows the surface plot of the measured E_ϕ polarization at 8.1 MHz. The plot displays a wavy surface with four minima located approximately at phi equal to

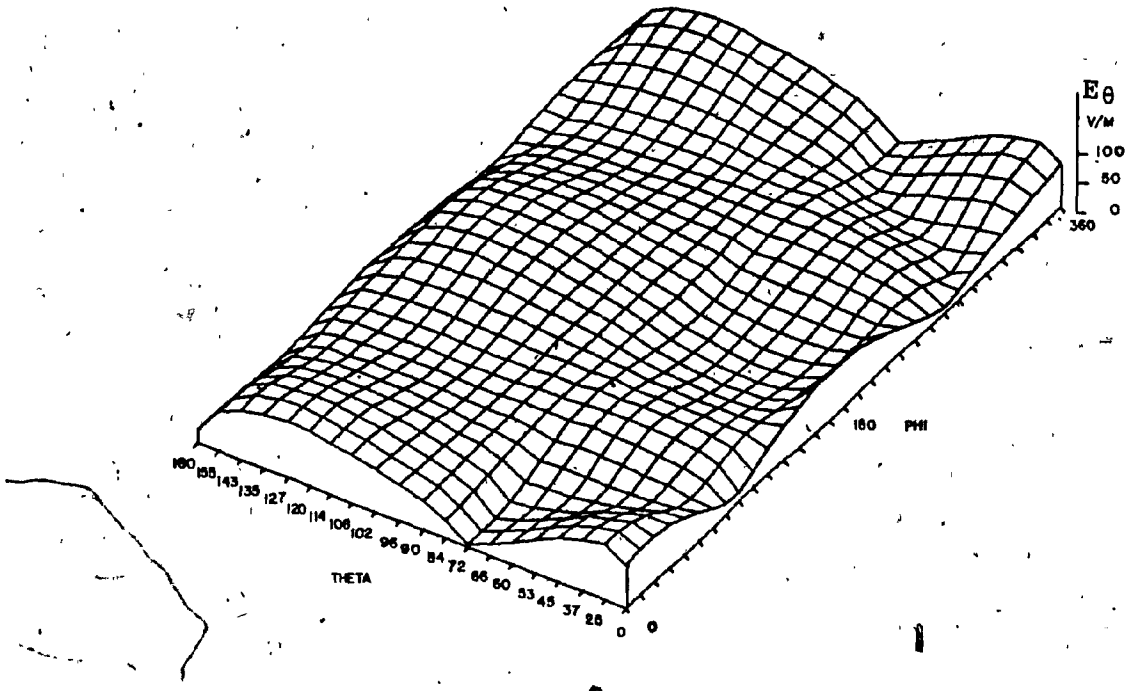

(a)

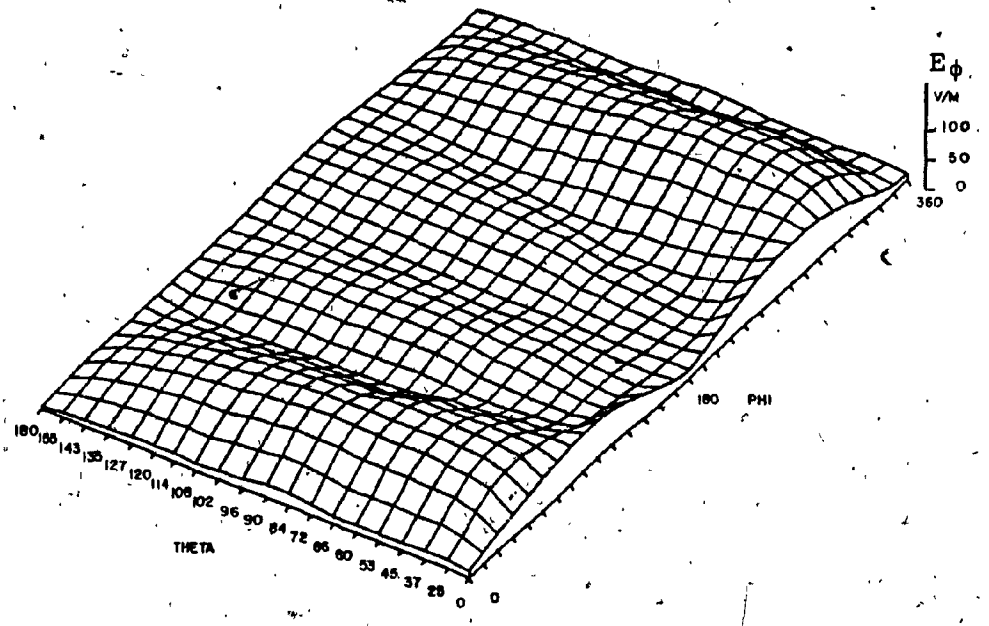

(b)

Fig. 5.32 Tranline antenna surface plots of the measured conical patterns at 8.1 MHz, for (a) E-theta polarization, (b) E-phi polarization.

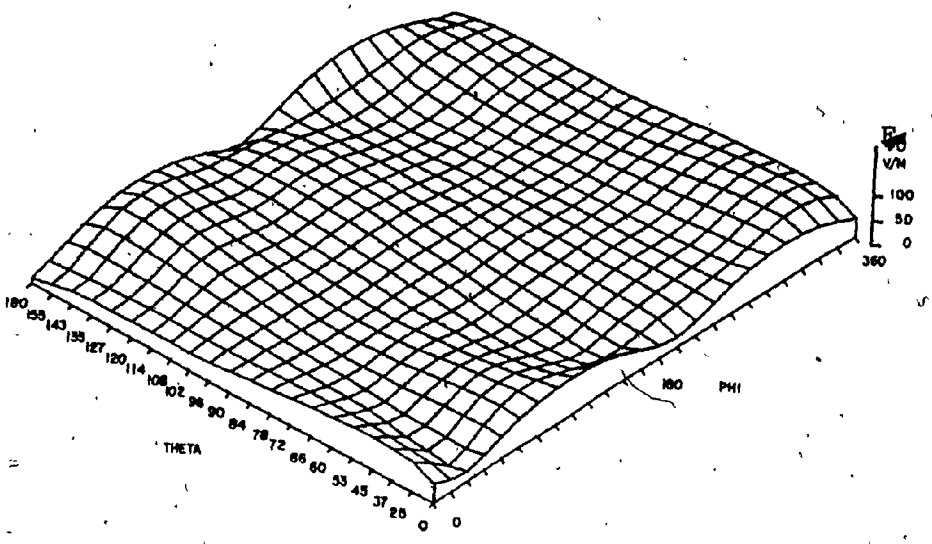

(c)

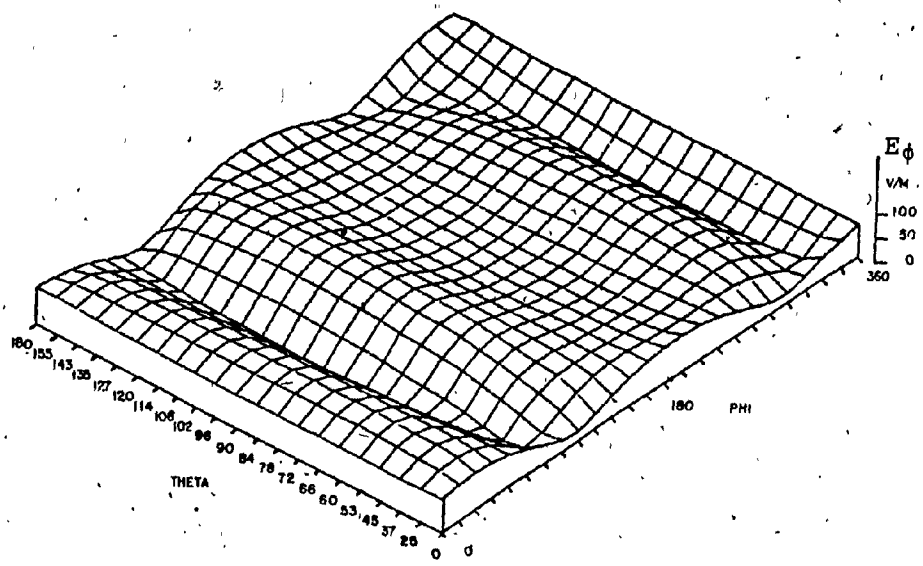

(d)

Fig. 5.32 (cont'd), Tranline antenna surface plots of the conical patterns obtained using the TRN18 model at 8.1 MHz, for (c) E-theta polarization, (d) E-phi polarization.

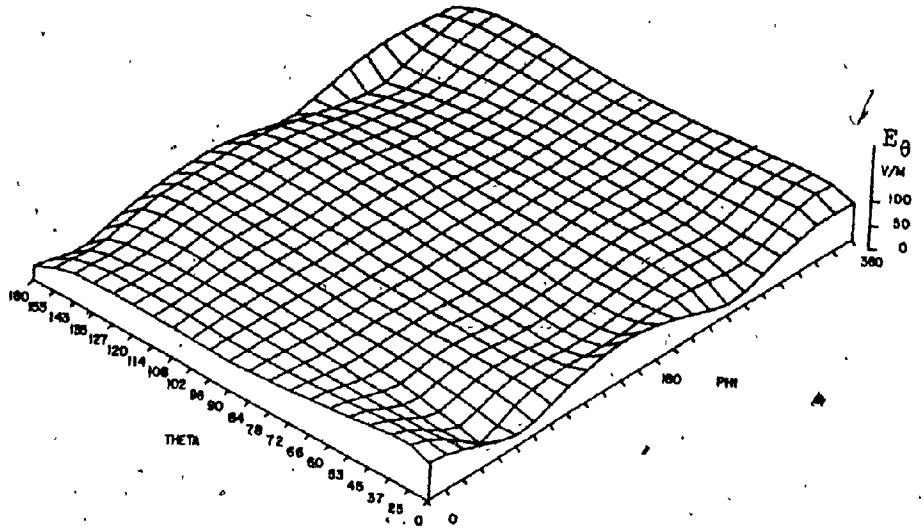

(e)

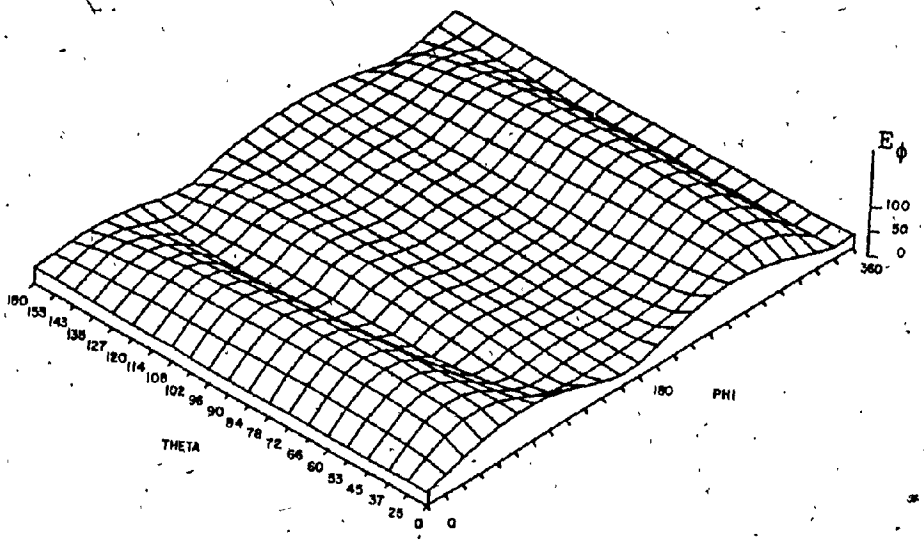

(f)

Fig. 5.32 (cont'd), Tranline antenna surface plots of the conical patterns obtained using the tuned TRN40 model at 8.1 MHz, for (e) E-theta polarization, (f) E-phi polarization.

0, 96, 180 and 240 degrees. This explains the butterfly figure seen in the azimuth pattern at 8.1 MHz. The surface plot of the computed E_ϕ polarization obtained by using the simple "TRN18" model at 8.1 MHz is shown in Fig. 5.32(d). This figure shows that the simple model reproduces three of the four lobes seen in the measured surface. This major disagreement was seen in the azimuth pattern of Fig. 5.12(d). Better agreement is obtained between the measured E_ϕ surface and the computed surface using the complex model, shown in Fig. 5.32(f). The improvement in this surface can be seen in the four lobe structure and in the level of the same patterns, which corresponds reasonably well to the measured surface. This indicates that the distribution of power between E_θ and E_ϕ is about the same for the complex model as it is for the measured model.

In earlier sections of this chapter the azimuth patterns of various computer models showed some disagreement with the measured pattern at 8.1 MHz. However by examining the surface plots of a complete set of radiation patterns, the computed surfaces always agree with the basic structure of the measured surfaces.

5.6 Alternative Loop Antenna Locations on the Sea-King

The "Tranline" name in this section designates a loop antenna which is oriented in a horizontal plane as shown in Fig. 2.1. The loop can also be oriented in other planes, such as the "vertical" loop and the "bottom" loop in Figs. 5.33-34.

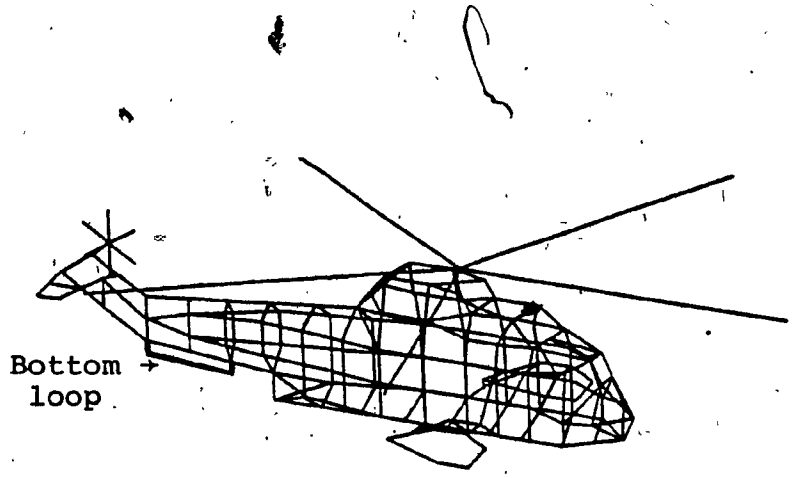

Fig. 5.33 Bottom loop antenna mounted on the tuned TRN40 model of the Sea-King helicopter.

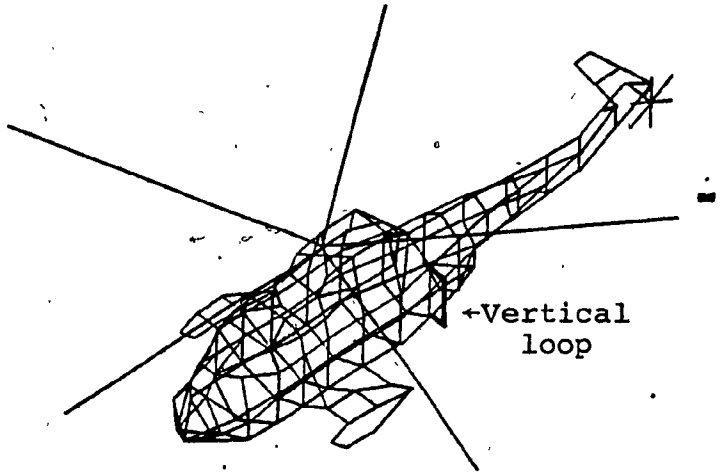

Fig. 5.34 Vertical loop antenna mounted on the tuned TRN40 model of the Sea-King helicopter

This section compares the performance of the Tranline "vertical" loop and "bottom" loop designs, based on computer modelling using the tuned TRN40 model. Section 3.1 of this thesis described the angular section which must be covered by an HF antenna mounted on a helicopter. The antenna must radiate a maximum amount of power in the vertically polarized component over the angular sector 30 degrees from the horizon, as shown in Fig. 2.6. The evaluation techniques given in chapter 3 have shown that the Tranline antenna in the location used for the scale model measurements is a poor radiator of the vertical component at the lower end of the HF band. Therefore, an alternate location to that of Fig. 2.1 is needed to improve the amount of vertical radiation around 2 MHz. The assessment parameters $\%E_\theta$ and $\%E_\theta^*$ are used here to compare the computed performance of the "vertical" and the "bottom" loop antennas, and the Tranline antenna on the Sea-King helicopter. In each case the effects of the rotor blade position on the radiation patterns are assessed. This section will attempt to suggest an alternative location to the present Tranline antenna mounted on the CHSS-2 Sea-King helicopter.

5.6.1 Comparison of Various Loop Antennas

The "vertical" and the "bottom" loop antennas mounted on the tuned "complex" TRN40 model are first analyzed at 2.0 MHz using the NEC program. A loop is considered to show superior performance to the Tranline antenna in the measured location, if it has a considerably higher $\%E_\theta$ and $\%E_\theta^*$. Recall that $\%E_\theta$ is

defined as the ratio of the power radiated in the vertical polarization to the total power radiated by the antenna. The $\%E_\theta^*$ is defined as the ratio of the amount of power radiated in the vertical polarization in the useful sector to the total power radiated by the antenna.

In Section 3.5.2 the H/V ratio was used to compare the Tranline antenna and the "bottom" loop examined by RAE [28]. However the H/V ratio is a poor indicator of the performance, and here the antennas will be compared using the power-derived parameters $\%E_\theta$ and $\%E_\theta^*$. A complete set of radiation patterns was generated for the "bottom" loop mounted on the tuned TRN40 model shown in Fig. 5.33. At 2.0 MHz the "bottom" loop produces a $\%E_\theta$ equal to 48% compared to 19% from the Tranline antenna. The $\%E_\theta^*$ of the "bottom" loop is 19% whereas the Tranline antenna has a $\%E_\theta^*$ of about 5%. Thus the "bottom" loop radiates four times as much power in the useful field component in the useful angle sector as does the Tranline antenna.

Using the same feed point as the measured Tranline antenna, a "vertical" loop is mounted on the tuned TRN40 model as shown in Fig. 5.34. This antenna runs down toward the bottom of the fuselage with a length of 1.83 m. Using the NEC program, a complete set of radiation patterns was obtained at 2.0 MHz. The "vertical" loop is much superior to the Tranline antenna in the measured location. It has a $\%E_\theta$ of about 60%, which amounts to a 40% more than that of the Tranline antenna. The $\%E_\theta^*$ of the "vertical" loop is 30% which is about 6 times that of the

Tranline antenna at 2.6 MHz. The "vertical" loop radiates more vertical component than both the "bottom" loop and the Tranline antennas.

The assessment parameters of the three antennas, namely the Tranline, the "vertical" loop and the "bottom" loop were computed for the frequency band from 2.0 to 14.0 MHz. Figs. 5.35 through Fig. 5.37 show the radiation pattern efficiency η_p, the $\%E_\theta$ and $\%E_\theta^*$ respectively. The pattern efficiency (η_p) of Fig. 5.35 shows that the "vertical" loop has a constant pattern efficiency (η_p) of about 45% between 2.0 and 6.0 MHz. Above 6.0 MHz the η_p of the "vertical" loop rises slightly to about 55%. The "bottom" loop has an η_p of about 40% between 2.0 and 6.0 MHz. The η_p curve of the "bottom" loop has a maximum at 8.0 MHz of about 61%. The curve decreases to about 32% at 12.0 MHz. The η_p curve of the Tranline antenna is described earlier in Chapter 3, and it is higher than the "bottom" loop by about 22% at 2.0 MHz, and 17% higher than the "vertical" loop at the same frequency. The η_p of the Tranline antenna becomes similar to the "vertical" loop between 4.0 and 6.0 MHz, but still higher than the "bottom" loop by about 5% in the same band. Above 6.0 MHz the Tranline antenna has an η_p approximately equal to the average value of η_p for both "vertical" and "bottom" loops. No clear choice can be made between the three antennas based on the η_p curves, and it is necessary to investigate the other assessment parameters namely $\%E_\theta$ and $\%E_\theta^*$. Fig. 5.36 shows the $\%E_\theta$ of the three antennas described above as a function of frequency. The $\%E_\theta$ curve of

the "bottom" loop shows that the loop has a high $\%E_\theta$ of about 48% at 2.0 MHz. The curve drops to about 26% at 6.0 MHz. At 8.0 MHz the "bottom" loop has a maximum $\%E_\theta$ of 82%. This frequency is considered to be resonant since the curve shows a rapid drop to about 32% at 12 MHz. On the other hand the "vertical" loop has $\%E_\theta$ curve with the minimum value of about 40% occurs at 8.0 MHz. The $\%E_\theta$ value at 2.0 MHz is 60%. This loop radiates more vertical power than both the "bottom" loop and the Tranline antenna at 2.0 MHz. The $\%E_\theta$ curve obtained from the Tranline antenna is a scaled down version of the $\%E_\theta$ curve produced by the "bottom" loop. At 2.0 MHz the Tranline antenna has a $\%E_\theta$ of about 17% compared to 60% produced by the vertical loop and 48% produced by the "bottom" loop. Only at 8.0 MHz does the Tranline antenna radiate more $\%E_\theta$ component than the "vertical" loop. The $\%E_\theta$ at this frequency is about 53% for the Tranline antenna compared to 40% for the "vertical" loop. Thus the resonant behaviour seen in both the "bottom" loop and the Tranline $\%E_\theta$ curves around 8.0 MHz is no longer true in the case of the "vertical" loop. Fig. 5.37 shows the $\%E_\theta^*$ curves for the three antennas described above. These curves have the same characteristics as those of $\%E_\theta$ curves seen in Fig. 5.36. The "vertical" loop radiates 28% of its total power into the useful angular sector 30 degrees from the horizon in the vertical component E_θ at 2.0 MHz. At 8.0 MHz the "bottom" loop has a higher $\%E_\theta^*$ than the other two antennas. It produces 50% of useful power compared to 23% obtained by the Tranline antenna and 15% obtained by the "vertical" loop.

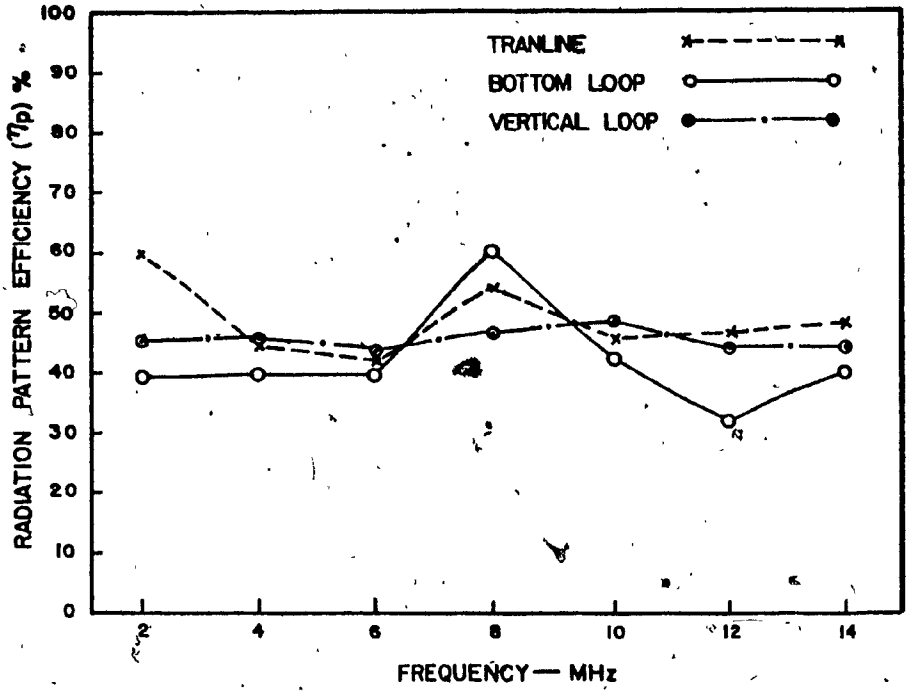

Fig. 5.35 Radiation pattern efficiency for the Tranline, bottom loop, and the vertical loop antennas as a function of frequency.

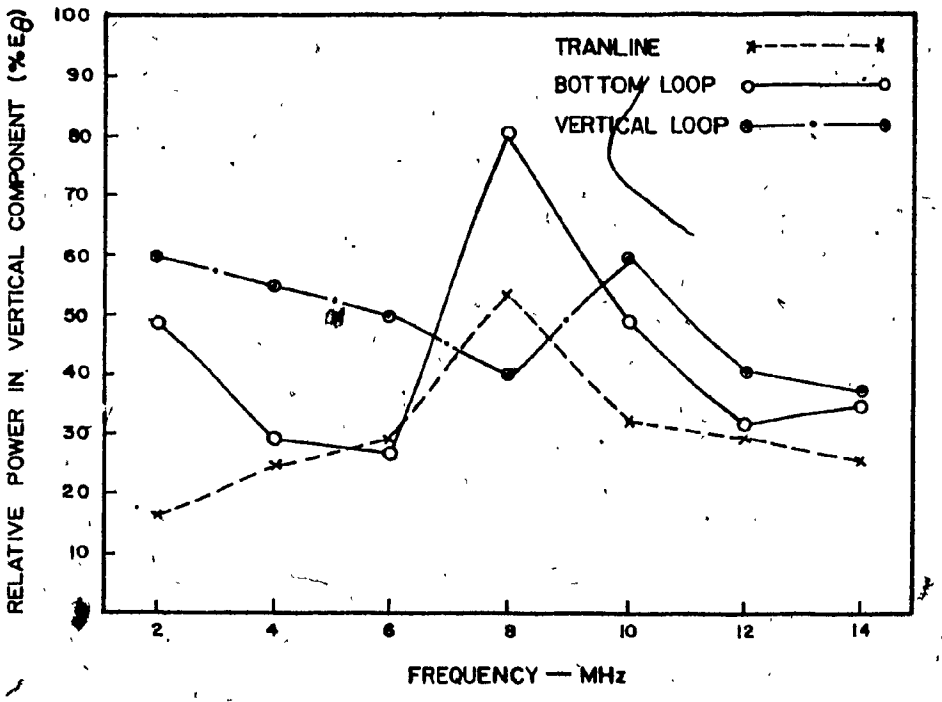

Fig. 5.36 Relative power contained in E_θ ($\%E_\theta$) for the Tranline, the bottom loop and the vertical loop antennas as a function of frequency.

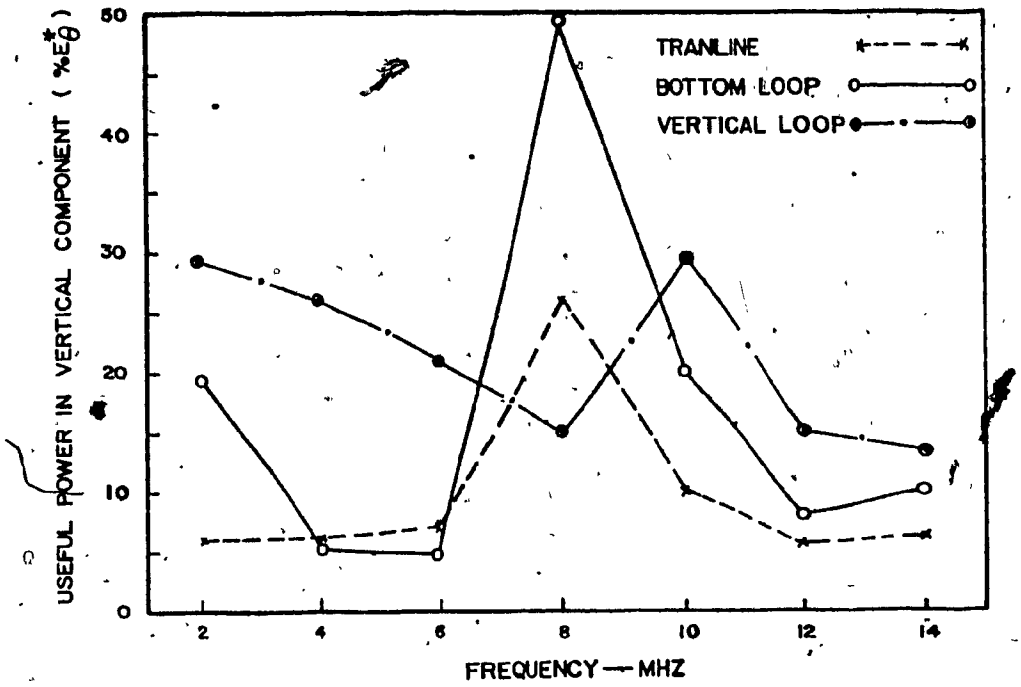

Fig. 5.37 Useful power contained in E_θ ($\%E^*_\theta$) for the Tranline, the bottom loop and the vertical loop antennas as a function of frequency.

The power derived assessment parameters of the Tranline antenna, the "bottom" loop, and the "vertical" loop were presented in this section. They showed that the "vertical" loop is far superior to the Tranline and the "bottom" loop in terms of vertical radiation at the lower end of the HF band. The assessment parameters also indicate that the Sea-King/"vertical" loop combination do not provide resonant paths around 8 MHz. The effects of the rotor blade position on each of the three

antennas' performance are considered in the next section, so that an assessment of best possible antenna performance can be obtained.

5.6.2 Effects of the Rotor Blade Position

In Section 3.6 the effects of the rotor blade position on the patterns of the Tranline antenna were assessed for two blade positions, namely the "forward" or "F-blade" position and the "backward" or "B-blade" position as shown in Fig. 2.7. The rotor blade position caused considerable changes in the radiation patterns at frequencies between 8.0 and 10 MHz. Fig. 3.12 showed the azimuth patterns of the Tranline antenna at 8.1 MHz and 10 MHz. The rotor blade position caused the amplitude of the pattern to change by 2 dB at 8.1 MHz and 5 dB at 10 MHz. The computed azimuth patterns of the Tranline antenna using the "tuned" TRN40 for the two blade positions are shown in Fig. 5.38(a-b). At 8.1 MHz, Fig. 5.38(a) shows the E_θ and E_ϕ polarization for the "F-blade" and "B-blade" positions. A difference of about 3 dB can be seen between the E_ϕ patterns of the two blade positions, whereas the E_θ patterns are of the same orientation and level for each blade position. Fig. 5.38(b) shows the azimuth patterns of the tuned TRN40 model with the "F-blade" and "B-blade" positions at 10 MHz. A difference of about 3 dB can be seen in the E_ϕ patterns, whereas a 1 dB difference is observed in the E_θ patterns. Recall that a 5 dB difference was seen in the measured patterns at 10 MHz. The discrepancy in these results is due to the low

level of the measured E_θ pattern, which makes it vulnerable to spurious reflection from the range's surface.

In this section the effects of the rotor blade position on the radiation pattern of the "bottom" and "vertical" loop antennas are assessed by computer modelling, and compared to this effect for the Tranline antenna. Fig. 5.39(a) shows the azimuth patterns of the "bottom" loop at 8.0 MHz for the two blade positions. The E_θ pattern is not sensitive to the blade position. However the figure shows a major difference between the "F-blade" and the "B-blade" patterns for the E_ϕ component. The "B-blade" pattern has shallower nulls than those seen in the "F-blade" pattern at the port and starboard sides of the helicopter. The four lobe structure seen in the "F-blade" E_ϕ pattern are represented by the "B-blade" pattern, with two lobes at the same level, and with two lobes lower in amplitude by 4 dB. Fig. 5.39(b) shows the azimuth pattern of the "bottom" loop at 10 MHz for the two blade positions. The figure indicates that the rotor blade position has no effect on the radiation patterns at this frequency. Fig. 5.40(a) shows the azimuth pattern of the "vertical" loop for the two blade positions at 8.0 MHz. The E_θ polarization presents a difference in the field strength of about 2 dB between the patterns for the two blade positions. The E_ϕ patterns are close to each other to within 1 dB in both cases. At 10 MHz, Fig. 5.40(b) shows that the rotor blade position has very little effect on the radiation patterns of both polarizations.

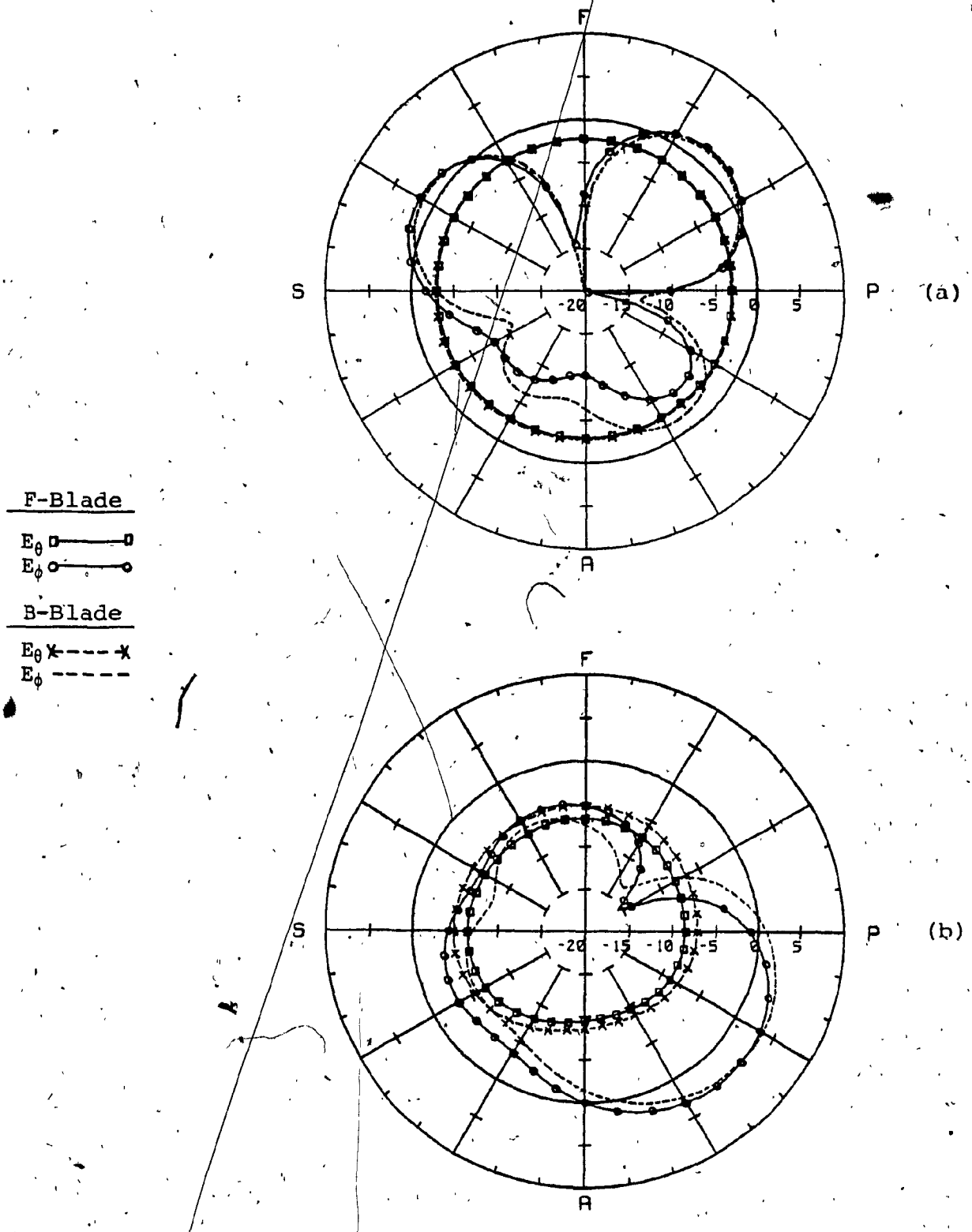

Fig. 5.38 Tranline antenna azimuth patterns obtained using the tuned TRN40 model at (a) 8.1 MHz, (b) 10 MHz, for the two rotor blade positions of Fig. 2.7.

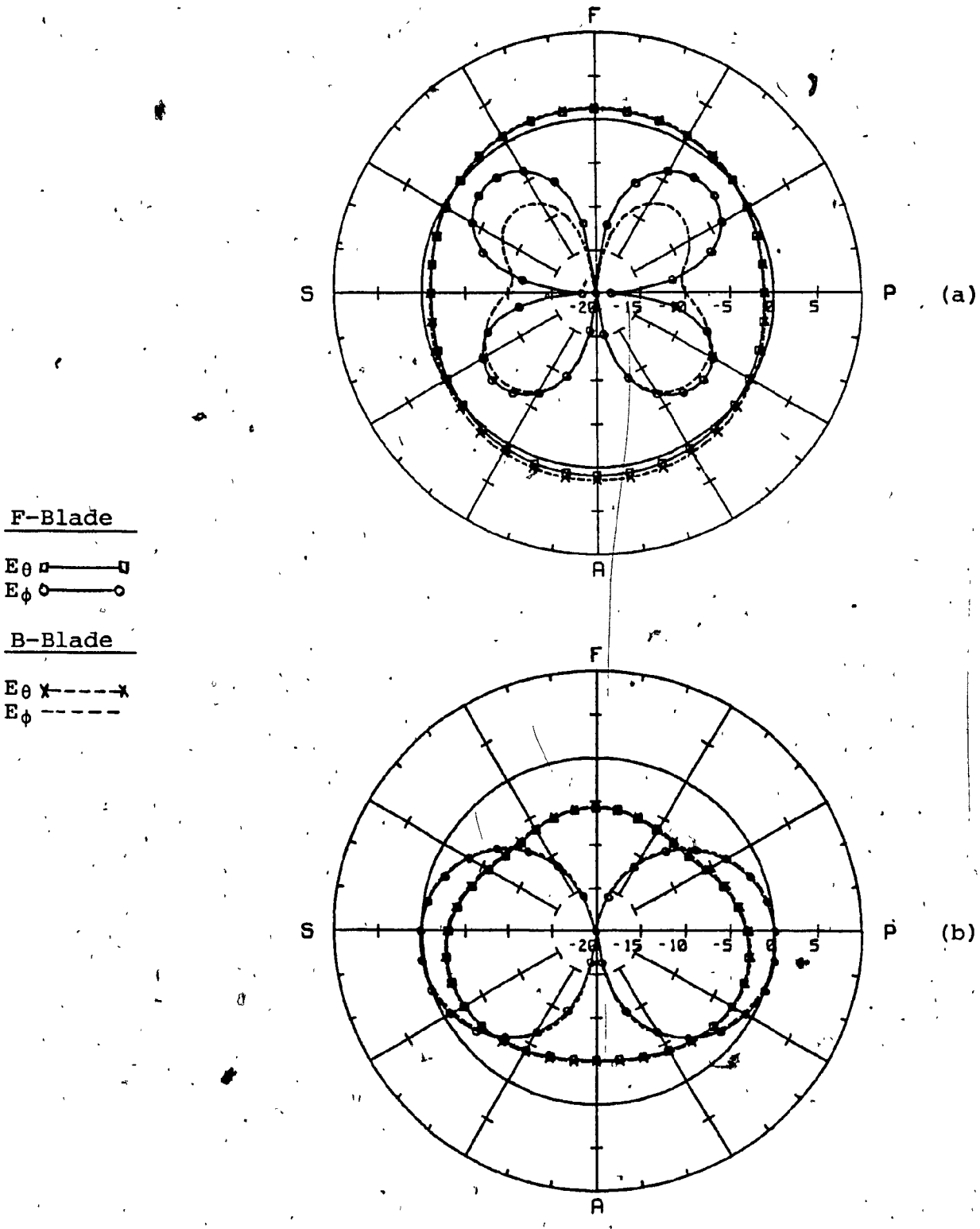

Fig. 5.39 Bottom loop antenna azimuth patterns obtained using the tuned TRN40 model at (a) 8 MHz, (b) 10 MHz, for the two rotor blade positions of Fig. 2.7.

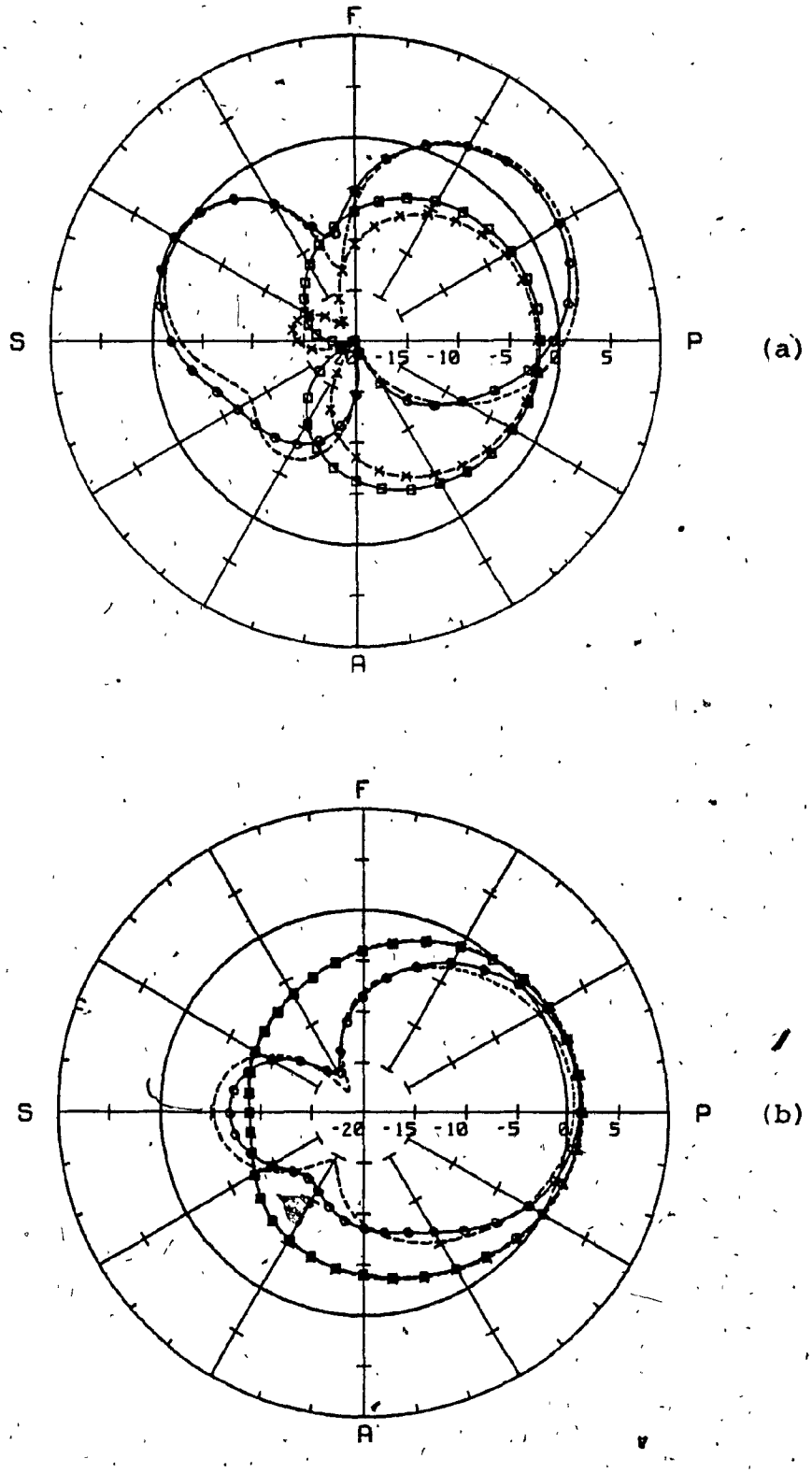

Fig. 5.40 Vertical loop antenna azimuth patterns obtained using the tuned TRN40 model at (a) 8 MHz, (b) 10 MHz, for the two blade positions of Fig. 2.7.

Using the "complex" TRN40 model / Tranline antenna combination, Fig. 5.31 showed the current distribution flowing on the rotor blades in the "F-blade" position at 8.1 MHz. It was seen then that blade numbers 3 and 4, which are oriented toward aft of the helicopter support a strong amount of current. Fig. 5.41 shows the current distribution on the rotor blades oriented in "B-blade" position. In this case three blades become strongly coupled to the model. These blades are oriented toward aft of the helicopter, whereas the "F-blade" position has only two blades oriented toward aft of the helicopter. Such changes in the position of the RF current would cause perturbation in the radiation patterns at this resonant frequency. The effect of the rotor blade position on the "vertical" loop patterns is minimal compared to the "bottom" loop or the Tranline antenna. Thus from pattern consideration alone, the "vertical" loop is considered to be the most suitable antenna among the three antennas examined. It has the highest $\%E_\theta$ at the lower end of the HF band, and the least pattern modulation due to the blade position. As far as this work is concerned, the "vertical" loop has additional advantage over the "bottom" loop. Its feed point is identical to that used for the existing Tranline and wire antennas mounted on the Canadian CHSS-2 Sea-King. This is convenient since the antenna coupler is physically located inside the fuselage at this position.

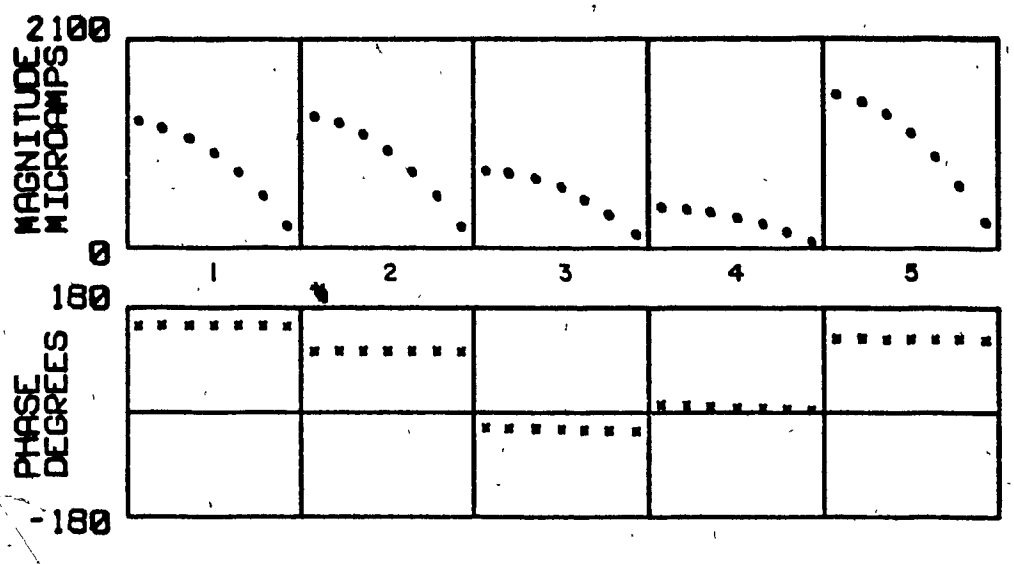

Fig. 5.41 Current distribution on the rotor blades in the backward position, obtained using the tuned TRN40 model at 8.1 MHz with the Tranline antenna mounted on the port side of the model.

5.7 Summary

This chapter has presented three wire-grid models of the Sea-King helicopter, namely the "simple" stick model, the "intermediate" model and the "complex" model. Each of these models was analyzed with the Tranline antenna mounted on the port side of the helicopter using the NEC program. Parametric studies were applied to the simple model to adjust its fuselage radius for a better agreement between the computed radiation patterns and the measured patterns. Results obtained using the complex model are superior to those of the simple and intermediate models. At resonant frequency the complex model required tuning so that its resonant path length is equal to

that of the scale model used in the measurements. A "tuned complex" model produces a set of radiation patterns closer to the measured patterns than those obtained with the "untuned" complex model at the resonant frequency. Finally this chapter explored the possibility of relocating the Tranline antenna. This is done by comparing the performance of various loop antennas mounted at different locations on the "tuned complex" model of the Sea-King helicopter.

Throughout this chapter, the numerically "predicted" radiation patterns are evaluated by a direct comparison with measured patterns as polar or surface plots. The performance of antennas mounted on a wire-grid model is assessed by evaluating the performance parameters. In summary the evaluation techniques used in this chapter present the need for further studies on the computer models of the Sea-King helicopter. A discussion of further work needed is presented next in the concluding chapter.

CHAPTER 6

CONCLUSIONS AND RECOMMENDATIONS

6.1 Introduction

This chapter summarizes the work reported in this thesis. Comments are made about the experimental and analytical results and their usefulness in searching for an optimum location for the Tranline antenna in terms of its performance. Emphasis is placed on the usefulness in such an evaluation of certain assessment parameters which can be obtained directly from the computations.

6.2 Assessment of the Measurements

The NRC antenna range has proven fully satisfactory as a facility for the measurement of the patterns of the Tranline antenna on the Sea-King helicopter. The problem of reflection from the range's surface was overcome by using "fences" as described in Section 2.2.5. The use of a miniature solid state battery-powered oscillator inside the helicopter as a transmitter has eliminated the spurious RF signal induced on

high resistance cables that have been used in past measurements. The patterns show good "correlation" in the sense that phi=0 degrees and phi=90 degrees elevation pattern field values agree well with the corresponding field values measured in the azimuth pattern, and this holds for both polarizations. The recording of the radiation patterns simultaneously on polar plots and on punched paper tape has made the measured patterns readily transferable to the PDP11/20 computer to form a digital data base of measured values. The digital records of measured patterns are used for the reproduction of polar plots in comparison with computations, and for the numerical calculation of the isotropic reference level of the patterns, and of the assessment parameters.

The evaluation of the Tranline antenna radiation patterns is based on the "assessment parameters" derived from the set of conical patterns and from the power radiated by the antenna. These assessment parameters are the "radiation pattern efficiency (η_p)", the "relative power contained in the vertical component E_θ ($\%E_\theta$)", and the "useful power contained in E_θ ($\%E_\theta^*$)", where the useful power is that radiated by the antenna in the angular sector ± 30 degrees from the horizon. The use of the above assessment parameters shows that the Tranline antenna is a poor radiator in the vertical polarization at the lower end of the HF band. The Sea-King/Tranline combination has a $\%E_\theta$ value of about 19% at 2.6 MHz. At 8.1 MHz the $\%E_\theta$ is about 60%. This indicates a resonance of the helicopter which is strongly excited by the Tranline antenna

at this frequency. The measured patterns show that the rotor blade position has a considerable effect on the Tranline antenna performance between 8 and 10 MHz.

In summary, although the measurements of the Tranline antenna radiation patterns are difficult to obtain, they allow a comprehensive evaluation of the antenna performance, and provide a base of measured patterns for comparison with analytical results obtained from the wire-grid models of the Sea-King helicopter.

6.3 Overview of the Analytical Results

The theoretical basis for the Numerical Electromagnetic Code (NEC) computer program is described in Chapter 4. However the main thrust of the analytical work presented in this thesis is the development of wire-grid models of the Sea-King helicopter. Three wire-grid models have been developed, namely the "simple" stick model, the "intermediate" model and the "complex" model. Each of these models was analyzed using the NEC program with the Tranline antenna mounted on the port side of the helicopter. This allowed the computation of the RF current distribution flowing on the model's wires and consequently the calculation of the far field radiated in both the E_θ and E_ϕ polarization.

The TRN11 "simple" model which uses a uniform radius of 0.1 m shows reasonable agreement between computed radiation patterns and the measured patterns at 2.6 MHz, and good

agreement can be seen in the azimuth pattern at 6.0 MHz for both polarizations. Such good agreement is reflected in the computed $\%E_\theta$ which is equal to the measured value at this frequency. However the use of 0.1 m for the fuselage radius of the "simple" model resulted in a smaller portion of the total power being radiated in the E_ϕ component than was seen in the measured patterns, at 2.6 MHz and 4.1 MHz. To overcome this insufficient E_ϕ radiation at these frequencies, the $\%E_\theta$ assessment parameter is used as described in Section 5.2.2 to adjust the fuselage radius to 0.3 m. The section also shows that wires which are parallel to the fuselage should be separated from it by at least 4 times the fuselage radius. This modified model called "TRN18" results in radiation patterns which agree better with the measured patterns than the TRN11 model's patterns, and the TRN18 model is considered to be "valid" between 2.0 and 6.0 MHz. The $\%E_\theta$ curve obtained using the TRN18 model corresopnds to the measured curve between 2.0 and 14.0 MHz, except for frequencies around 8.0 MHz the resonant frequency of the helicopter. By using the scheme of calculating the far field due to the currents flowing on certain wires of the model only, the loop formed by the antenna and its return path along the fuselage is identified as the main radiator at 2.6 MHz. At 8.1 MHz the current on the rotor blades shows a considerable contribution to the far field patterns and so is identified as part of the "principal path" of current flow near resonance. Such analysis gives insight into the modes of current flowing or the "principal paths" of current flow on the model, and into the

resonant behaviour of the model. The identification of such paths is the basis for further studies with more complex models.

The "intermediate" TRN30 model of the Sea-King helicopter presented in Section 5.3 demonstrates the changes in the radiation patterns that come about when the simple model is increased in complexity. The radiation patterns obtained using the "intermediate" computer model are superior to those obtained using the simple model, in the sense that the intermediate model's patterns are similar in shape to the measured patterns. However a large portion of the power is radiated into the E_θ component with this model than in the measurements, and so the E_θ component is at a higher level than in the measured patterns, when both are scaled to radiate the same total power. The density of the rectangular wire grids making up the fuselage of the "intermediate" model is not sufficient to provide a current path similar to that present on the actual scale model used in measurement. Addition of more wires to the "intermediate" model result in a complex model such as that described in Section 5.4.

The detailed TRN40 "complex" model of the Sea-King helicopter was developed at RAE and is used in Section 5.4. This model was analyzed at frequencies between 2.6 and 14.0 MHz using the NEC program. The computed radiation patterns obtained using the "complex" model with the Tranline antenna show good agreement with the measured patterns at all frequencies except 8.1 MHz. The complex model was "tuned" as follows. By

analyzing the "complex" model at frequencies near 8.0 MHz, it was shown that the 8.1 MHz measured patterns match the computer model's patterns at 7.8 MHz. This suggests that the "complex" wire-grid model resonates at a somewhat lower frequency than the scale model used for measurement. In order to "tune" the computer model to a higher frequency, the rotor blades were shortened by five percent and then the computed pattern at 8.1 MHz matches the measured pattern. The "tuned" complex model has the resonant path length equal to that of the resonant path of the scale model.

The "tuned" complex model is used to compare the performance of loop antennas at different locations from that of the present Tranline antenna. Based on the values of the assessment parameters derived from the radiation patterns of loop antennas at three locations, the "vertical" loop of Fig 5.34 has the highest $\%E_\theta$ among all the loop antennas examined at 2 MHz in this thesis. Also, the rotor blade position showed very little effect on the "vertical" loop radiation patterns.

Further studies on the Sea-King wire-grid models are needed. The next section describes the major topics that require further work as a continuation of this thesis.

6.4 Need for Further Work

This thesis has presented a comprehensive methodology for developing wire-grid models of aircraft with HF communication

antennas. This technique requires an extensive set of radiation patterns to be measured on a scale model, and the patterns were used to establish the validity of the computer model and further to tune the computer model so that it resonates at the same frequency as the scale model. Once established in this way, the computer model can be used to study other antennas similar to those used in the measurements, to arrive at an improved design for the HF antenna, such as the "vertical" loop presented in this thesis.

The modelling technique has some shortcomings which may be alleviated by further research. The work presented here needs further investigation into the behaviour of the RF current modes that exist on a computer model at resonant frequencies. A more complex wire-grid model of the Sea-King helicopter than those presented in this thesis might be needed to predict the far field radiation patterns at the higher end of the HF band. Chapter 4 described the "surface patch" modelling techniques. A surface representation of the Sea-King helicopter would give the antenna engineer an appreciation of the difference between the wire and surface modelling techniques. The antenna impedance computed directly by the NEC program can be unreliable especially near resonant frequencies. The comparison of computed and measured impedance values was outside the scope of this thesis. This topic needs a detailed study, and it would require further development in the theoretical aspects of the numerical method used herein.

Although many topics can be considered as an extension to the work presented in this thesis, the most important one in the author's opinion is further investigation of the simple stick model. Such investigation should be based on the concepts that were collected from the analysis of the "complex" model, specifically the "tuning" idea. This is important because it might expand the frequency band in which the simple model is valid.

APPENDIX - A

Tranline antenna principal plane patterns measured in the HF-band, (2.6 - 30 MHz).

$\theta = 90^0$ $\phi = 0^0$ $\phi = 90^0$

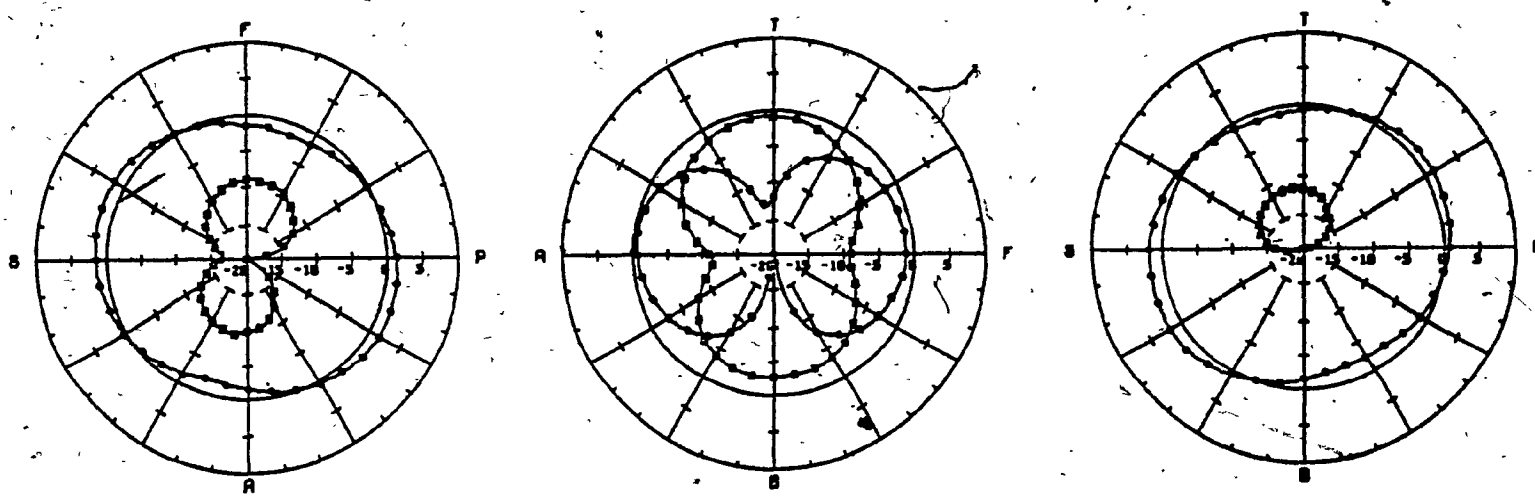

Tranline antenna principal plane patterns measured at 2.6 MHz for both polarizations, E_θ o——o and E_ϕ ●——● . Isotropic level is indicated as a solid circle, (dB-scale).

$\theta=90^{o}$ $\phi=0^{o}$ $\phi=90^{o}$

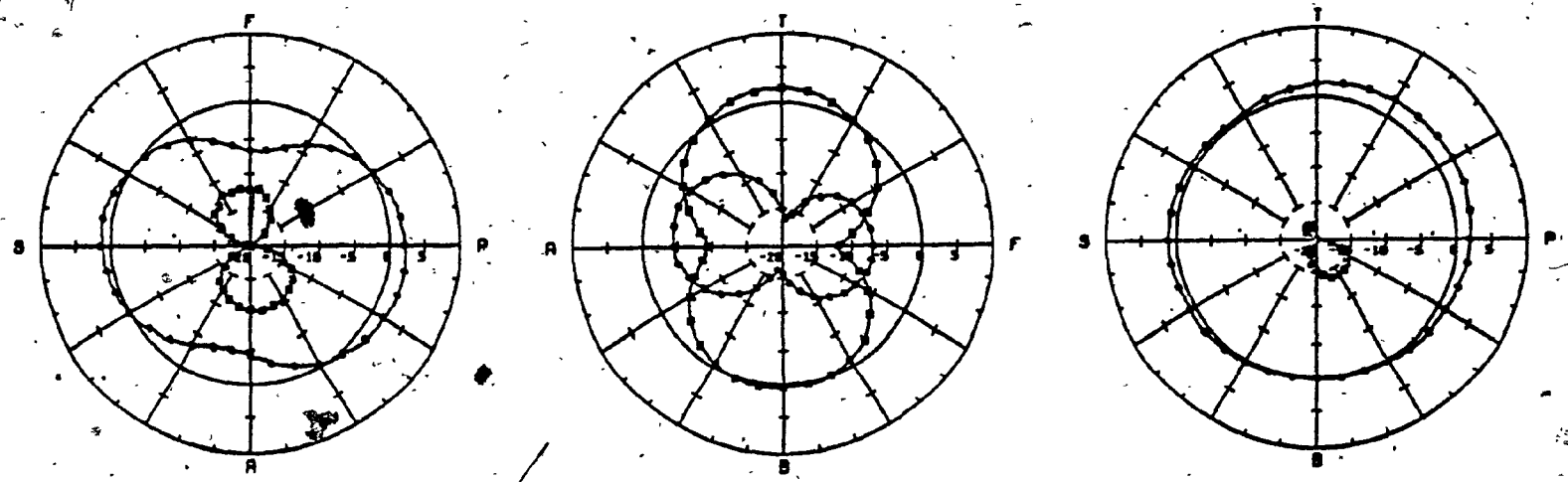

Tranline antenna pricipal plane patterns measured at 4.1 MHz for both polarization, E_θ □——□ and E_ϕ ●——●. Isotropic level is indicated as a solid circle, (dB-scale).

$\theta = 90^0$ $\phi = 0^0$ $\phi = 90^0$

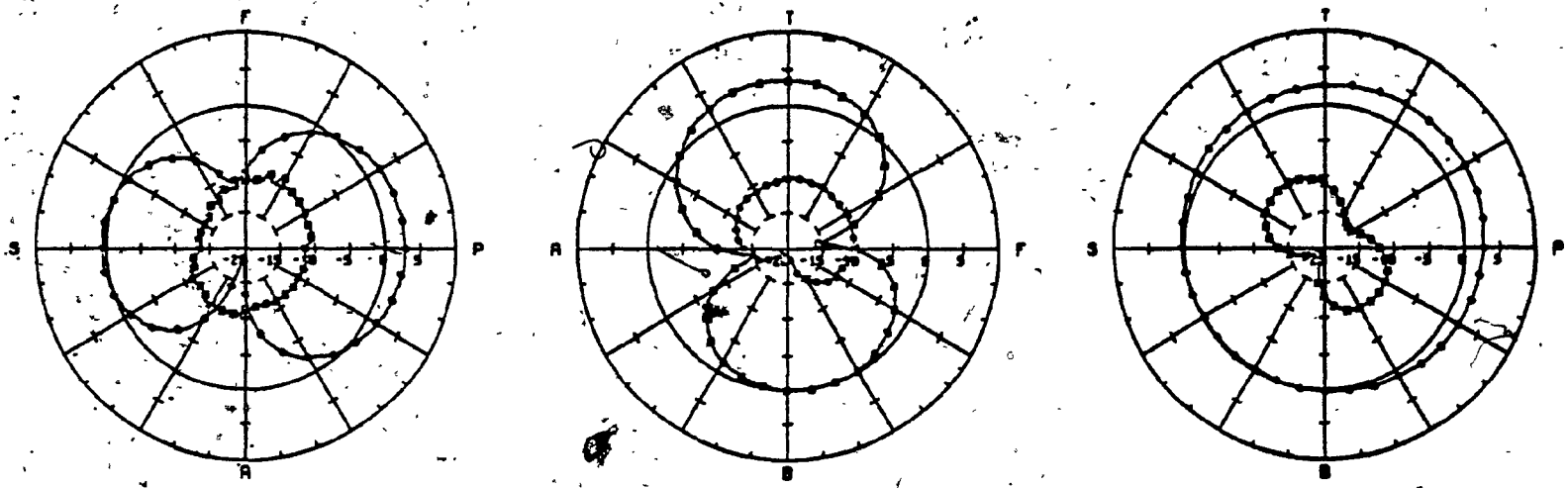

Tranline antenna principal plane patterns measured at 6 MHz for both polarizations, E_θ ▫——▫ and E_ϕ •——•. Isotropic level is indicated as a solid circle, (dB-scale).

$\theta = 90^{o}$ $\phi = 0^{o}$ $\phi = 90^{o}$

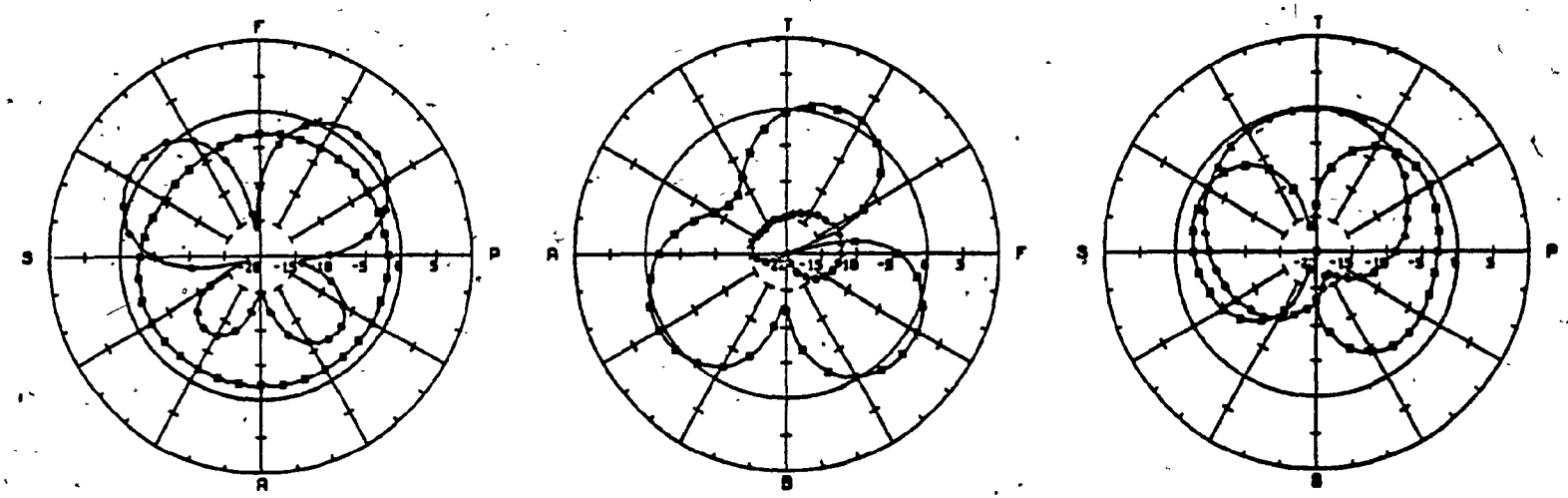

Tranline antenna principal plane patterns measured at 8.1 MHz for both polarizations, E_{θ} ▫——▫ and E_{ϕ} ●——●. Isotropic level is indicated as asolid circle, (dB-scale).

$\theta = 90^{o}$ $\phi = 0^{o}$ $\phi = 90^{o}$

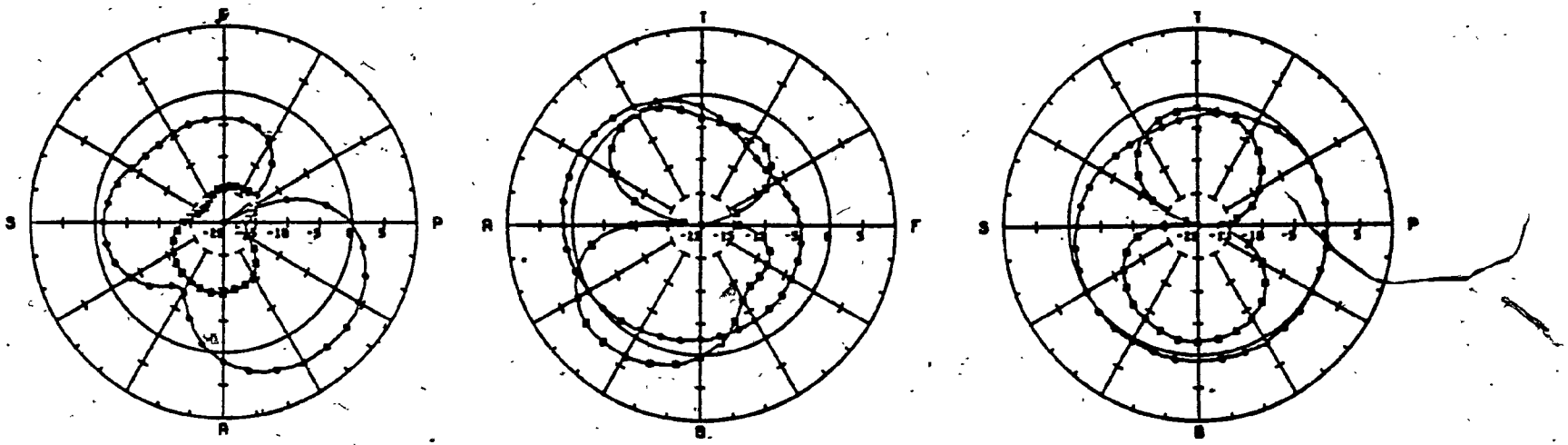

Tranline antenna principal plane patterns measured at 10 MHz for both polarizations, E_θ o——o and E_ϕ •——• . Isotropic level is indicated as a solid circle, (dB-scale).

$\theta = 90^{o}$ $\phi = 0^{o}$ $\phi = 90^{o}$

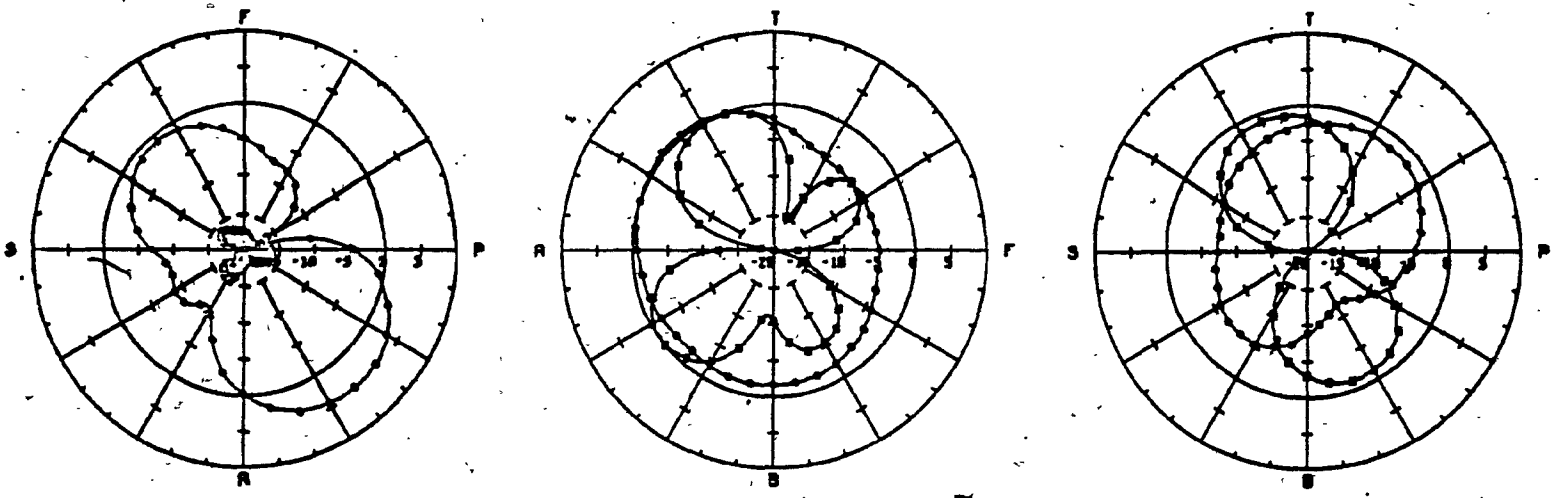

Tranline antenna principal plane patterns measured at 12 MHz for both polarizations, E_θ ▫——▫ and E_ϕ •——• . Isotropic level is indicated as a solid circle, (dB-scale).

$\theta = 90^0$ $\phi = 0^0$ $\phi = 90^0$

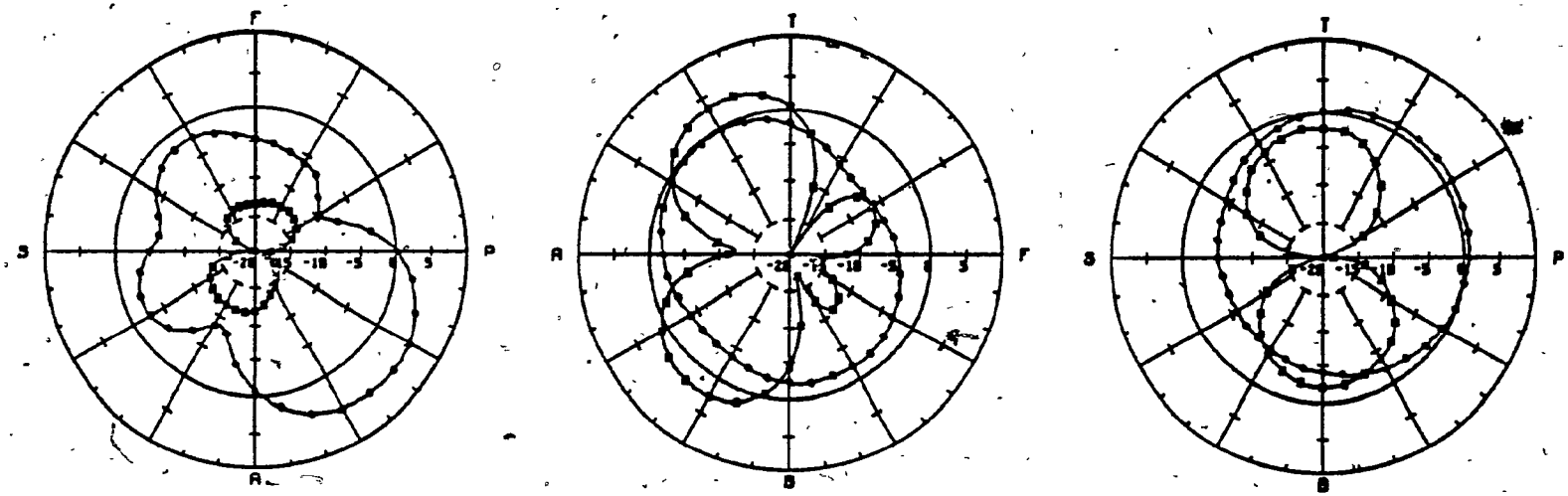

Tranline antenna principal plane patterns measured at 14 MHz for both polarizations, E_θ ▫——▫ and E_ϕ ●——●. Isotropic level is indicated as a solid circle (dB-scale).

$\theta = 90^0$ $\phi = 0^0$ $\phi = 90^0$

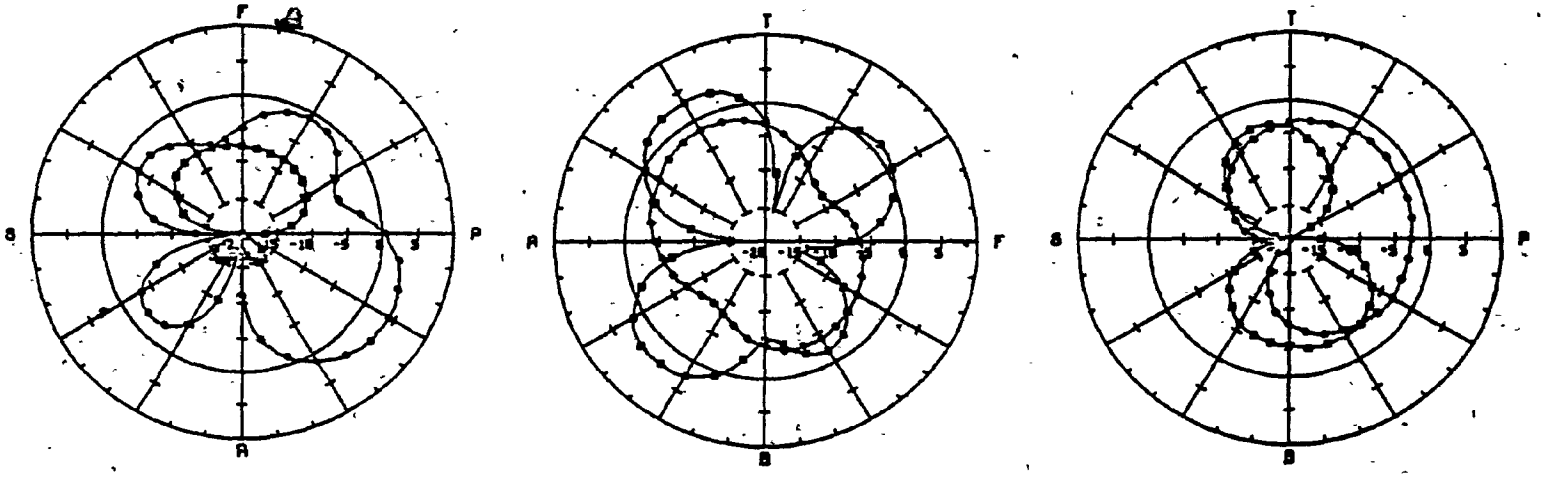

Tranline antenna principal plane patterns measured at 16 MHz for both polarizations, E_θ ▫——▫ and E_ϕ •——• . Isotropic level is indicated as a solid circle , (dB-scale).

$\theta=90^0$ $\phi=0^0$ $\phi=90^0$

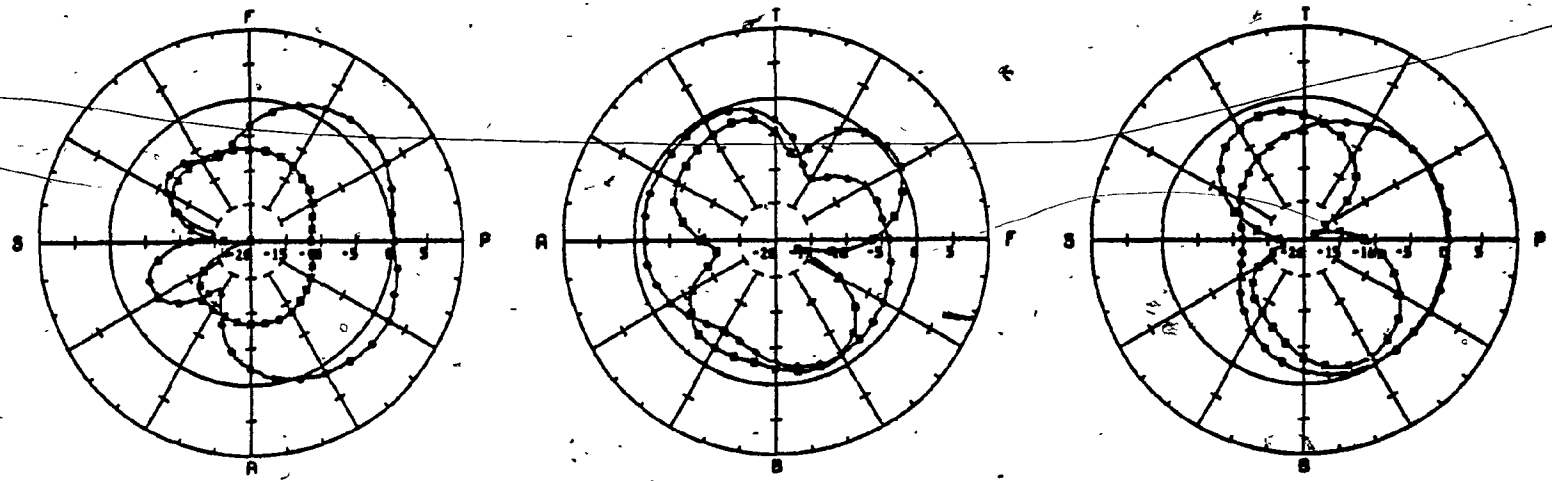

Tranline antenna principal plane patterns measured at 18 MHz for both polarizations, E_θ o——o and E_ϕ •——• . Isotropic level is indicated as a solid circle, (dB-scale).

$\theta = 90^{o}$ $\phi = 0^{o}$ $\phi = 90^{o}$

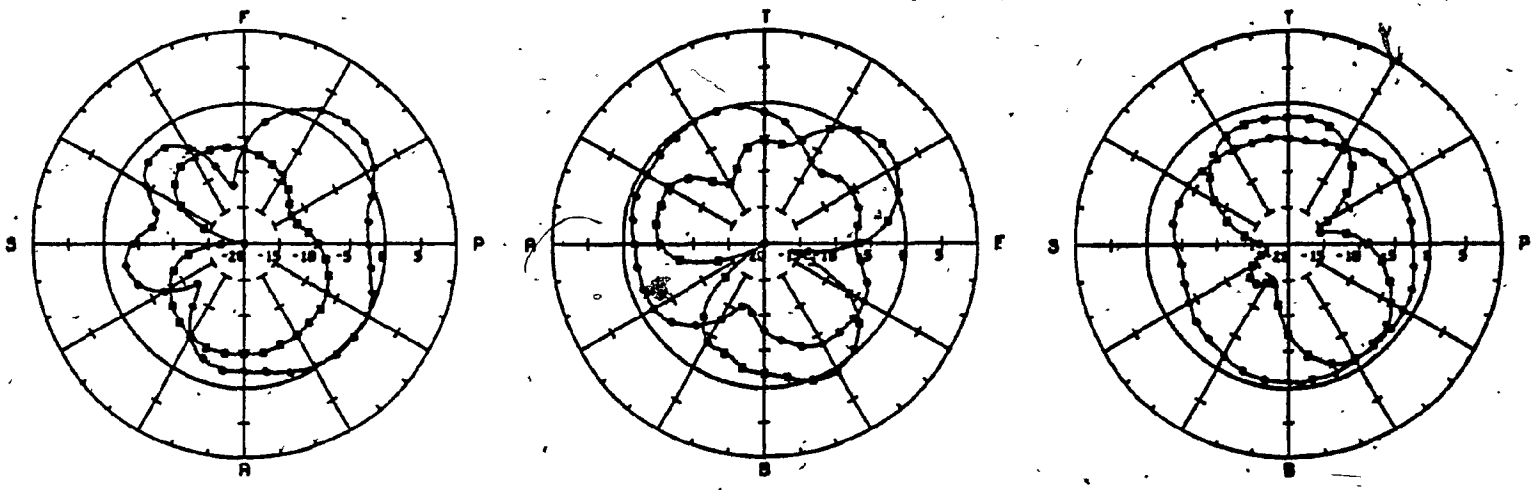

Tranline antenna principal plane patterns measured at 20 MHz for both polarizations, E_θ ▫——▫ and E_ϕ ●——● . Isotropic level is indicated as a solid circle, (dB-scale):

$\theta = 90^0$ $\phi = 0^0$ $\phi = 90^0$

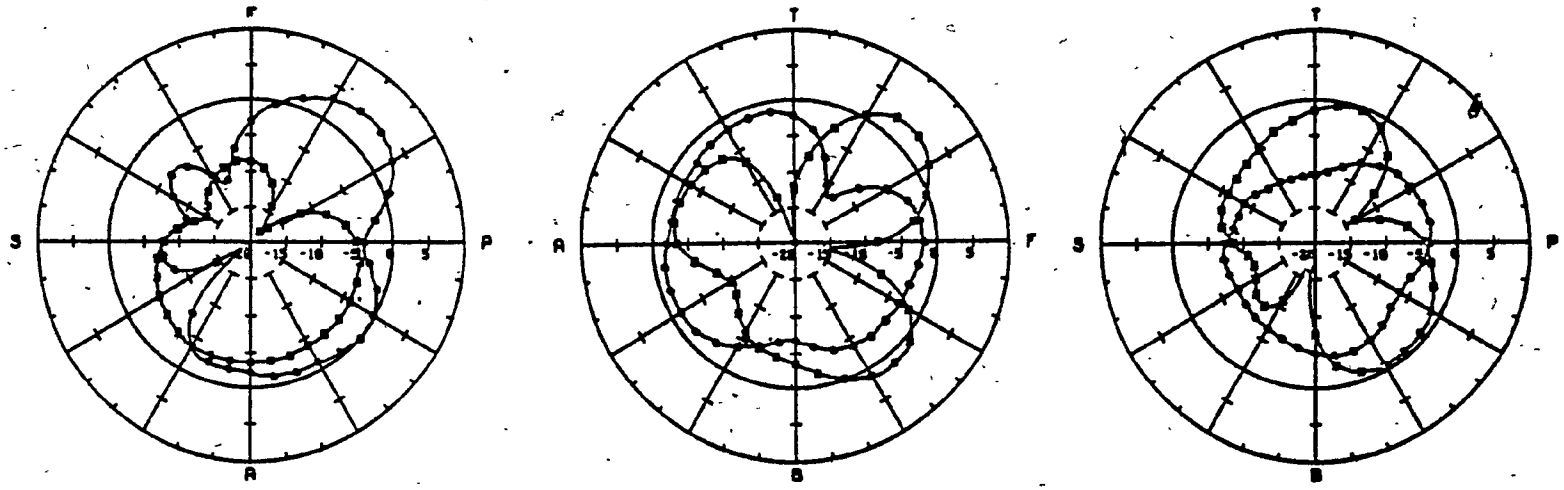

Tranline antenna principal plane patterns measured at 22 MHz for both polarizations, E_θ o——o and E_ϕ ●——● . Isotropic level is indicated as a solid circle, (dB-scale).

$\theta = 90^{o}$ $\phi = 0^{o}$ $\phi = 90^{o}$

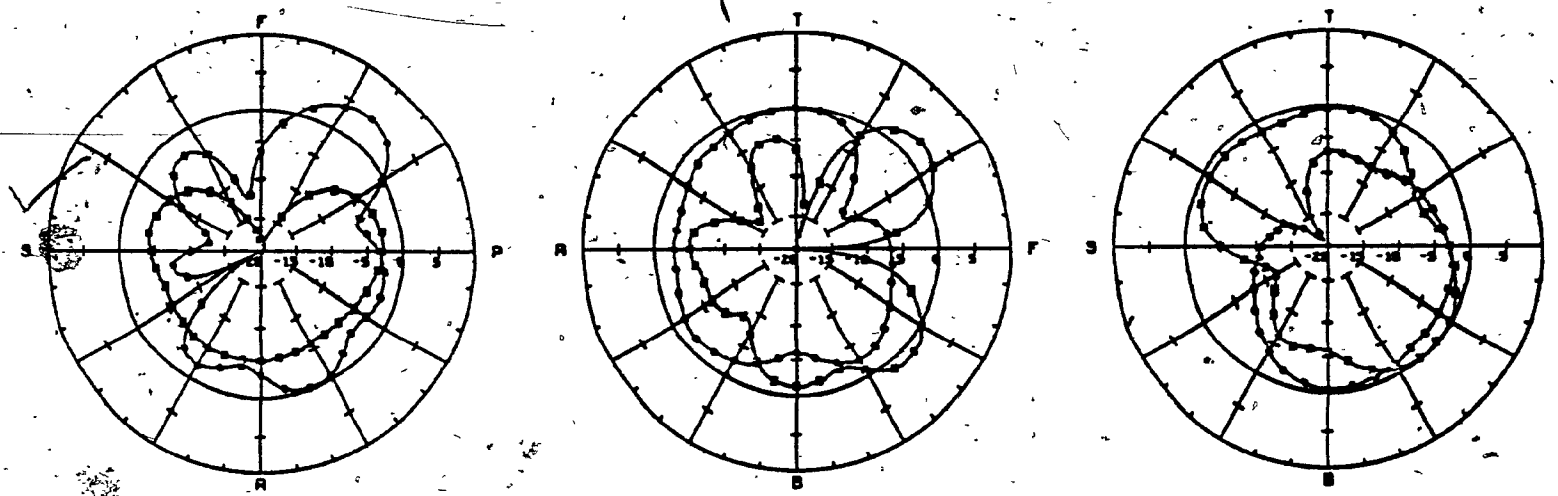

Tranline antenna principal plane patterns measured at 24 MHz for both polarizations, E_{θ} ▫——▫ and E_{ϕ} •——• . Isotropic level is indicated as a solid circle, (dB-scale).

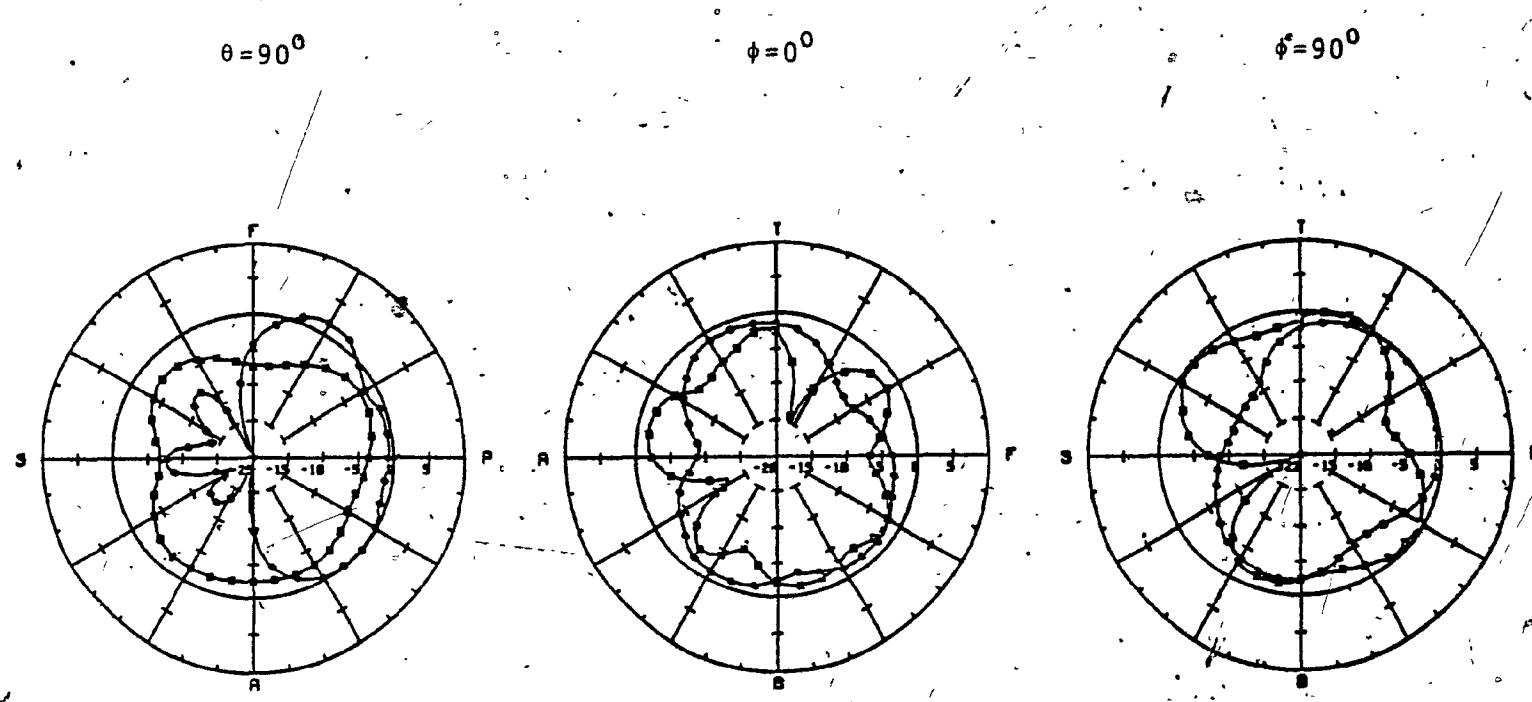

Tranline antenna principal plane patterns measured at 26 MHz for both polarizations, E_θ ▫——▫ and E_ϕ ●——● . Isotropic level is indicated as a solid circle, (dB-scale).

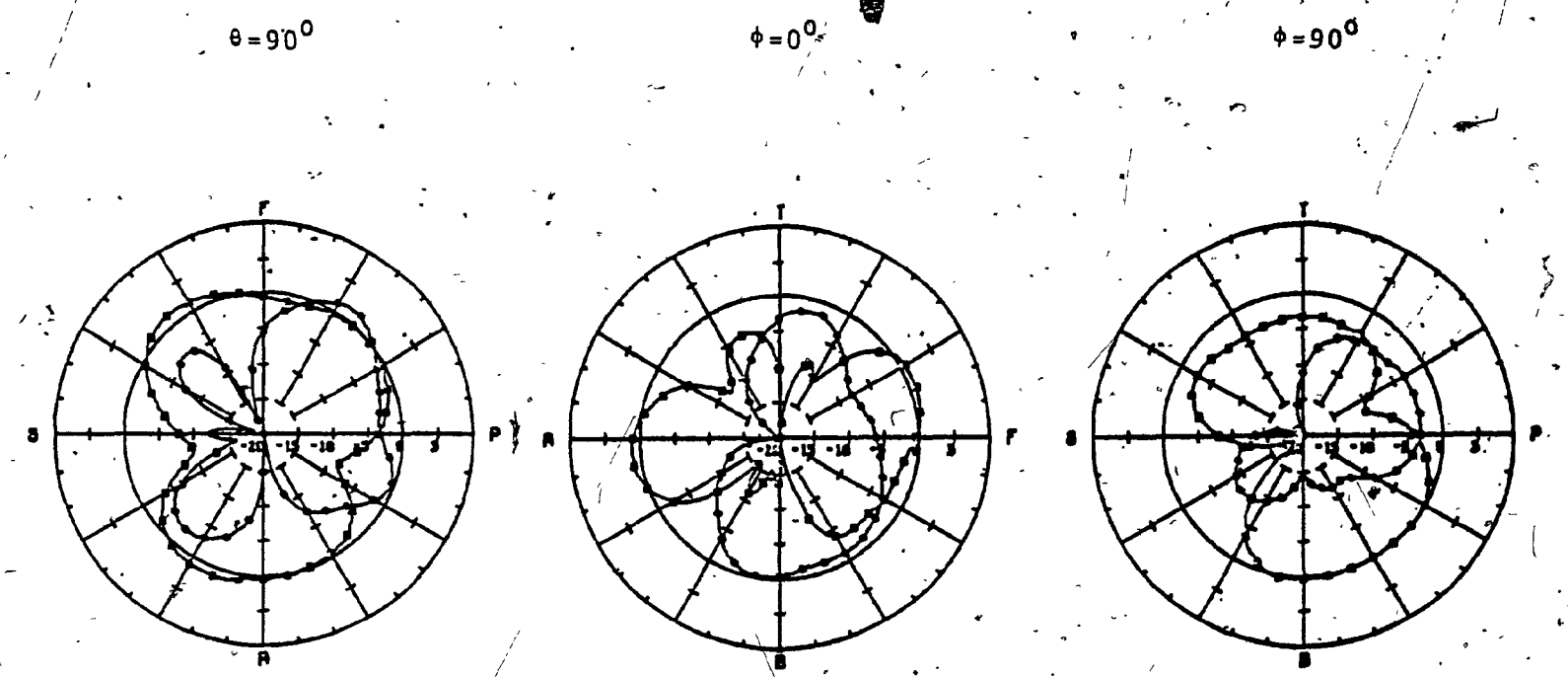

Tranline antenna principal plane patterns measured at 28 MHz for both polarizations, E_θ o——————o and E_ϕ •——————• . Isotropic level is indicated as a solid circle, (dB-scale).

$\theta = 90^0$ $\phi = 0^0$ $\phi = 90^0$

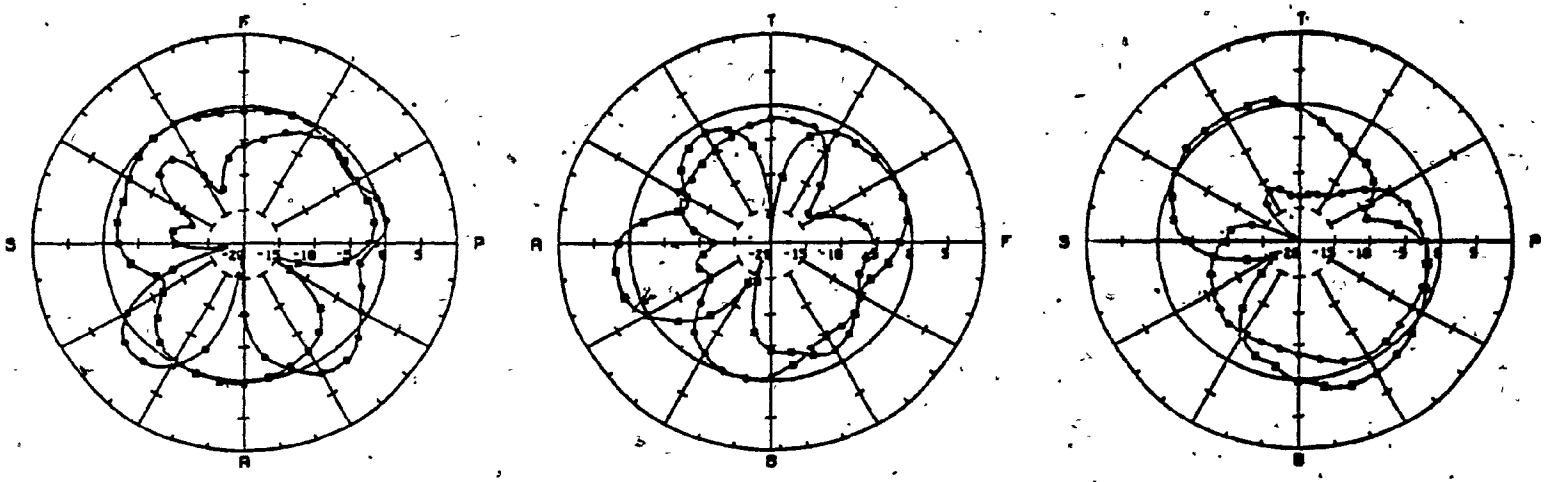

Tranline antenna principal plane patterns measured at 30 MHz for both polarizations, E_θ ▫——▫ and E_ϕ •——• . Isotropic level is indicated as a solid circle, (dB-scale).

REFERENCES

[1] G. Sinclair, E. C. Jordan and E. W. Vaughan, "Measurements of Aircarft Antenna Patterns Using Models," Proceedings of I.R.E., Vol. 35, pp. 1451-1462 Decemder, 1947.

[2] C. K. Adkar, "Radiation Pattern Measurements on Nine HF Antennas for the Sikorsky CHSS-2 Helicopter," Canadair Report No. RAR-00-103, Montreal, April, 1964.

[3] J. Y. Wong and C. A. Muilwyk, "Rotor Modulation Studies of an HF Wire Antenna for the CHSS-2 Helicopter," NRC Report ERB-710 July, 1965.

[4] J. D. Cosgrove and R. C. Fenwick, "Recent Developments in HF Helicopter Antennas," from Radio Antennas for Aircrafts and Aerospace Vehicles," edited by W. T. Blackband, pp. 119-148, November, 1967.

[5] Internal DGAEM/DND Menorandum on the Sea-King/Tranline antenna installation, Ottawa, 1978.

[6] J. E. Brown, "Radiation Pattern Measurements of a Sea-King Loop Aerial by Scale Modelling," RAE Technical Report No. 79037, England, 1979.

[7] Y. Bahsoun and J. Hazell, "Radiation Pattern Measurements of a Tranline Antenna on a Scale Model of the CHSS-2 Sea-King Helicopter," ERB-929, NRCC No. 18883, Ottawa, December, 1980.

[8] J. H. Richmond, "A Wire-Grid Model for Scattering by Conducting Bodies," IEEE Transaction on Antennas and Propagation, Vol. AP-14, pp. 782-786, November, 1966.

[9] E. K. Miller and B. J. Maxum, "Mathematical Modelling of Aircrafts and Supporting Structures," ECOM Contract ADDB07-C-0456, Report No. ECOM-0456-1, MB Associates, San Ramon, California, February, 1970.

[10] S. J. Kubina, "Radiation Characteristics of Vehicle Mounted Antennas and Their Application to Comprehensive System Design," Ph.D. Thesis, Department of Electrical Engineering, Mc Gill University, Montreal, August, 1972.

[11] J. I. R. Owen, "Wire Grid Analysis of HF Aerial for the Toronado and the Sea-King," Royal Aircraft Establishment, Technical Report TR. 77154, England, October, 1977, (Restricted).

[12] R. L. Tanner and M. G. Andreasen, "Numerical Solution of Electromagnetic Problems," IEEE Spectrum, Vol. 4, pp. 53-61, September, 1967.

[13] C. W. Trueman, S. J. Kubina, A. Skalina and T. J. F. Pavlasek, "Interactive Graphics in Antenna Design," Proceedings of IEEE Conference and Exposition, pp. 46-47, Toronto, 1977.

[14] E. K. Miller, R. M. Bevensee, A. J. Poggio, R. Adams, F. J. Deadrick and J. A. Landt, "An Evaluation of Computer Programs Using Integral Equations for the Electromagnetic Analysis of Thin Wires Structure," Report No. UCRL-75566, Rev. 1, Lawrence Livermore Laboratory, Livermore, California, March, 1974.

[15] C. W. Trueman, "Average Field Matching Wire Antenna Moment Method and Aircraft HF Antenna Application," Ph.D. Thesis, Department of Electrical Engineering, Mc Gill University, Montreal, April, 1979.

[16] MIL-A-9080 (U.S.A.F.), Military Specification for Antenna Liaison Communications Equipment, February, 1954.

[17] J. V. Granger, "System Consideration in Aircraft Antenna Design," I.R.E. Transaction on Airborne Electronics, Vol. AE-1, pp. 1-2, December, 1951.

[18] Y. Bahsoun and S. J. Kubina, "A Digital Data Base for the Numerical Calculation of Isotropic Level and Radiated Power by an Aircraft Antenna," Concordia University, Loyola Campus, Electromagnetics Laboratory, TN-EMC-81-06, Montreal, August, 1981.

[19] J. Hazell, "Modification to Sinclair Radio Laboratories Model Range Antenna System," NRC/ERB-879, Ottawa, April, 1973.

[20] W. A. Cumming, "Radiation Measurements at Radio Frequencies: a Survey of Current Techniques," I.R.E. Proceedings, Vol. 47, pp. 705-735, 1959.

[21] IEEE Standard Test Procedures for Antennas, IEEE STD 149-1979, published by IEEE, 1979.

[22] "Micro-Wave Antenna Measurements," Scientific Atlanta, July, 1970.

[23] F. Preikschat, "Screening Fences for Ground Reflection Reduction," Microwave Journal, pp. 46-50, August, 1964.

[24] Scientific Atlanta, INC. Instruction Manual, Model 1863, tape recorder, October, 1965.

[25] F. E. Terman, "Radio Engineering," third edition, Mc-Graw-Hill, 1947.

[26] H. Jasik, "Antenna Engineering Handbook," Mc-Graw-Hill, 1961.

[27] J. Y. Wong, "A Proposed Method for Evaluating the Performance of an HF Shipborne Antenna," NRC Report ERB-647, Ottawa, September, 1963.

[28] I. R. Owen, J. E. Brown, and M. S. Smith, "A Comparison of Scale Model Measurements Using Vertical Range with Wire Grid Analysis for HF Antenna radiation," Royal Aircraft Establishment, Technical Memo RAD-NAV 107, June 1979,

[29] Antenna Coupler Manual, 490S-1, Collins Radio Company, December, 1970.

[30] J. Carswell, "Current Distribution on Wing-Cap and Tail-Cap Antennas," I.R.E. Transaction on Antennas and Propagation, Vol. AP-3, pp. 207-212, October, 1955.

[31] J. V. N. Granger and T. Morita, "Radio Frequency Current DiStributions on Aircraft structures," Proceedings of the I.R.E., Vol. 39, pp. 932-938, August, 1951.

[32] G. J. Burke and A. J. Poggio, "Numerical Electomagnetic Code, (NEC)," Program Description Theory, Naval Ocean System Center, San Diego, California, 92152, July, 1977.

[33] S. J. Kubina, C. W. Trueman, A. Skalina and E. Cerny, "Application of Multi-computer System with Interactive Graphics," Proceedings of the fifth Man-Computer communications conference, Calgary, pp. 199-207, September, 1977.

[34] G. A. Thiele, "Wire antennas," from "Computer Techniques for Electromagnetics," R. Mittra, editor, Pergammon press, New York, 1973.

[35] W. Ghiorgis, "Wire Grid Analysis of Antennas Near Conducting Surfaces," Ph.D. Thesis, Department of Electrical Engineering, Mc Gill University, Montreal, March, 1972.

[36] R. F. Harrington, "Field Computation by Moment Methodes," The Mac Millan Co., New York, 1968.

[37] G. J. Burke and A. J. Poggio, "Numerical Electromagnetic Code," Users Manual, Naval Ocean System Center, San Diego, California, 92152, July, 1977.

[38] A. Brown, "Simulation of a TEKTRONIX 4010 Computer Terminal (SIMTEK)," Concordia University, Loyola Campus, Montreal, April, 1975.

[39] K. A. Ai-Badwaihy and J. L. Yen, "Extended Boundary Condition for Perfectly Conducting and Dielectric Bodies: Formulation and Uniqueness," IEEE Transaction on Antennas and Propagation, Vol. AP-23, pp. 546-551, July, 1975.

[40] NOS Version 1 Reference Manual, Volume 1, Publication No. 60435400, Control Data Corporation, St. Paul, Minnesota, 55112, December, 1980.